Book of Abstracts. Symposium Lightweight Design in Product Development

Zurich, 14.06. – 15.06.2018

Conference Proceedings

Publication date:
2018-06-14

Permanent link:
https://doi.org/10.3929/ethz-b-000283432

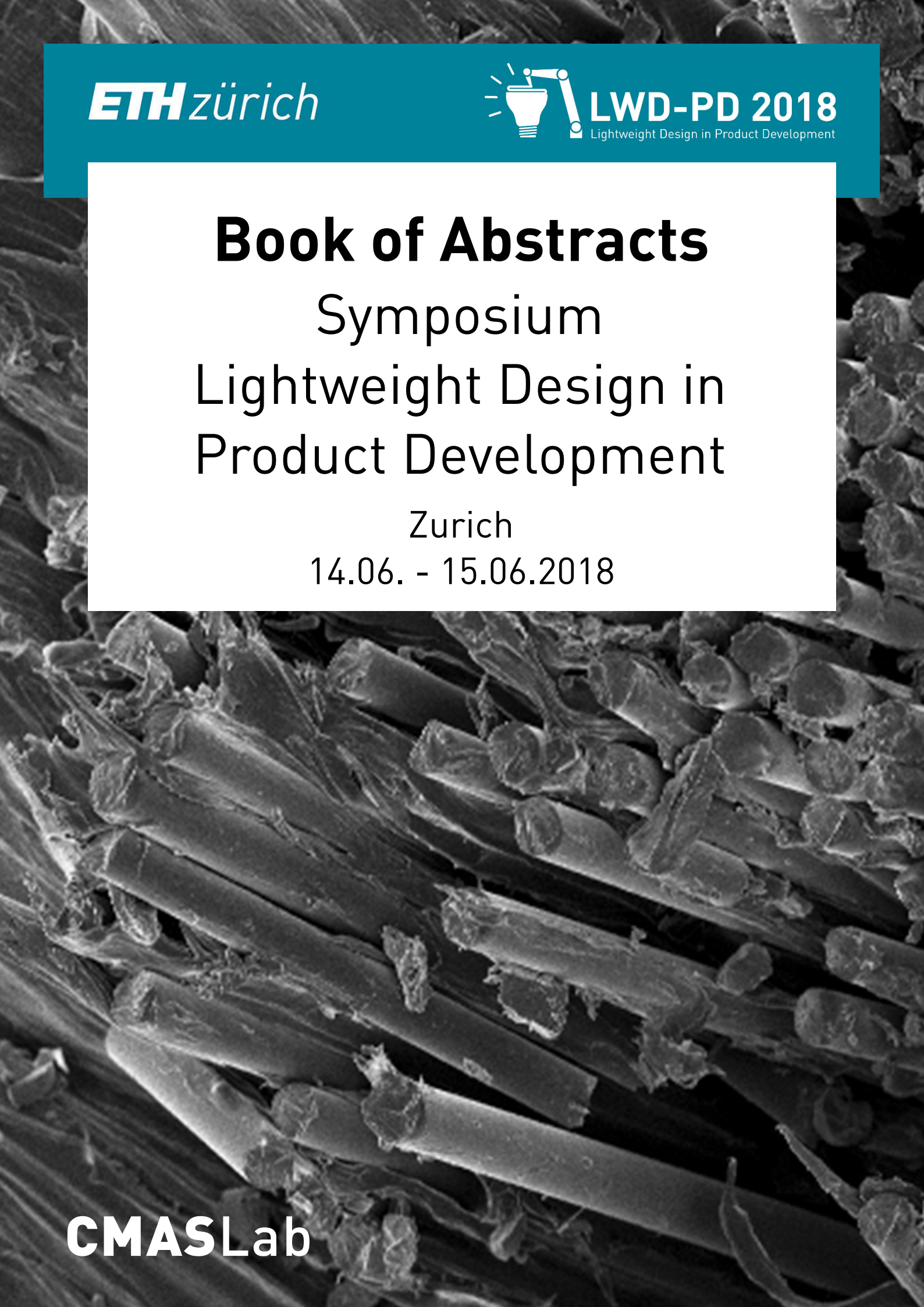

ETH zürich

LWD-PD 2018
Lightweight Design in Product Development

Book of Abstracts

Symposium Lightweight Design in Product Development

Zurich
14.06. - 15.06.2018

CMASLab

Symposium *Lightweight Design in Product Development 2018*

Editorial

The symposium *Lightweight Design in Product Development* (LWD-PD18) was held June 14th – 15th 2018 at ETH Zurich, Switzerland.
Today more than ever, economic growth, prosperity and mobility need to be balanced with the limited availability of natural resources and energy reserves. In this context, lightweight systems play a central role by the realization of sustainable products and components, minimizing material and energy consumption over the entire design life. The design space available to engineers is continuously expanded by novel material systems and fabrication technologies entering the market. At the same time, novel multidisciplinary design tools, methods and approaches, new data and information technologies are revolutionizing products and the way they are designed and fabricated.

The symposium thus selectively addressed and discussed actual topics along the entire value chain from material to design and fabrication, sharing research achievements at the leading edge of research and application and discussing and exchanging ideas on future trends.

A wide variety of lightweight design subject areas were covered over five main tracks: Engineering of Composites, Modular Lightweight Design, Multifunctional Lightweight Systems, Additive Manufacturing for Lightweight Design, Advanced Materials and Processes.

The organizing committee would like to thank all volunteers, participants, speakers and most of all the researchers who enabled the symposium to become such an outstanding success.

Zurich, June 2018

Paolo Ermanni
Mirko Meboldt
Sandro Wartzack
Dieter Krause
Markus Zogg

Symposium *Lightweight Design in Product Development 2018*

Content

Symposium *Lightweight Design in Product Development 2018* (LWD-PD18)
Zurich, Switzerland, 14th–15th June 2018

COMPUTER AIDED INTERNAL OPTIMIZATION (CAIO) METHOD FOR FIBER TRAJECTORY OPTIMIZATION: ENHANCING APPLICABILITY

H. Voelkl[1], M. Franz[2] and S. Wartzack[3]

[1]Friedrich-Alexander-University Erlangen-Nürnberg (FAU), Engineering Design, voelkl@mfk.fau.de
[2]FAU, Engineering Design, franz@mfk.fau.de
[3]FAU, Engineering Design, wartzack@mfk.fau.de

1. INTRODUCTION

Bionic solutions to technical problems led to fascinating algorithmic approaches in structural design – for example, transferring the principle of tree fiber growth to optimal fiber layout in fiber-reinforced plastics (FRP), called the Computer Aided Internal Optimization Method (CAIO) [1]. It is based on aligning the orthotropic axes of FRP with the "force flow" [1], i.e. maximum principal normal stress trajectories (MPNST), which consequently leads to a reduction of shear stresses. As shear stresses are among the main causes for matrix failure [2], this leads to a significant increase in strength. Fig. 1 shows the flow chart of the CAIO method.

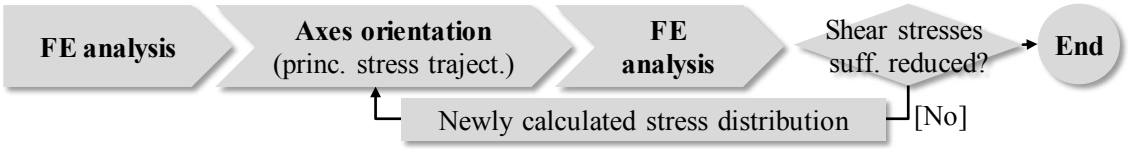

Fig. 1: Flow chart of the CAIO method adapted from [1].

Following an initial finite element (FE) analysis with isotropic material, the orthotropic material axes are aligned with MPNST (more precisely, principal normal stress trajectories with maximum absolute eigenvalues [3]). Using these new orientations, another FE analysis is conducted. If shear stresses are significantly reduced [1] or fiber angles don't change significantly [3], the calculation ends; otherwise it continues with the next iteration.
Even though the method has been applied and its working principle scrutinized in several contributions [3; 4] there is still some work to be done to bring CAIO into practice. Specifically, for areas of isotropic multi-axial stress states, the selection of MPNST becomes non-unique [3] – this means in practice, it's unclear in which direction fibers have to be put. Fig. 2 illustrates this problem.

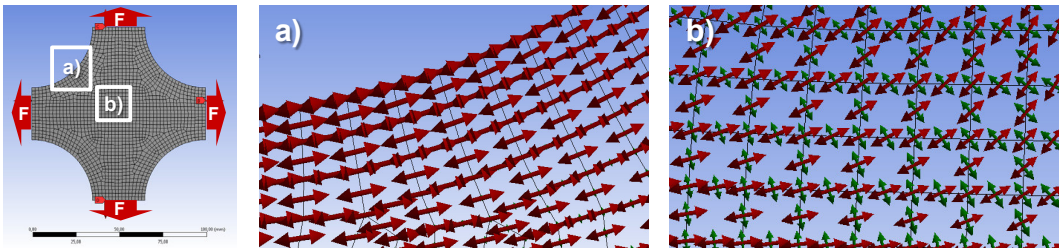

Fig. 2: a) Areas with unique MPNST; b) Areas with non-unique MPNST

Experience shows these stress states typically appear in real-world examples with complicated geometries and load cases. Solutions to this problem have been discussed, like selecting MPNST with maximum absolute eigenvalues instead of signed eigenvalues [3] ("maximum absolute") or searching for finite elements within proximity with unambiguous fiber directions [5; 6] and adapting their orientation ("proximity search"). However, there is a lack of deeper scrutiny. This extended abstract compares these two approaches to tackle the problem. Comparison is done both visually and in terms of stiffness and strength, measured using Puck matrix failure criterion. The extended abstract is limited to plane stress states; convergence history is given for each example.

2. EXTENDING THE CAIO METHOD FOR LOCAL MULTI-AXIAL STRESS STATES

To scrutinize the impact of multiaxial stress states on the overall outcome of the CAIO method, a two-step examination process is followed: (1) Find regions of multiaxial stress states for a given demonstrator. (2) Compare stiffness and strength results of the optimized fiber layouts when applying "maximum absolute" and "proximity search".

(1) Fig. 3 shows the principal normal stress directions of a simple plate with a notch. It is subjected to bending load at one edge and fixed on the left boundary. For this example, two regions of multiaxial stress states evolve – close to force application (A) and in regions where tension and compression principal stresses intervene (B). Region B is much more heavily stressed than region A (see vector lengths corresponding to eigenvalues).

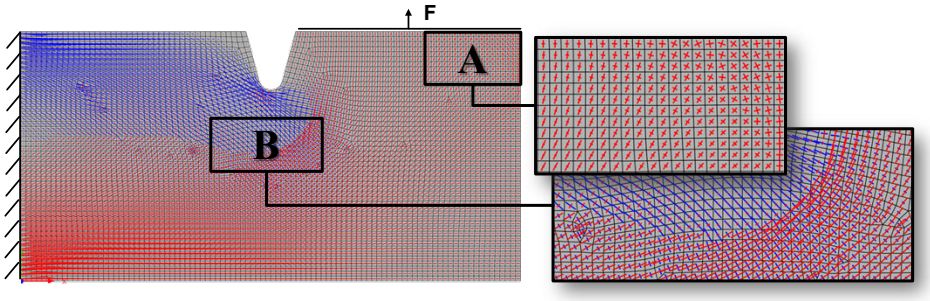

Fig. 3: Plate with a notch under bending load, principal normal stress trajectories (red = tension, blue = compression)

(2) The results of the CAIO method applied to this example are presented in Fig. 4 after 10 iterations (strain energy difference smaller than 0.1 %). The "maximum absolute" result without any interference with fiber direction during the optimization process is shown on the left in Fig. 4a. Using the "proximity search" method from [5] a different principal normal stress direction field evolves – and thus different fiber orientations, especially in Region B (Fig. 4b). Elements with similar absolute eigenvalues of first and second principal stress trajectories (± 20%) ("isotropic" stress states) are shown in Fig. 4c. These are the elements where "proximity search" selects suitable, uniquely selectable fiber trajectories from elements in the vicinity.

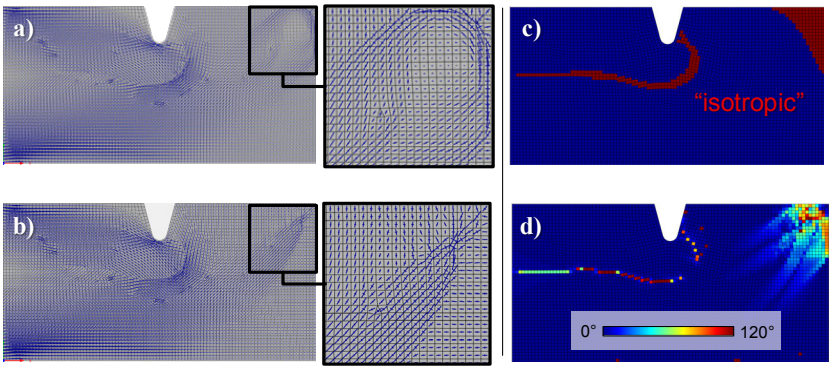

Fig. 4: Visual results. a) Usual "maximum absolute" CAIO results, b) "Proximity search" modified CAIO result, c) Elements with detected multiaxial stress states (all iterations) where "proximity search" is applied, d) Fiber angle difference between "maximum absolute" and "proximity search".

Fiber orientations are not significantly altered in regions of unique MPNST, yet quite strongly altered especially in region A. In the tension-compression region B, orientation differences are very high locally, depicting 90° deviations. Fig. 5 presents numerical results: strain energy sum (stiffness) in the course of ten iterations and Puck matrix failure values (strength) visually in the third iteration, see break criterion above.

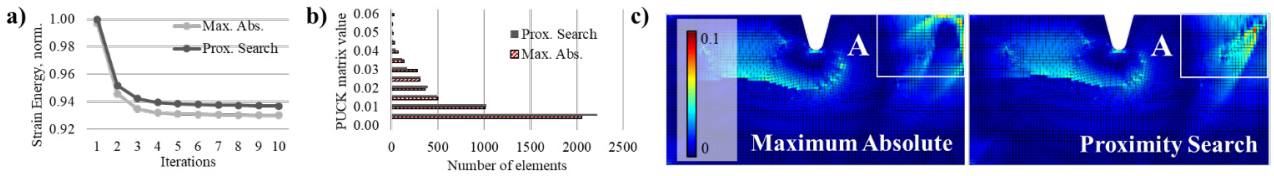

Fig. 5: Numerical results. a) Convergence history of the total strain energy (normalized to max = 1), b) histogram of Puck matrix failure values, c) Puck matrix failure criterion values.

Interpreting these results, stiffness only differs slightly between the two calculation methods (about 0.7 %). Hypothetically, the reason for this behavior could be that the orientation of the orthotropic fiber axis in elements with multi-axial stress states does not have a huge stiffness effect – fiber orientation might always be "equally bad". The strength results show bigger differences especially in region A (force application), which corresponds to the differences in fiber orientation (Fig. 4d).

This might stem from a secondary effect of load transfer due to locally different fiber angles picked from neighboring unambiguous-MPNST elements. More widely distributed Puck values are observed in region A when using proximity search (Fig. 5b), the histogram in Fig. 5c shows that "proximity search" shows lower Puck matrix values than "maximum absolute" a bit more frequently and vice versa.

In the following, application to a real-world example shall reveal whether the upper observations can be repeated: no significant stiffness increase or decrease; differences in fiber orientation close to boundary conditions and loads; and more widely distributed/frequently lower Puck matrix failure values.

3. APPLICATION TO A MOUNTING BRACKET

In real-world applications, part geometries often consist of 3D-shapes. To scrutinize the two CAIO method variations under more practical conditions, a mounting bracket under torsional load applied to the inner mounting holes, illustrated in Fig. 6a, is chosen. The part is fixed at the outer holes. Figs. 6b and 6c show the results after 10 iterations with proximity search (± 20%). The elements with an "isotropic" stress state (red) in the last iteration are shown in Fig. 6b, emphasizing selection A as an example area for applying proximity search. Studying the differences of the Puck matrix failure values in Fig. 6c, there is no regular pattern which could be seen as correlated to the "isotropic" elements.

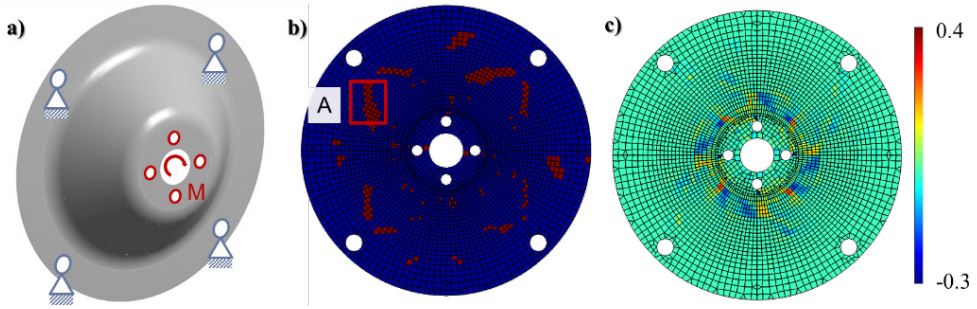

Fig. 6: a) Three-dimensional mounting bracket under torsional load, b) Elements with "isotropic" multiaxial stress states in the last iteration when "proximity search" is applied, c) differences in Puck matrix failure values between "maximum absolute" and "proximity search".

Analysing the stiffness results in Fig. 7a the "proximity search" provides slightly less stiff designs than the conventional CAIO method. As described before, from the numerical point of view the fiber is not placed in the best way, but nonetheless the fiber direction computed by "proximity search" helps designing bigger areas of similar fiber angles. Fig. 7b shows a detailed view of the fiber directions computed with the two presented methods. Area A contains several Finite Elements with "isotropic" stress state. The "proximity search" leads to a more uniform result. Additionally to the stiffness evaluation there can be seen no significant stiffness change after the fifth Iteration, indicating fast convergence in terms of stiffness. The observation of the fiber angle difference in Fig. 7c shows high local deviations between the methods but no correlation with the "isotropic" elements of the last iteration (Fig. 6b).

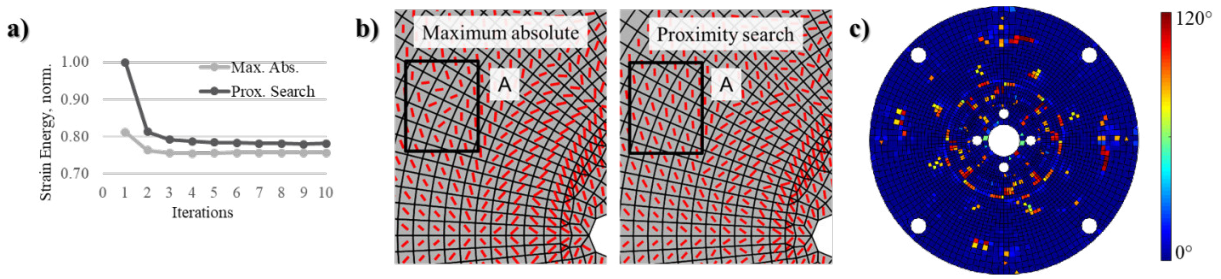

Fig. 7: Numerical results after ten iterations a) Convergence history of the total strain energy (normalized to max = 1), b) Fiber directions computed with "maximum absolute" CAIO and with "proximity search" CAIO, c) Fiber angle difference between "maximum absolute" and "proximity search".

4. CONCLUSION

The "proximity search" adaption to the CAIO method [5] was scrutinized and compared to the typical fiber trajectory selection within CAIO ("maximum absolute"). Both stiffness, strength and uniformness of fiber layout were examined. No clear pattern was found concerning strength. However, although providing slightly less stiff results, the "proximity method" produces more regular – and thus easier-to-manufacture – fiber layouts for the given demonstrator.

REFERENCES

[1] REUSCHEL, D. et al. "Optimization of fiber arrangement with CAIO (computer aided internal optimization) and application to tensile samples", *Transactions of the Built Environment*, 1999, Vol. 37: pp. 247–255.

[2] SCHÜRMANN, H., *Konstruieren mit Faser-Kunststoff-Verbunden. 2. Auflage*, Springer, Berlin, Heidelberg, 2007.

[3] SPICKENHEUER, A.: *Zur fertigungsgerechten Auslegung von Faser-Kunststoff-Verbundbauteilen für den extremen Leichtbau auf Basis des variabelaxialen Fadenablageverfahrens Tailored Fiber Placement*, Ph.D. thesis, Technische Universität Dresden, 2014.

[4] CHENG, G et al., "On sufficiency conditions for optimal design based on extremum principles of mechanics", *Journal of the Mechanics and Physics of Solids*, 1997, Vol. 45: pp. 135–150.

[5] KLEIN, D., *Ein simulationsbasierter Ansatz für die beanspruchungsgerechte Auslegung endlosfaserverstärkter Faserverbundstrukturen*. Ph.D. thesis, Friedrich-Alexander-Universität Erlangen-Nürnberg, 2017.

[6] Klein, D. et al., "Introduction of a computational approach for the design of composite structures at the early embodiment design stage", *ICED15*: 2015, pp. 105-115

Symposium *Lightweight Design in Product Development 2018* (LWD-PD18)
Zurich, Switzerland, 14th–15th June 2018

HYBRID LIGHTWEIGHT DESIGN FOR STRUCTURAL COMPONENTS – A TECHNICAL, ECONOMIC AND ECOLOGICAL POTENTIAL ANALYSIS

Jerome Kaspar[1] and Michael Vielhaber[1]
[1]Institute of Engineering Design (Saarland University), Germany. kaspar@lkt.uni-saarland.de

1. INTRODUCTION

Today, lightweight measures compete with many other CO2 abatement levers (e.g., electrification with strong interdependency to weight) in the transport sector, particularly within the automotive industry. Thus, composite materials are being marketed to industrial companies as a superlative lightweight alternative to the wide variety of aluminum and steel alloys already being used and technologically optimized in structural applications for years. However, do these innovative materials (i.e., CFRP) substantially feature the desired game-changing issue facing the challenge of transferring new lightweight-oriented concepts through each phase of the product development process in accordance with unique technical, economic and ecological specifications? Or, do actually hybrid concepts exceed the overall cost-benefit performance as a result of their specifically tailored and customer-driven properties even with regard to an advanced multi-material systems design?

Concerning this matter, the scientific contribution presents a module-driven systematic approach for the early conceptual stage of product development regarding a potential analysis of designing hybrid material components based on an integrated cross-component lightweight and material-oriented development (IC2-LMOD) methodology [1,2].

2. LIGHTWEIGHT AND MATERIAL-ORIENTED FRAMEWORK – EXTENSION OF HYBRID DESIGN

Covering this challenging topic, a systematic material selection has already been valued for decades, particularly more and more successfully with the scientific contribution by Ashby [3] and its computational screening approach [4]. Thus, and compared to former perspectives on material aspects paired with at least to some extent production-oriented know-how [5-6] within the decision-making process in product development, Ashby's methodology clearly defines four main phases to the final choice of material: (1) translating material-related requirements, (2) screening by eliminating materials or material subclasses failing to perform, (3) ranking by comparing most promising candidate materials, and (4) seeking supporting information by validation of material properties. Integrated procedures considering geometry-depending aspects are indeed being fundamentally addressed [7-9], however, it is carried out in detail only insufficiently analogous to processing-specific matters [10]. Accordingly, the systematic analysis of potentials along with its actually conceptual or detailed component design of hybrid structures proves to be rather difficult up until now, since all three aspects (design, process, and material) have essentially to be taken into account in a fully integrated perspective. In this regard, current approaches by Kleemann et al. [11] (CPM/PDD based extended mapping matrices identifying strategies to develop multi-material components), Lauter [12] (modular layout to conceptually design hybrid structures correlated to design guidelines and planning of manufacturing processes) and Ashby et al. [13] (more detailed view on technical dimensioning of sandwich, foam as well as lattice, and straightforward segmented structures) present initial procedures, even though they do not give any technical, economic and ecological evaluation and ranking possibilities or suggestions for selecting a most-beneficial component design compared to conventional (monolithic) solution alternatives with regard to the respective application case and its individual weighting of prioritizations.

Against this inadequate background in the scientific state of the art, the fundamentally developed framework of an integrated cross-component lightweight and material-oriented development (IC2-LMOD) with a central view on the joint section design [1,2] is extended by a methodological potential analysis and design of hybrid structures, at first on the component-specific side (see Fig. 1). In doing so, and originating from the basic engineering idea of a gradually guided system analysis (clarification and functional conception), the structurally ingenious extension directly steps into the initial screening of diverse but equally potential lightweight engineering concepts (component pre-design / *gray marked section*). Following a modular procedure, an investigation of categorically expedient (design) layouts and materials of one individual component (of the composed subsystem or system) is carried out first regarding its assignable or rather operating loads and space. As a result, for example, sandwich structures are subject to a more detailed examination in the following design scheme if the available installation space is reduced to a (flat) plate design while forces are limited to predominant bending. Second, the basic material layout takes place, where the conventional (monolithic) component pre-design keeps – to a certain extent – a reference to the strategic hybrid design. Consequently, the multifarious dimensioning of previously determined, individual concepts is provided by its technical feasibility and weight (primary key performance indicator) in a first instance. Based on a set-based compilation of the lightest alternative solutions of each eligible structural family (monolithic, segmented hybrid, and sandwich layout), finally all well-thought-out solutions are holistically assessed according to technological, economic and ecological criteria including local prioritizations of each attributes (e.g., specific manufacturing challenges). In the end, an overall

ranking indicates the potentials of hybrid concepts compared to conventionally monolithic solutions globally depending on the company's strategic focus ("green image") or customer-oriented demands (significance of cost in compact cars vs. premium and luxury segment). A more detailed process planning and cost optimization ensuing increased efficiency need to be tackled hereafter while, on the one hand, successful proposals from previous projects will be evaluated, and on the other hand, currently gained knowledge get documented to prevent similar challenges in future, at the same time.

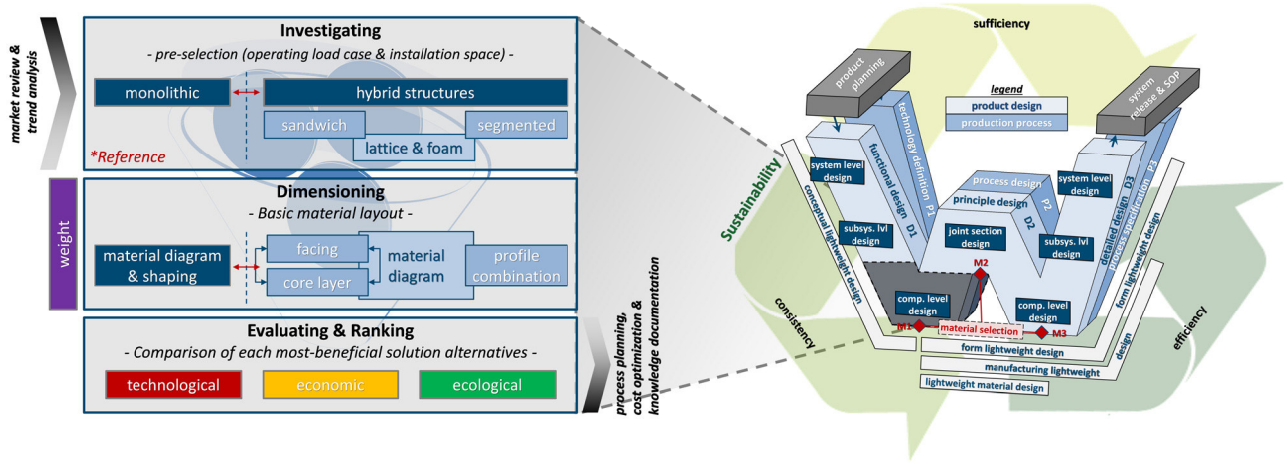

Fig. 1: IC2-LMOD methodology extended by potentials of designing hybrid structures

3. HYBRID LIGHTWEIGHT DESIGN AND RANKED ASSESSMENT

Focusing on the hybrid lightweight design of structural components with a needed cross-sectional study, the procedure to gradually adjust the geometry of segmented solutions (e.g., rectangular hollow sections with two oppositely reinforced plates from FRP or high-strength steel) is depicted in Fig. 2. An approximately same methodology may be performed also with regard to sheet shaping sandwich structures including the implementation of lattice and foam compositions for both hybridization classes.

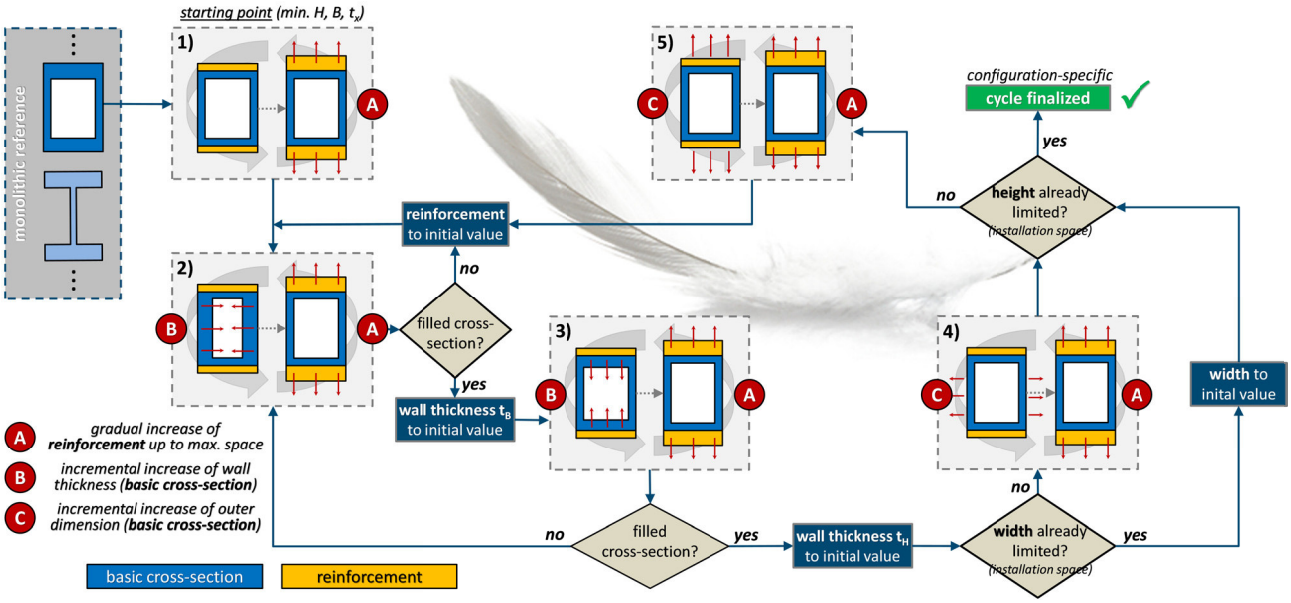

Fig. 2: Procedure for geometry variations of hybrid-segmented structures

As shown in Fig. 2, the basic and most appropriate cross-sectional layout(s) originate from an initial estimation as a function of the relatively weighted, for example, 30 percentage torsional and 70 percentage bending load associated with its available dimensions, which continuously is getting successively adjusted with the interacting reinforcement attempts. In this case, the variation cycle starts with the material-driven reference geometry of the basic monolithic dimensioning and then proceeds with the schematically shown procedure (mutually sensitive wall thickness variations) up to the final hybrid concept for the given (multi-dimensional) load case and installation space with regard to a simultaneously strength and stiffness-limited lightweight design of a specific configuration. Coming up with an optimized solution, further favorable compositions of different design layouts and/or choices of material pass through the process. In doing so, the hybrid-segmented design is not just limited to singular profiles with layered facings made of various materials as illustrated in Fig. 2, but also concerning multifaceted profile-reinforced structures.

Finally, the individually best (by weight), distinguishable (by structure or material) solution alternatives are comparably assessed by further technological (e.g., possibility for serial production), economic (e.g., material cost) and ecological (e.g., primary energy consumption) attributes. Ranked by a globally customized prioritization of the four main criteria of technological, economic, ecological and lightweighting feasibility as well as performability, the holistic potentials of hybrid concepts regarding a specific application case can be tabularly identified in direct comparison to exclusively monolithic solutions, and hence the considerably monetary and non-monetary effort estimated (e.g., in terms of the additionally needed join-ability aspect of its individual materials in hybrid layouts). Accordingly, the transparent assessment of all lightweight concepts is brought to the next level enabling a speedier application and implementation of hybrid concepts.

4. DISCUSSION AND OUTLOOK

Starting from a broad range of scientific approaches to cover lightweight design as such or systematically helps to find the most-beneficial choice of material particularly in terms of hybrid structures, this contribution stresses the need for a technical, economic and ecological potential analysis of designing hybrid material components relating to the early conceptual stage of product development. Thus, an extension of the underlying IC2-LMOD framework including a procedure for geometry variations of hybrid-segmented structures is demonstrated. At this point, the currently still manually (step-by-step) practiced procedure to variate, analyze and optimize the complex and interrelated issues in finding hybrid concept solutions is now being steadily transformed into a numerically (mathematically not solvable with Lagrangian analytical mechanics for a weight-optimized material distribution of symmetrical/asymmetrical profiles) multi-criteria decision-making approach, analogous to the already happened calculation of monolithic alternatives [2]. The main challenge here lies in the even bigger diversity of reciprocal parameters (multi-segmented layout) on top of the iteratively double or multiple inclusion of assorted material properties (several materials, keyword: *composite beam* [14]) within the sophisticated algorithm cycle. A subsequent validation of the extended methodology is ultimately targeted, for example, for a body-in-white section of the automotive industry [15].

Notwithstanding the above, furthermore the original idea of the IC2-LMOD methodology regarding cross-component aspects (e.g., component 1 + joining + component 2) has additionally to be focused, since hybrid structures may possess more extensive challenges in its local (component-related) and global (subsystem-related) joint section design taking into account a concurrent determination of most-beneficial joining technologies of all adjacently defined components. Moreover, the multi-cross-dimensional and multi-criteria decision analysis (MCD²A) of a fully assembly line with its material throughput and utilization rates, cycle times, and much more faces a new challenge [16]. Thus, the development of a utility-based software tool supporting the engineer with all these complex and correlated concurrent considerations is getting more and more indispensable, as initially proposed in [17].

REFERENCES

[1] J. Kaspar et al., “Cross-component systematic approach for lightweight and material-oriented design”, DS 85-1 Proceedings of NordDesign 2016: 2016, pp. 332–341.

[2] J. Kaspar et al., “Integrated cross-component lightweight and material-oriented development methodology – The embodiment design cycle”, Procedia CIRP, 2018; 70: 481–486.

[3] M. F. Ashby, *Materials selection in mechanical design*, 4th ed., Butterworth-Heinemann: 2011.

[4] Granta Design Ltd. CES Selector, version 15.10.8: 2016. www.grantadesign.com

[5] K. H. Illgner, “Werkstoffauswahl für den Konstrukteur”, *VDI-Z,* 1979; 121 (10): 1027–1030.

[6] G. E. Dieter, *Engineering design: a materials and processing approach*, Mc-Graw-Hill: 1983.

[7] M. F. Ashby, “Materials and shape”, *Acta Metallurgica et Materialia*, 1991; 39(6): 1025–1039.

[8] P. M. Weaver et al., “Material limits for shape efficiency”, *Progress in Material Science,* 1997; 41: 61–128.

[9] D. Pasini, “Shape transformers for material and shape selection of lightweight beams”, *Materials & Design,* 2007; 28: 2071–2079.

[10] M. F. Ashby, “Selection strategies for materials and processes”, *Materials & Design,* 2004; 25: 51–67.

[11] S. Kleemann et al., “A methodological approach towards multi-material design of automotive components”, *Procedia CIRP*, 2016; 60: 68-73.

[12] C. Lauter, *Entwicklung und Herstellung von Hybridbauteilen aus Metallen und Faserverbundkunststoffen für den Leichtbau im Automobil*, Dissertation, Universität Paderborn: 2014.

[13] M. F. Ashby et al., “Designing hybrid materials”, *Acta Materialia*, 2003; 51(19): 5801–5821.

[14] E. J. Sapountzakis, “Nonuniform torsion of multi-material composite bars by the boundary element method”, *Computers and Structures,* 2001; 79: 2805–2816.

[15] J. Kaspar et al., “Systemeffizienter Hybridleichtbau – Ein technischer, wirtschaftlicher und ökologischer Potenzialvergleich im Anwendungsfeld Karosseriebau”, *16. Gemeinsames Kolloquium Konstruktionstechnik*: 2018, submitted.

[16] S. A. Choudry et al., “Concurrent assessment of material and joining technology in lightweight engineering”, *5th International Conference on Sustainable Design and Manufacturing (KES-SDM-18)*: 2018, in press.

[17] J. Kaspar et al., “Concurrent and geometry-dependent selection of material and joining technology – an initial utility-based systematic decision-making tool”, *The 12th Annual IEEE International Systems Conference (SysCon)*: 2018, pp. 767–774.

Symposium *Lightweight Design in Product Development 2018* (LWD-PD18)
Zurich, Switzerland, 14th–15th June 2018

REQUIREMENTS FOR EXPERIMENTAL VALIDATION TO ANALYZE THE BUCKLING OF UNSTIFFENED CFRP CYLINDERS

Tobias S. Hartwich[1], Jan Oltmann[1] and Dieter Krause[1]
[1]Hamburg University of Technology, Institute of Product Development and Mechanical Engineering Design, Germany.
tobias.hartwich@tuhh.de, j.oltmann@tuhh.de, krause@tuhh.de

1. INTRODUCTION

Thin and unstiffened cylinder shells made of carbon fiber reinforced plastics (CFRP) are structural components used in aerospace engineering. One recent prominent example is the Falcon 9, which has such a cylindrical interstage between the first and second stage made of composite materials [1]. Because of their high radius-thickness-ratio the critical failure is buckling. At the same time in aerospace engineering there are high weight and safety requirements which increase the need for precise and non-conservative knockdown factors.

Today, the prediction of the critical buckling load follows NASA design guidelines developed in the 1960s [NASA SP-8007] by deterministic design procedures using empirical knock-down factors based on test of metal structures with different boundary conditions [2]. However, for these structures there exist a high number of uncertainties. These include geometric [3, 4] and load imperfections [5], introduced disturbances during manufacturing and mounting as well as material and model uncertainty [6]. Therefore, with a deterministic design approach the level of safety is not possible to quantify and it leads to conservative designs for composite materials. New approaches have to be developed and requirements for experimental validation and numerical prediction of buckling loads have to be specified.

2. REQUIREMENTS FOR TESTING

So-called shim tests were carried out by Hühne where shims of different sizes placed at various positions between the cylinder and the test rig. Depending on the positions and sizes of the shim he shows that the buckling loads decreases. For instances, a 0.4 mm thick shim reduces the buckling load up to about 27% [5]. Kriegesmann computes that a small deviation of 0.009° from the ideal angle of load introduction reduces the buckling load up to 17% [7]. In [4] it is also demonstrated by Schillo that the geometrical imperfection have much smaller influence than load imperfections. Therefore, especially the testing on the multiaxial hexapod test rig have to be analyzed based on previous results in order to reduce undesired lateral forces on to the cylinders. Previously test on this test rig showed high lateral forces in a magnitude of 4.0 % to 6.2 % of the buckling load [4].

However, the measurement of geometric imperfections and other disturbances like small deformations introduced during the mounting process have to be considered. These geometric deformations are able to be determined with optical measurement systems like the ATOS-System. Material parameters, like the fiber volume ratio, fiber orientation or the Young-Modulus have to be determined by coupon tests and resected samples of the cylinder. If all impact factors and their distributions are known they can be taken into account for the model. Finally, with experimental data from the buckling test the quality of the model prediction and a level of safety can be calculated.

3. EXPERIMENTAL TESTING

The cylinders are clamped in a fixture developed by Schillo [4]. This fixture reduces the introduced geometric imperfection and stresses through the mounting process. Before and after the mounting the cylinders are measured by an ATOS-system to determine the fest-fit radius and form deviations. These data will be used for modelling the cylinders.

The buckling test are carried out on the hexapod test rig of the TUHH. The Hexapod test rig is a 6D movement platform to execute static and dynamic tests. The control system of the test rig now enables multi axial static tests that can be displacement and load controlled as well as in a hybrid mode that allows an independent choice of the control in all 6 dof. For the buckling tests this control system enables different test procedures compared to 1D-buckling tests to reduce lateral forces. The differences of displacement control and load control on the lateral loads in x- and y-direction are investigated.

In Fig. 1 the experiment set up is shown. The bottom of the clamping is fixed with screws on a 6-dof-load cell is placed. So that, existing lateral forces can be measured. The load introduction is realized by a centered 1-dof-load cell which is connected to the cylinder through a ball and socket. Furthermore, the displacements are measured internally in all direction. For crosschecking the displacement in axial direction is measured with an external optical sensor, either.

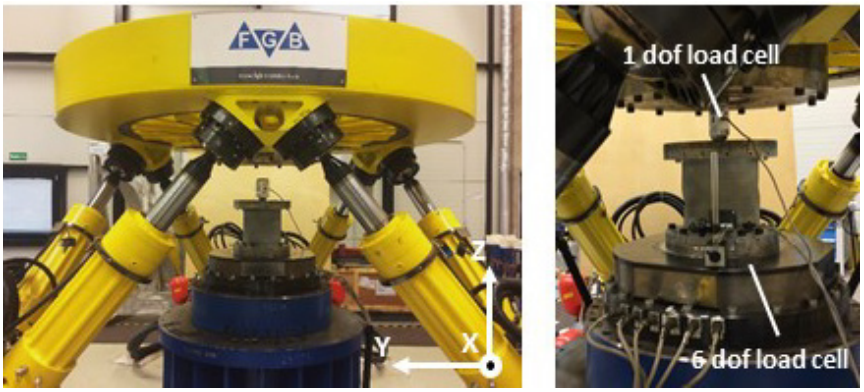

Fig. 1: Mounted cylinder in the Hexapod test rig

Five tests are carried out. In Table 1 the overview of the control parameters of the test are shown. The tests are executed as a hybrid and displacement controls. Because of the decrease of buckling load between the first and second hybrid-controlled test this test is repeated twice.

Table 1: Control mode of the experiments

	Translation			Rotation		
Test	x	y	z	x	y	z
1,2,3	Force controlled	Force controlled	Displacement controlled	Angle controlled	Angle controlled	Angle controlled
4,5	Displacement controlled	Displacement controlled	Displacement controlled	Angle controlled	Angle controlled	Angle controlled

4. TEST RESULTS

For the test an already used cylinder from Schillo [4] is used. In [4] a buckling load of 55.4 kN was reached. This test was carried out with a three-dimensional displacement-controlled method. Therefore, the actual tests are only carried out to investigate qualitatively the influence of the control system on the lateral forces.

In Fig. 2 the test results are shown. In radial direction the displacements and moments are added vectoral to one value. The first three experiments are carried out with a hybrid control. The lateral forces are up to the buckling almost zero. Indeed, the radial displacements increase with the axial displacement. From first to the second experiment the buckling load decreases from 56.62 kN to 43.93 kN. The buckling load from the second and third experiment reduces to 39.17 kN. The fourth and fifth are carried out with a displacement-control. There were very small radial displacements. But the lateral force increases before the buckling up to 1,76 kN and 1,37 kN. The buckling load is with 41,52 kN and 42,11 kN in the same range as the second and third hybrid-controlled tests. A real comparison of the these test under different conditions is not meaningful because the cylinder was already damaged from previous experiments from Schillo where delamination during the buckling occurred [4]. However, buckling loads in the same order are achieved.

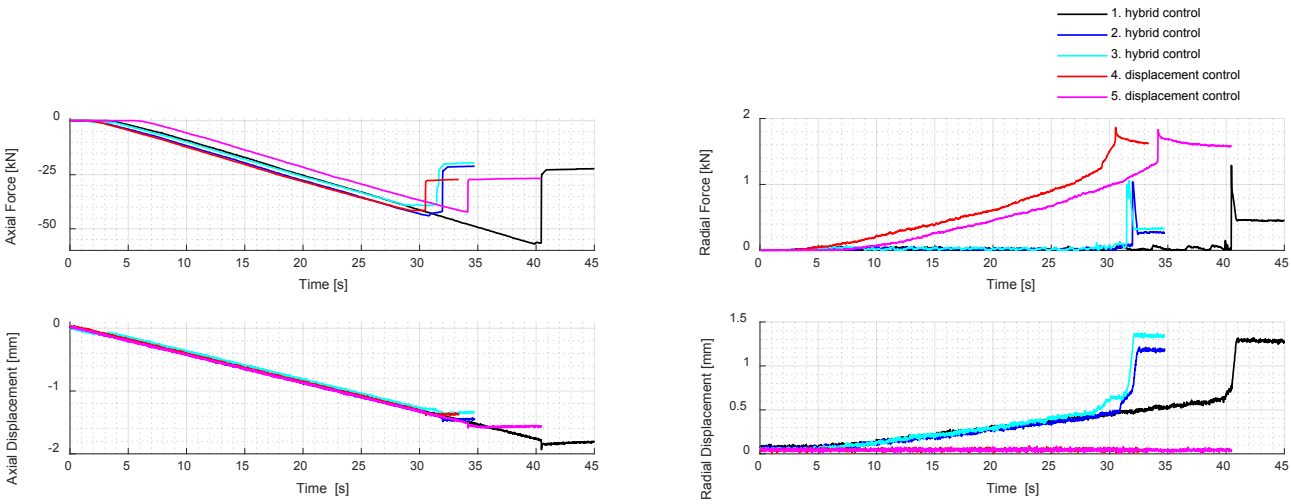

Fig. 2: Measured forces and displacements

The occurrence of the radial displacement in the hybrid-controlled tests can be interpreted as a centering of the cylinder. Due geometric imperfection the cylinders might not be able to center perfectly in the clamping. Furthermore, as a result of a fixturing the cylinders clamping with screws in the test rig the fixture is not completely centered in the test rig. However, theses radial displacements can also be a correction of other imperfections which effect the buckling load and have to take into account. This has to be further investigated.

5. CONCLUSION AND OUTLOOK

The requirements for experimental validation and numerical prediction of buckling loads are presented. One developed measure against lateral forces was applied with the hybrid control of the hexapod test rig. With a hybrid control the lateral force can be reduced. But one drawback is the increase of the radial displacement. This radial displacement can be interpreted as centering of the cylinder. Further investigations have to discuss this effect and which test method - the displacement control or the hybrid control - is closer to the real application.

5. ACKNOWLEDGEMENT

This research was funded by the German Research Foundation (DFG).

REFERENCES

[1] SpaceX, *Homepage Falcon 9,* 2017, http://www.spacex.com/falcon9.
[2] J. P. Peterson et al., *NASA SP 8007 - Buckling of thin-walled circular cylinders,* 1968. Hampton, VA, United States.
[3] W. T. Koiter, "The Stability of Elastic Equilibrium"*, Ph.D. Thesis,* 1970.
[4] C. Schillo et al., “Experimental and numerical study on the influence of imperfections on the buckling load of unstiffened CFRP shells,” *Composite Structures,* 2015, vol. 131, pp. 128–138.
[5] C. Hühne et al., “Sensitivities to geometrical and loading imperfections on buckling of composite cylindrical shells,” *Proceedings - European Conference on Spacecraft Structures, Materials and Mechanical Testing,* 2002.
[6] C. Schillo et al., “Reliability based calibration of safety factors for unstiffened cylindrical composite shells,” *Composite Structures,* 2017, vol. 168, pp. 798–812.
[7] B. Kriegesmann, "Probabilistic Design of Thin-Walled Fiber Composite Structures", *Ph.D. Thesis*, 2012, Hannover.

Symposium *Lightweight Design in Product Development 2018* (LWD-PD18)
Zurich, Switzerland, 14th–15th June 2018

DURABILITY ANALYSIS OF CO-CURED REINFORCED POLYMER – ALUMINUM INTERFACES

Georgios Pappas[1], John Botsis[2]
Ecole Polytechnique Fédérale de Lausanne (EPFL), LMAF, STI, Lausanne, CH-1015 Switzerland.
[1] georgios.pappas@epfl.ch
[2] john.botsis@epfl.ch

1. INTRODUCTION

The current demand for strong yet stiff and lightweight structural components in transportations and civil structures has been rapidly increasing primarily due to the common objective of energy saving for environmental and economic aspects. Moreover, bioengineering and biomechanical applications demand production of tailor specific components with optimal specific stiffness and strength similar to natural materials and living tissues. To this end, fiber reinforced polymers (FRPs) offer several advantages in the design of modern structures. Nevertheless, the low hardness of FRPs restricts their use in machine elements and structural components with inevitable demanding contacts such as bearings, joints, gears etc. In the quest of optimal design, complicated parts consisting of hybrid material pieces are recently designed and used in high end applications such as aerospace, automotive, sports, etc. Commonly mechanical locking of combined multi-material parts is favored, avoiding bonded interfaces wherever possible. The reason for the latter is the difficulty in robust characterization of adhesively bonded interfaces and the number of parameters that affect the durability of the resulted joint such as material nature, mechanical and chemical surface treatment, surface purification and curing conditions [1] etc. The amount of mentioned parameters provides a wide range of tensile and shear strengths from a couple to hundred MPa, while fracture toughness can vary from ten to a couple of thousand J/m^2 depending also on fracture mode and mode mixity [1, 2]. While the shearing and tearing critical fracture resistance is reported always higher than the corresponding mode I toughness, the equivalent shear strength can be higher, lower or of the same range with the analogous tensile strength.

FRPs can be jointed with metallic, ceramic or polymeric pieces to form hybrid material parts. The FRPs pre-cured before the joint is created necessitating mechanical (bolting or riveting) or adhesively bonded joint or they can be co-cured with the counterpart, as it is done for example in the production of sandwich beams or GLARE™. The co-curing process has the advantage of the single fabrication step; however it requires thorough preparation and includes potential effect of residual stresses as well as lower modularity. Nevertheless proper design can lead to elimination of stress concentrators which coupled with geometry optimization result in higher weight gain.

The purpose of this study is to investigate the feasibility of a hybrid FRP-aluminum structural component of a robotic exoskeleton. The investigation of the concept involves durability analysis of the global structure and its correlation with the local stress state of the created polymer-aluminum interface. Parameters such as functionality, material, processing and geometry are taken into consideration. The durability of the resulting interface is evaluated by means of interface strength and multi-mode fracture toughness. To conduct the feasibility analysis, strength and fracture testing are conducted and combined with pertinent systematic FE simulations involving cohesive contact modeling. Preliminary results show that the effect of residual stresses due to the co-curing process governs the durability of the created joint. To reduce their effect, the local compliance of the multi-material components is altered along with modification of the aluminum parts' local geometry.

2. CONCEPT DEFINITION AND METHODS

Component Characteristics and Definition of Constrains

The analysis reported herein refers to an element designed to replace an existing hip bracing component of the *VariLeg* lower limb exoskeleton (see Fig. 1(a)), developed by pd|z and RELab, ETHZ [3]. This hip component has to support the weight of the patient, house the gait actuation motor and connect the two leg supports with each other. Thus, it is the core of the exoskeleton subjected to combined bending and torque moments while connecting the moving parts with the human hip and pelvis. The substitute component results from a pioneer design of aluminum-carbon fiber reinforced polymer (CFRP) co-cured part, developed in collaboration with pd|z and CMASLab. The manufacturing concept comprises manual stacking of prepreg CFRP layers in a quasi-iso layup, on a disposable molding polymer core created by additive manufacturing and the aluminum component/housing of the actuation motor (see Fig. 1(b)). The created piece is cured using standard autoclave procedures at maximum curing temperature of 80°C and the major part of the inner polymer core is discarded after cycle's end. This process allows for a lightweight and at the same time patient specific part to be created, improving the adaptation time and experience of the patient.

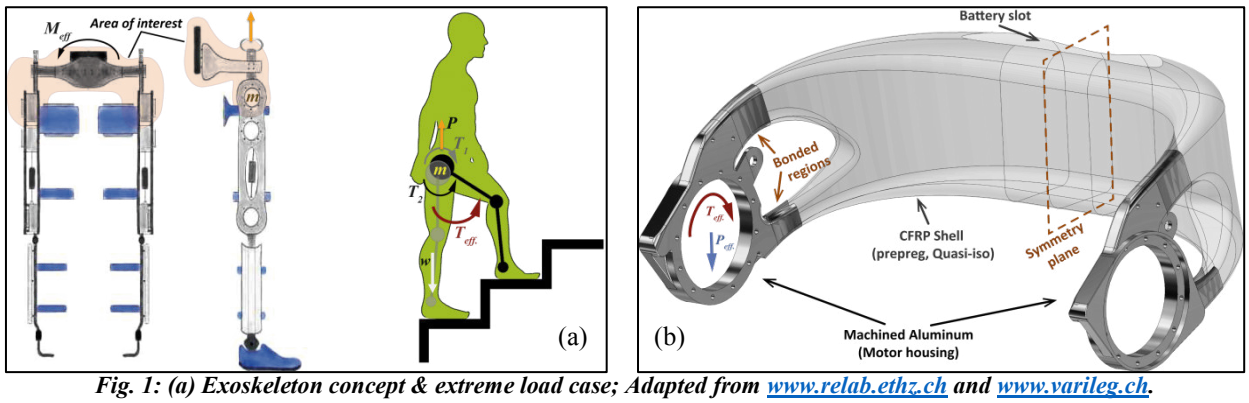

Fig. 1: (a) Exoskeleton concept & extreme load case; Adapted from www.relab.ethz.ch and www.varileg.ch.
(b) Hip component advanced design; initial input.

Numerical Scheme

In order to evaluate the stresses developed in the bonded Aluminum-CFRP region, a numerical model is built in Abaqus Standard v6.12 [4], with the aluminum part discretized using 3D linear tetrahedral elements (Abaqus C3D4) and the CFRP structure with linear quadrilateral, shell elements with reduced integration (Abaqus S4R) and assuming 2mm thickness. The two parts are connected using contact pairs with cohesive interaction properties in the bonded surfaces. The traction separation relation's linear stiffness coefficients are set to default penalty values (10× the stiffness of the involving elements). In these preliminary design optimization stages, no damage parameters are implemented, since the durability of the interface is evaluated with a strength criterion. Typical linear elastic isotropic material properties are considered for the aluminum domain, while quasi-iso ($[0/90, \pm45]_{xs}$) laminate orthotropic properties are considered for the composite shell region, based on the chosen CFRP material (woven cross-ply, cured-ply thickness ~0.19mm, SIGRA TEX PREPREG CE 8201-200-45S). The symmetric case is only considered for this model while an effective extreme moment (M_{eff}) and normal force (P_{eff}) (Fig. 1(b)) are applied in the center of hip actuation motor's position. These extreme loads are developed during the stair-climbing and were measured in-situ by the Laboratory for Mechanical Systems Engineering, EMPA and correspond to 245 Nm and 300 N respectively. Moreover, a temperature difference of -60°C is implemented to simulate the thermal shrinkage of the co-cured part, using the corresponding thermal expansion coefficients for each used material. The described model is solved in consequent iterations by optimizing the local geometry and the interphase material, by considering an auxiliary adhesive layer, minimizing the resulted normal and in-plane shear tractions on the bonded surfaces.

Experimental Scheme

As it has been already mentioned the strength and toughness of polymer-metallic interfaces vary significantly and depend on various details. For this study the aluminum surfaces are treated with sandblasting, grit removal with abundant water and degreasing with alcohol and finally pure acetone, as such processes are demonstrated to enhance durability of such bonds. As it will be discussed later, an adherent epoxy layer promotes the durability of the joint, thus the critical interface to evaluate is of aluminum-epoxy. In order to measure the shear strength of the interface, double shear lap (DSL) specimens are fabricated and tested following the ASTM standard [5], while butt joints are planned to measure the equivalent normal strength. Double cantilever beam (DCB) specimens based are fabricated and tested based on the ISO standard [6] to evaluate the mode I fracture toughness while mode II tests are already in process.

3. RESULTS AND DISCUSION

Preliminary Analysis

The preliminary numerical results show that the thermal stresses due to the cool-down step account for ~ 80% of the interface tractions at the extreme load conditions, which for the initial design are comparable with the strength of an ordinary epoxy, with some even higher peaks observed on the transition points, as depicted in Fig. 2. The reason for those high tractions is the important thermal expansion coefficient mismatch, since the one of the CFRP (in-plane) is one order of magnitude larger than that of aluminum ($2.2e\text{-}6°K^{-1}$ vs. $2.4e\text{-}5°K^{-1}$). Thus, the designed geometry is expected to fail right after the end of autoclave's cool-down step, and for this reason further adjustments are proposed.

Design Optimization for Stress Relief and Experimental Results

As explained already the reason of the high interface tractions originates from the higher shrinkage of the aluminum part combined with the high modulus of the CFRP which "resists on" the adaptation of the shell structure. To reduce the later effect an additional more compliant layer of 0.45mm pure epoxy is considered in the FE model which results in a reduction of the maximum shear tractions at ~1/5 and ~ 1/3 on the normal ones. The epoxy is modeled to correspond to the Gurit SA-80 [7] toughened with glass fibers (9% in mass), prepreg epoxy adhesive film, the use of which preserves all the characteristics of the co-curing fabrication concept. Nevertheless, the expected interface tractions after the curing

process and under the extreme loading conditions are still high (>30 MPa), compared also with the DSL preliminary results of the designed interface, shown in Fig. 3(a). As illustrated in Fig. 3(a) the ultimate shear strength is ~33 MPa while the expected yield point is ~22 MPa, with mixed cohesive-adhesive failure. The calculated mode I critical toughness is ~70 J/m^2 and the ultimate one ~270 J/m^2.

To further reduce the stiffness gradient on the bonded regions hollow sections are tested with the FE scheme and additional minor reduction of the developed surface tractions is evaluated. However, some extended areas of high stresses are still present on the curved regions as seen in Fig 3(b) -left-. As depicted in this deformed state due to the thermal cool-down step, the aluminum part that has greater tendency for shrinkage, hence it is blocked from the CFRP shell, especially in the curved corners that its rigidity is higher. Further optimization of the traction profile is obtained by elimination of the curved regions that leads to relaxation of the local locking and the aluminum part can follow the shape imposed by the CFRP shell (see Fig 3(b) -right-). Interestingly, no local weakening of overall hybrid geometry is observed since the part is highly reinforced on the bonding regions that comprises hybrid aluminum - CFRP domains.

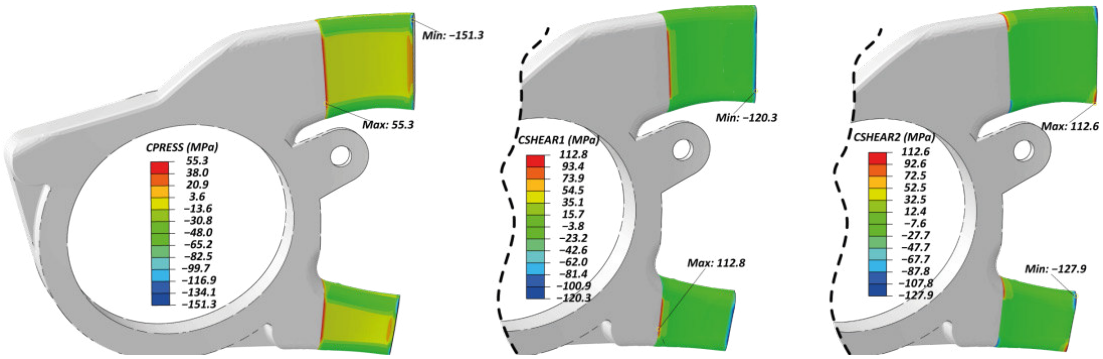

Fig. 2: FE results of cohesive contact stress profile: (i) Normal; negative is in tension, (ii) Shear Vertical (iii) Shear Horizontal.

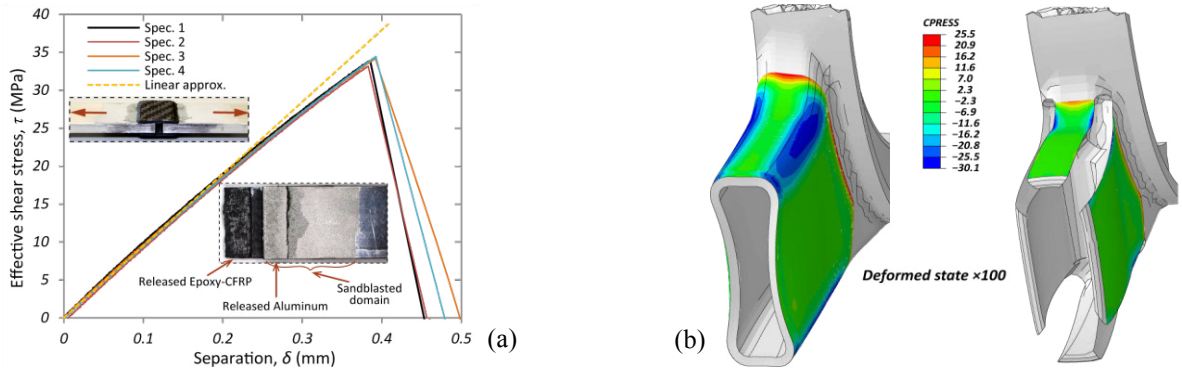

Fig. 3: (a) DSL Stress-separation and fractography in insert. (b) FE results of cohesive contact normal stress profile due to thermal shrinkage (deformations×100).

ACNKOWLEDGEMENTS

This work is funded by the *SFA Advanced Manufacturing* initiative of the ETH Board, under the "*Individualized cost-efficient and sustainable ultra-lightweight structural components"* project. The design of the hip exoskeleton component is developed in collaboration with pd|z and CMASLab, ETHZ in close cooperation with Mr. R. Kussmaul and Mr. M. Biedermann.

REFERENCES

[1] K. Ikegami, T. Fujii, H. Kawagoe, H. Kyogoku, K. Motoie, K. Nohno, T. Sugibayashi, and F. Yoshida, "Benchmark tests on adhesive strengths in butt, single and double lap joints and double-cantilever beams," *Int. J. Adhes. Adhes.*, vol. [6]16, no. 4, pp. 219-226, 1996.

[2] B. F. Sørensen and J. T. Goutianos S., "Strength scaling of adhesive joints in polymer–matrix composites," *Int. J. Solids Struct.",* vol. 46, pp. 741-761, 2009.

[3] St. Schrade, K Dätwyler, M. Stücheli, K. Studer, D.-A. Türk, M. Meboldt, and R. Gassert, "Development of VariLeg, an exoskeleton with variable stiffness actuation: first results and user evaluation from the CYBATHLON 2016, " *J. Neuroeng. Rehabil.*, vol. 15, pp. 1743-0003, 2018.

[4] © Systèmes Dassault, *Abaqus Analysis User's Manual (v6.12)*.: Dassault Systèmes Simulia Corp, 2012.

[5] ASTM Standard D3528 − 96, *Standard Test Method for Strength Properties of Double Lap Shear Adhesive Joints by Tension Loading*. West Conshohocken, PA, United States of America: ASTM International, 2016.

[6] ISO 25217, *Adhesives-Determination of the mode 1 adhesive fracture energy of structural adhesive joints using double cantilever beam and tapered double cantilever beam specimens*, 1st ed. Geneva, Switzerland: ISO Standard, 2009.

[7] Gurit SP™. (2017, July) SE 80, toughened prepreg epoxy adhesive film. General datasheet. [Online], http://www.gurit.com.

Symposium *Lightweight Design in Product Development 2018* (LWD-PD18)
Zurich, Switzerland, 14th–15th June 2018

MODELING OF TRANSVERSE SHEAR BEHAVIOR IN CORRUGATED LAMINATES

Daniel T. Filipovic[1], Gerald R. Kress[2]
[1]ETH Zurich, Switzerland. fidaniel@ethz.ch
[2]ETH Zurich, Switzerland. gkress@ethz.ch

1. INTRODUCTION

Corrugated laminates have been discussed as candidate materials for morphing wing applications lately since they show highly anisotropic stiffness properties [1]. They can reach high bending stiffness values about the direction of corrugation, whereas the extensional compliance in the same direction is rather low. This has given rise to the publication of various models for the calculation of their homogenized structural properties in research in the last years (e.g. [2]).

An interesting remaining question is the behavior of corrugated laminates under transverse shear loading. As in sandwich structures, a lot of material may be located away from the bending-neutral-axis. This leads to excellent bending stiffness properties; however, transverse shear compliance is expected to have a considerable influence on the total deflection of the laminate under transverse load [4]. We have therefore developed an efficient finite element model, which is able to calculate the behavior of corrugated laminates under transverse shear loading [5]. The computational cost is very low, since the model requires a planar mesh only. The underlying theory is generally valid and can be applied for the calculation of shear effects in cross-sections of any shape.

2. MODELING APPROACH

The following considerations are based on the model presented in [5]. If a composite plate or beam is loaded with a transverse shearing force, the resulting bending moment will vary linearly in out-of-plane direction, which is equivalent to a linearly varying curvature. We select a coordinate convention where the cross-section lies within the y-z-plane, therefore x refers to the out-of-plane direction.

$$\kappa_{xx} = \kappa'_{xx}(x - b) \tag{1}$$

Eq. 1 describes the linear variation of the curvature, with κ'_{xx} being a parameter and b the total length of the laminate. The aforementioned concepts can be further elaborated in order to obtain the general form of the displacement field – here presented in matrix notation:

$$\boldsymbol{u}(x, y, z) = \hat{\boldsymbol{u}}(x, z) + \boldsymbol{X}_0(y, z) \tag{2}$$

The contribution $\hat{\boldsymbol{u}}$ in Eq. 2 is known a priori and can be understood as load information term. It contains deformation modes pertinent to the given load case and is thus dependent on the parameter κ'_{xx}. The unknown contribution $\boldsymbol{X}_0$ describes cross-sectional warping caused by the shearing force. Since the latter is constant in every cross-section, the respective displacement field component does not depend on the out-of-plane coordinate x.

The finite element formulation of Eq. 2 can be derived using the principle of virtual displacements:

$$\int \delta \boldsymbol{X}_0^T \left[\boldsymbol{L}^T \overline{\overline{\boldsymbol{C}}} (\boldsymbol{L}\hat{\boldsymbol{u}} + \boldsymbol{L}\boldsymbol{X}_0) \right] d\Omega = 0 \tag{3}$$

The linear operator $\boldsymbol{L}$ in Eq. 3 is used to calculate the strains from the displacements whereas $\overline{\overline{\boldsymbol{C}}}$ is the stiffness matrix used in Hooke's law. Eq. 3 still represents a strong form; in order to obtain the weak variational form with respect to $\boldsymbol{X}_0$ integration by parts needs to be applied.

Since $\boldsymbol{X}_0$ does only depend on the spatial coordinates and the linear operator is applied to the load information term twice, the resulting system of equations for the finite element formulation does not depend on the out-of-plane variable x any more. Therefore, a planar mesh only is needed in the finite element routine with the planar elements possessing three displacement-degrees-of-freedom. Hence, the given three-dimensional problem has been reduced to a quasi-two-dimensional problem.

3. RESULTS

For illustrating the behavior of corrugated laminates subjected to transverse shear loading, some peculiar shear stress distributions are shown. They were derived for the case of a [0°] carbon composite corrugated laminate with four layers and a half amplitude of $h = 25$. We use a unit-cell approach in our model; accordingly, the behavior of an extended corrugated laminate is modeled by implementing periodicity boundary conditions at either end of the unit cell. The latter has a width of $p = 100$ in the selected example.

For reasons of simplification, we will use the local xst- instead of the global xyz-coordinate-system. The s-direction is oriented along the mid-plane of the laminate, whereas the t-direction is perpendicular to it and points in through-thickness-direction. Therefore, for the limiting case of a plate, the two coordinate systems are identical. Note also that the following plots do not show the element-wise stress values but show – more accurately – the distribution at the optimal stress points of every element. Positive stress values are shown in yellow-red, negative values in cyan-blue and vanishing stresses in white.

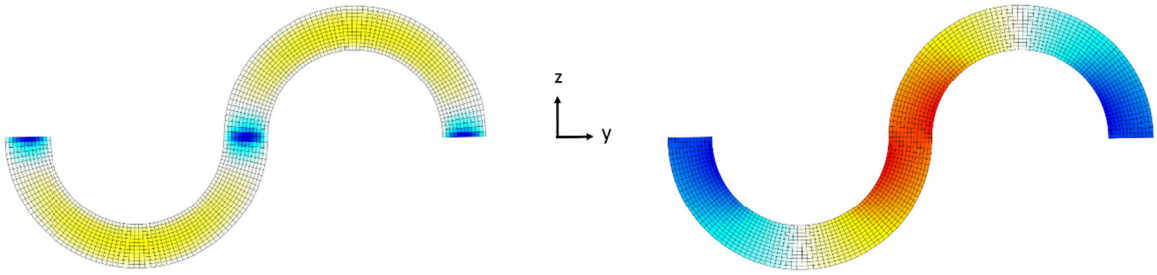

Fig. 1: τ_{xt} (left) and τ_{xs} (right) shear stress distributions.

The stress distribution in Fig. 1 on the left corresponds to the τ_{xt} shear stress. The edges of the laminate are traction free, thus highlighting the fact that the model is able to correctly map the natural boundary conditions. The blue shear stress peaks have shown to be characteristic for corrugated laminates. Their intensity is much higher than the τ_{xt} stress values in the rest of the laminate.

The τ_{xs} shear stress distribution can be found in Fig. 1 on the right. The maximum and minimum stress values have the same absolute values and are about one order of magnitude higher than the extremae of the τ_{xt} shear stress.

The previously shown shear stress results have been verified using a conventional finite element software resulting in the identical characteristics as in the presented model. Having obtained meaningful shear stress distributions, it is possible to calculate transverse shear stiffness values for corrugated laminates [5].

The aforementioned theory is generally valid and can be applied to all types of planar cross-sections. Representing a classical example, Fig. 2 shows the characteristic shear stress distributions in an I-shaped aluminum beam subjected to a transverse force in z-direction:

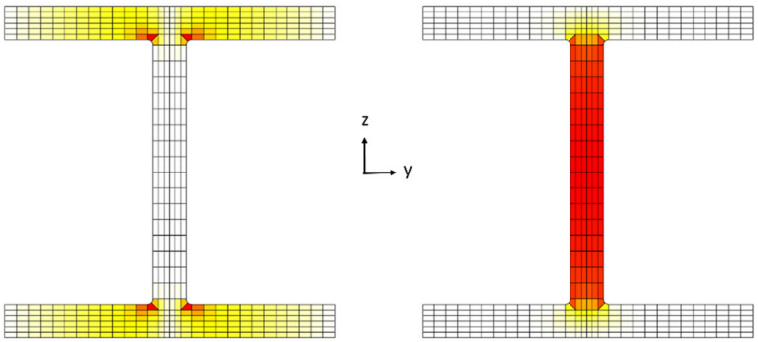

Fig. 2: $|\tau_{xy}|$ (left) and $|\tau_{xz}|$ (right) shear stress distributions.

Also in this example the boundary conditions are respected, furthermore the shear stress distribution coincides well with analytical considerations (linear distribution in flanges, quadratic distribution in web and maximum value at neutral axis).

4. CONCLUSIONS

A finite element formulation for the calculation of corrugated laminates transverse shear behavior has been derived and programmed. The model is able to correctly predict the resulting shear stress distributions in corrugated laminates, independent of dimensions or lay-up. Verification using a volumetric model in a conventional FEM software has shown a very good agreement between the results.

The main benefit of the new program is that it is able to calculate transverse shear effects using a planar mesh only; therefore, the model is very efficient. Hence it well suited for being used for design purposes.

5. ACKNOWLEDGEMENTS

The presented model and results were elaborated in the framework of a project supported by the Swiss National Science Foundation (project no. 169468).

REFERENCES

[1] T. Yokozeki et al., "Mechanical properties of corrugated composites for candidate materials of flexible wing structres", *Composites: Part A.*, 2006; 37: 1578-1586.
[2] G. Kress et al., "Corrugated Laminate Homogenization Model", *Composite Structures*, 2010; 92: 795-810.
[3] G. Kress et al., "Corrugated Laminate Analysis: A generalized plane-strain problem", *Composite Structures*, 2011; 93: 1493-1504.
[4] C. Thurnherr et al., "Highly anisotropic corrugated laminates deflection under uniform pressure", *Composite Structures*, 2016; 154: 31-38.
[5] D.T. Filipovic et al., "A planar finite element formulation for corrugated laminates under transverse shear loading", Submitted to *Composite Structures*, 2018.

Symposium *Lightweight Design in Product Development 2018* (LWD-PD18)
Zurich, Switzerland, 14th–15th June 2018

MODULAR RAPID DESIGN OF MULTI-MATERIAL LIGHTWEIGHT TRUSS STRUCTURES – A NOVEL APPROACH

T. Rathert[1], C. Witzgall[1], S. Wartzack[1],
[1]Friedrich-Alexander-University Erlangen-Nuremberg, Engineering Design, Germany. rathert@mfk.fau.de

1. INTRODUCTION

In lightweight design, the multi-material design is often referred to as hybrid design. The best properties of different materials are combined here. The individual elements each offer a solution, but in addition can achieve optimization in a combined state. Consequently, the design of highly loaded and complex structures is allowed, while at the same time significant weight savings can be achieved. In detail, for each position of the component, the material is used which possesses all the material properties required at this location. Furthermore, the availability and operational capability of the materials as well as their costs become decisive factors. Critical areas are reinforced with high-priced but also more efficient materials. Cheaper materials are used for less important intermediate areas. Of course, the material must meet the requirements of all points of consideration. The respective strengths of the materials can be combined with each other. This allows new materials to be combined with conventional materials. By using a material mix, it is possible to exploit the entire lightweight design potential.

2. PROBLEM STATEMENT AND AIMS

As KLEIN, WITZGALL and WARTZACK have shown by using the example of a bike frame, the composite suitability of framework structures is only given for uniaxial loaded sections. Figure 1 displays the low composite suitability of the connector regions of a bike frame. Due to deflections within the flux of force, the stress state within these areas is (at least) biaxial, which is very unfavorable for composite materials. [1] The observations described for the bicycle frame can be generalized for all sorts of trusses.

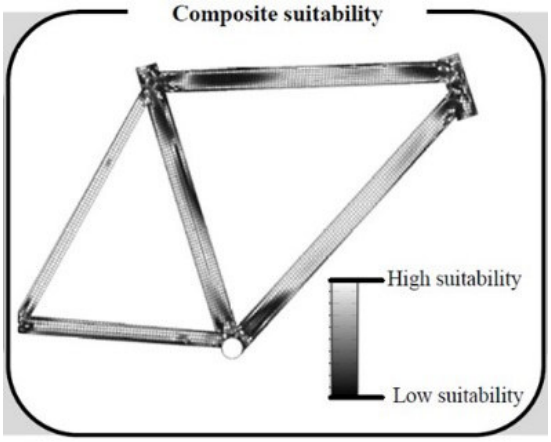

Fig. 1: Suitability of composite material.

For this reason, the aim of this contribution is to show how to simply use the right material in the right place, thus allowing to optimally exploiting their beneficial lightweight properties. To do so, anisotropic composite tubes will be used in sections of uniaxial stresses and isotropic connectors will be utilized to join them.

One further aspect which has to be taken into account are the high development costs of composite products. Modern composite design and manufacturing methods are poorly standardized and their implementation usually causes high costs in design and production. Therefore, a method for the dimensioning and optimization of multi-material lightweight design systems in modular rapid design is to be introduced. This allows the cost-effective development of lightweight support structures based on standardized composite profiles. Using the example of a motorcycle frame, the method will be evaluated and discussed.

2.1 TRUSS TOPOLOGY OPTIMIZATION

Methods for topology optimization can be diversified by definition of design space: continuous structures on the one hand, and discrete structures on the other [2]. The continuous design space, however, is not suitable for the generation of a hybrid structure based on predefined standard profiles and nodes, since the result must be redesigned into a discrete skeleton structure. In general, the optimization of a topology space made up of discrete structures is done via discrete and connected zones. Within these, predefined structure elements can either be selected, inserted or removed by the optimizer. When optimizing a discrete truss structure, the zones of the design space are defined by beams. For this

purpose, e. g. in the process of redundant truss topology optimization (TTRR = TRUSS-TOPOLOGY-ROBUST-REDUNDANT), according to MOHR [3], the points distributed in space are connected by as many beams and as many different variations as possible. Subsequently, the beams that are relevant to the optimum are selected from this basic structure based on the evaluation criteria - typically stiffness and volume. The output of the results then takes place via the information on the cross-section, the start and end point of the selected beams. This means that all required information is available for creating the product's embodiment design in the CAD system.

2.2 INTERPRETATION OF THE OPTIMISED DESIGN PROPOSAL

Although all data are generally available for the geometry generation in CAD, the calculated cross-section values of the truss topology optimization represent continuous nominal values. But there is not always a suitable semi-finished product. For a successful reconstruction in CAD, it is not only necessary to transfer the result data from the TTRR process, but also to perform an interpretation of the result.

For this purpose, the nodes are extracted from the result file and are imported directly into the CAD system by means of an offset coordinate system. Based on this information, a skeletal model can be generated in CAD, on which, in turn, the interpretation can take place. The resulting model initially contains no information about the cross-sectional areas. The cross sections of the individual bars are read from a separate result file and then sorted by size. Since a semi-finished product does not exist for every calculated nominal value, these values must first be interpreted with regard to the permissible semi-finished products and cross-sections. According to discreetly defined limits for the semi-finished products, the cross-sectional values of the result are divided into different classes. The semi-finished geometry is re-dimensioned by using these cross-sectional classes and then synthesized on the skeleton lines in CAD . Finally, predefined parametric node models are adapted according to the generated semi-finished products and installed on the nodes of the CAD model.

As a further advantage, the skeleton-based CAD model allows a direct derivation of a beam FE model that can be used for a post evaluation of the design.

3. CASE STUDY: MOTORCYCLE FRAME

Figure 2 shows the procedure used in this study: first of all, the available design space as well as load cases have to be defined. According to STOFFREGEN [4], the load that is decisive for the mechanical stress of the chassis components are essentially the wheel contact forces and the resulting moments. The largest individual forces occur at the wheel contact point on the front wheel during full braking (wheel contact force or braking force), as the force transmission is based on the limiting case of braking, in which the rear wheel lifts off and the total weight is fully supported by the front wheel.

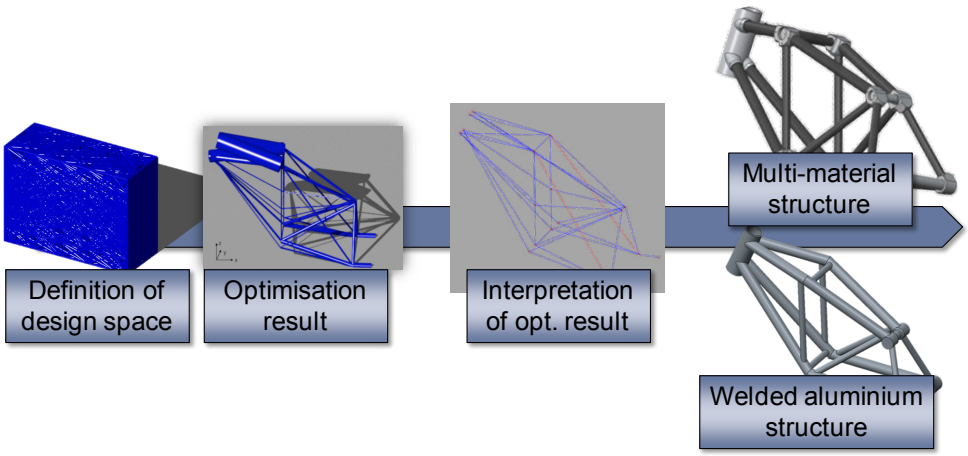

Fig. 2: Design process of modular rapid design

4. COMPARISON: WELDED ALUMINUM FRAME VS. HYBRID FRAME

In this chapter, the two designs presented are compared with each other. The advantages and disadvantages of the two versions are also highlighted. Table 1 quantitatively compares the two designs by means of stiffness and weight. The two designs shown in this work have a relative weight difference of 21.2%, which is achieved by using carbon fiber reinforced plastic and aluminum connectors. It was noted that the interface elements – i.e. the connection tubes for front fork, rear swing arm and spring / damper element - are identical in both designs, so on this basis, no major weight savings occur. However, since the two designs do not have exactly the same stiffness, it is necessary to introduce a comparison value in order to demonstrate absolute comparability. The comparison value is defined as the ratio of the

respective stiffness to the mass. It gives in the respective comparison a statement about what percentage the mixed design improves compared to the welded design in terms of weight with respect to the stiffness properties.

Table 1: Comparison of welded frame and multi-material frame

Type	Welded aluminium frame	Difference	Multi-material frame
Overall mass	12.93 kg	-21.2%	10.19 kg
Longitudinal stiffness	59.95 N/(kg mm)	+24.0%	74.35 N/(kg mm)
Lateral stiffness	19.14 N/(kg mm)	+33.5%	25.56 N/(kg mm)
Torsion stiffness	59.04 Nm/(kg °)	+13.1%	66.76 Nm/(kg °)

When compared to the welded design, the method of multi-material lightweight design (which as a result produces the frame design) can above all score with the weight saving element. With a relative weight saving of 21.2% compared to the welded design, it significantly reduces the weight with almost constant stiffness properties. In this work, tubes made of carbon fiber reinforced plastic were joined together by aluminum connectors, but the adhesive combination hardly limits the material combination. Simple and fast assembly will further reduce production costs.

5. SUMMARY, CONCLUSION

The multi-material lightweight design offers the great advantage of weight reduction by a very considerable amount compared to the aluminum-welded design. The model developed here, still has to undergo experiments in real cases to confirm the results. With the help of the newly developed connectors, it is possible not only to construct motorcycle frames, but also to expand the technique into other fields of application. Possible applications include automotive design and aviation. Depending on the application, the design developed in this work can create a great deal of added value compared to conventional designs such as welded design. With the multi-material design, a novel principle of the connection of pipe designs has been created. As it turns out, it offers some advantages over conventional weldments. Even in comparison with a lightweight design solution (which is already very good solution of the aluminum welding frame), the first elaboration of such a mixed design was convincing. It can be assumed that the shown stiffness values of the frame increase even further by attachments such as the electric motor and the accumulator.

The next step in further developing the new construction method is the transfer of the principle of the connectors and straight semi-finished products into an automated software tool. With the help of defined basic elements, which can be selected similarly to a modular system, the construction of a frame structure can almost be automated. In the basic function, the tool only has to have balls and tubes of various sizes as connector semi-finished products. By defining algorithms, one can also optimize the material removal and weight optimization of the connectors. As an example, the Advanced Framework extension (AFX), which is integrated in CREO, can be used.

In summary, this work serves as a basis for further research and development. On the one hand, we have shown that a demonstrator can be set up, on which experiments can be carried out and the developed connectors can be validated. On the other hand it is possible to create an automated design methodology as an extension for CAD programs.

ACKNOWLEDGEMENT

The authors thankfully acknowledge a funding of the federal ministry for Economic Affairs and Energy (BMWi) and the German Federation of Industrial Research Associations - AiF within the Central Innovation Programme for SMEs (ZIM) under grant number ZF4222610PO8.

REFERENCES

[1] D. Klein, C. Witzgall, S. Wartzack, “A novel approach for the evaluation of composite suitability of lightweight structures at early design stages”, *International Design Conference – DESIGN*: 2014, pp. 1093–1104.

[2] A. Schumacher, *Optimierung Mechanischer Strukturen - Grundlagen und Industrielle Anwendungen,* Springer Vieweg, 2013.

[3] D. Mohr, I. Stein, T. Matzies, C. Knapek, “Redundant robust topology optimization of truss”, *Optimization and Engineering*, 2014, Vol. 15, Nr. 4, pp. 945–972.

[4] Stoffregen, Jürgen, *Motorradtechnik: Grundlagen und Konzepte von Motor, Antrieb und Fahrwerk*, Vieweg + Teubner, 2010.

Symposium *Lightweight Design in Product Development 2018* (LWD-PD18)
Zurich, Switzerland, 14th–15th June 2018

EXAMING LIGHTWEIGHT DESIGN POTENTIAL OF THE HUMAN MUSCULOSKELETAL SYSTEM BY USING THE EXAMPLE OF AN ARTICULATED ARM ROBOT

Marcel Bartz[1], Henning Brand[2] and Beate Bender[3]
[1]Lehrstuhl für Produktentwicklung, Ruhr-Universität Bochum, Germany. bartz@lpe.rub.de
[2]Lehrstuhl für Produktentwicklung, Ruhr-Universität Bochum, Germany. henning.brand-j3s@rub.de
[3]Lehrstuhl für Produktentwicklung, Ruhr-Universität Bochum, Germany. bender@lpe.rub.de

1. INTRODUCTION

In recent years, bioinspired lightweight design has become increasingly important in technology. An important source is the musculoskeletal system, in which lightweight construction is achieved by the interplay of different principles, with the aim of minimizing bending stresses. In addition to a hierarchical bone structure that increases bone strength, the lightweight construction of the musculoskeletal mainly results from the interplay of three principles: minimization of bending loads through tension chording, functional adaptation through bone remodeling, and bending minimized movement control by the sensorimotor system [1].

The biological control and optimization strategies, which describe the interaction of these principles, run simultaneously in nature. Prevailing bionic solutions that use the lightweight design principles neglect the coordinated interplay of these principles. Moreover, transfer is limited to isolated principles, e.g. in the context of structure optimization as simultaneous implementation of bone remodeling processes [2, 3, 4, 5] or the use of tension chords and passive elements to minimize bending [6, 7, 8, 9]. Therefore, further potential for lightweight design can be expected.

Human extremities have kinematic similarities with technical systems that can be understood as open kinematic chains, e.g. articulated arm robots. Using this similarity, the lightweight design potential is investigated by introducing a new bioinspired lightweight design approach in this article. The development process lead to a simulation model. This model resulted from abstracting the aforementioned lightweight principles. To consider the interaction of the principles, the simulation model is implemented by coupling multibody simulation and topology optimization in an iterative process.

2. TRANSFER OF THE LIGHTWEIGHT PRINCIPLES OF THE MUSCOLUSKELETAL SYSTEM INTO THE TECHNICAL DESIGN PROCESS IN A BIOINSPIRED APPROACH

In order to apply the lightweight principles of bending minimization in their entirety to technical systems with similar kinematics to the extremities of the musculoskeletal system, the principle of motion generation must be adapted to that of the musculoskeletal system. Figure 1 shows the possible principles of motion generation for an open kinematic chain that consists of n elements with n joints. In the classical system, an articulated motor with the torque M_i is sufficient for the movement of individual element i. In the musculoskeletal system, the movement of an element is achieved over a variety of muscle forces. To generate movement, there are more forces than necessary, i.e. the system's kinematics is overdetermined. This is known as the redundancy problem of motion generation [1, 10]. According to this, a functional integration takes place, as the muscles allow not only movement but also a minimization of the bending load caused by tension chording. In order to use this for the technology, the operating principle (or the drive) of the technical system must be exchanged as shown in the lower part of figure 1 in the bioinspired system. The movement of an element i is generated by j tensile forces F_{ij}. In the field of biomechanics, mathematical optimization methods are used to determine possible movement forces (in this case muscle forces) [11]. In order to take the principle of bending minimization by means of tension chording into account in the design of technical systems, bending minimization will be included as a further criterion for the bioinspired system as part of the multibody simulation when determining the movement forces.

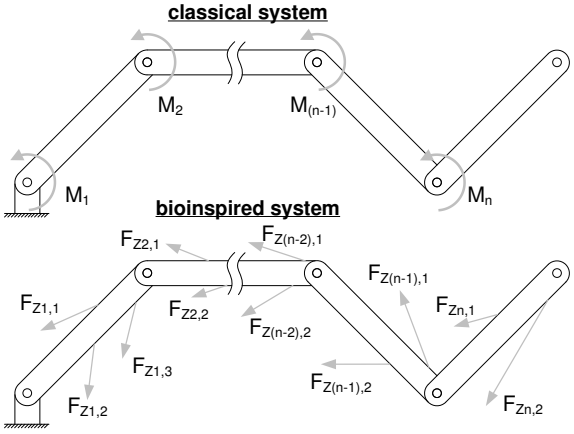

Fig. 1: Operating principle of motion generation: classical system (top); bioinspired system (bottom)

By exchanging the principle of generating motion it is possible to transfer the interplay of the three bending minimizing lightweight principles of the musculoskeletal system mentioned above. The minimization of bending loads through tension chording is realized by the integration of the bending moment minimization in the multibody simulation. The functional adaptation through bone remodeling is implemented by a topology optimization using finite element calculations. The bending minimized movement control by the sensorimotor system is realized by technical path planning. This path planning determines a path in which the bending moments resulting from inertia forces are minimized. The interaction of the three technical transformations of the lightweight principles is not being transferred in accordance to the biological model. Because the control and optimization processes taking place in biology run simultaneously, an exact quantification of the interaction cannot simply take place. For the transfer into the technical design process, a sequential procedure is therefore being used here to map the process in an iterative procedure. This is implemented in a new bioinspired approach for the design of open kinematic chains, shown in figure 2.

The coupling of determining a bending minimizing path via path planning with redundant movement forces is implemented by means of a multi-criteria optimization problem within the framework of multibody simulation. Subsequently, the topology optimization is carried out. In a classical approach, topology optimization is followed by geometry preparation and validation. Contrasting that, the new approach adds a back iteration from topology optimization to multibody simulation. A back iteration is necessary, because both the path planning and the force determination depend directly on the mass and the inertial forces. Both of which change due to the topology optimization. Consequently, the calculation loop must run until the mass no longer changes in order to get an optimal result.

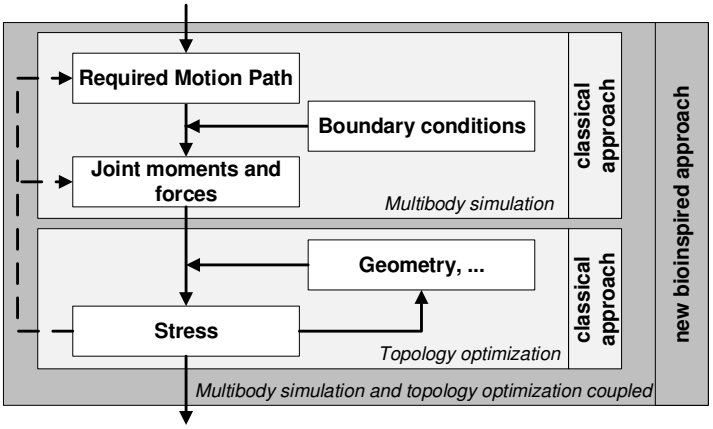

Figure 2: Extension of the classical to a bioinspired approach: The classical approach is supplemented by an iterative procedure by coupling topology optimization and multibody simulation (represented by the dashed arrows)

3. APPLICATION ON ARTICULATED ARM ROBOTS AND DISCUSSION OF THE RESULTS

The new bioinspired approach is applied to an articulated arm robot with two arm segments shown in the left part of figure 4. The aim of the application is to investigate the potential of lightweight construction and to determine advantages and disadvantages that arise by comparing the mass and strain energy of two robots. One robot is bioinspired with several tension chords, the other is a classically developed variant with a joint motor in each joint. Variants are compared in which each arm segment is designed with single, double or fourfold tension chord. The arrangement of the tension chords has been determined according to an algorithm that sets the attachment points in such a way that the integral of the bending moment along the arm segment becomes minimal. Additionally, one tension chord always engages at the end of the segment. The diagrams in figure 3 shows the bending moment curve and the mass and strain energy for the second arm segment in relative units, at a time step with a constant angular velocity.

The comparison shows that the simple system can reduce the maximum bending moment by about 70%. However, due to the inertia forces, further bending remains in the dynamic center of mass. Due to the lack of redundancies, the tension chord cannot influence the bending moment curve any further, but can only minimize the joint torque. A suitable interaction can be found under double tension strapping, which can reduce the maximum bending moment to less than 10% of that of the classical system. A fourfold tension strap can further minimize this moment, but not as much. The diagram shows that the mass of the systems decreases continuously with the number of tension chords. Under simple tension chording the mass is less than 50%, under double tension chording the mass is already less than 20% than the mass of the classical system. The strain energy of the systems under tension chording is below that of the classical system only with double and fourfold tension chording. The reason for this is that the stiffness decreases due to the lighter design. However, a high maximum bending moment remains in the system under simple tension chording, which leads to high deformation. This can only be minimized by means of redundant forces with several tension chords. The diagram does not show that the normal load increases in contrast to the reduction of the bending load. However, despite the increased normal load, this results in a lower mass and overall deformation.

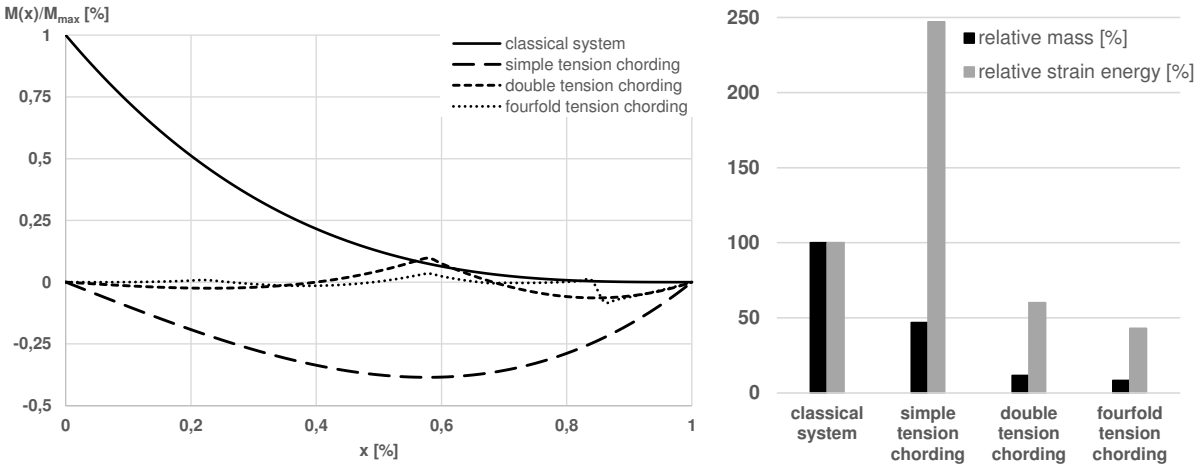

Figure 3: Bending moments along the beam axis of the second arm segment (left); comparison of the mass and strain energies (right)

The middle and right parts of figure 4 show the synthesized structures for the classical system and the system under double tension chording after multibody simulation and topology optimization. The results show that the mass can be reduced by more than 40% for both arm segments due to the bioinspired approach and that compression structures are formed due to the lack of bending stress.

Using an articulated arm robot as an example, the lightweight construction potential for technical systems was demonstrated by transferring the interplay of the lightweight construction principles of the musculoskeletal system. The combination of topology optimization and bend-minimized determination of movement force by means of tension chording can lead to a system with reduced mass by using an iterative method. This is countered by the disadvantages resulting from the exchange of the operating principles of the drive. Due to the increased elasticity of the form-fit driving tension chords, an expansion slip occurs when the force is applied, which the joint motors in the classical system do not exhibit. This results in a fundamentally different and more complex dynamic control and response behavior. The externally guided tension chords also change the safety requirements of the system, since the drive is no longer completely locked to the outside. Furthermore, the tension chords of the bioinspired system are only designed for a defined pick & place task. In the case of deviating load cases, it is not guaranteed that the construction is sufficiently protected against excessive bending stress. The transfer of the lightweight construction principles of the musculoskeletal system to an articulated arm robot represents a fundamental investigation of the lightweight construction potential. Further work is necessary to investigate the dynamic behavior and the adaptation to different load cases. There is also a need for research to open up further technical fields of application. The description of the human locomotor system as open kinematic chains permits further analogies to technical systems outside robotics.

Figure 4: Geometry of the articulated robot (left); results of the classical (middle) and bioinspired approach (right)

REFERENCES

[1] F. Pauwels, *Gesammelte Abhandlungen zur funktionellen Anatomie*, Springer-Verlag, Berlin, Heidelberg, New York, 1965.
[2] U. Witzel et al., *Finite-Element model construction for the virtual synthesis of the skulls in vertebrates: case study of diplodocus*, The anatomical record. Part A, Discoveries in molecular, cellular, and evolutionary biology, 283(2), 391–401, 2005.
[3] C. Matthek, *Design in der Natur*, Rombach GmbH+Co Verlagshaus KG, Freiburg, 1997.
[4] VDI-Richtlinie, *VDI 6224-3 (2017): Bionische Strukturoptimierung eines ganzheitlichen Produktentstehungsprozesses.*
[5] T. Ricken et al., *A triphasic model of transversely isotropic biological tissue with applications to stress and biologically induced groth*, Computational Materials Science, 39(1): 124-136, 2007.
[6] H. Witte et al., *Konstruktion vierbeiniger Laufmaschinen anhand biologischer Vorbilder*, Konstruktion 9-2000, 2000.
[7] B. Möhl, *A Composite Drive with Separate Control of Force*, 11th International Conference on Advanced Robotics 2003.
[8] S. Klug et al., *Design and Application of a 3 DOF Bionic Arm*, Proc. AMAM 2005, Ilmenau, Germany, 2005.
[9] A. Ananthanarayanan et al., *Towards a bio-inspired leg design for high-speed running*, Bioinspiration & Biomimetics, 2012.
[10] Richard et al., *Biomechanik*, Springer Vieweg, Wiesbaden, 2013.
[11] J. Rasmussen et al., *Muscle recruitment by the min/max criterion – a comperative study*, Journal of biomechanics, 2001.

Symposium *Lightweight Design in Product Development 2018* (LWD-PD18)
Zurich, Switzerland, 14th–15th June 2018

PRODUCT DEVELOPMENT PROCESS FOR HIGHLY INTEGRATED COMPOSITES LIGHTWEIGHT AUTOMOTIVE SYSTEMS

Jonathan Sprehe (formerly Schmidt)[1], Georg Jacobs[1] and Dave Cadwell[2]

[1]Institute for Machine Elements and Systems Engineering, RWTH Aachen University,
Steinbachstraße 54 B, 52074 Aachen, Germany
+49 241-80 27340
Email: jonathan.sprehe@imse.rwth-aachen.de; georg.jacobs@imse.rwth-aachen.de; web page: www.ikt.rwth-aachen.de

[2]BENTLEY MOTORS LIMITED,
Crewe, Cheshire, CW1 3PL, England,
Email: dave.cadwell@bentley.co.uk; web page: www.bentleymotors.com

1. INTRODUCTION

Modern lightweight products for the automotive industry are usually the result of a multi-disciplinary team, organized in different departments, often with the involvement of several suppliers. To structure such a development process, to define the most efficient design tools and to enable a comprehensible view onto the process is a challenging but necessary objective within lightweight design.

The corporate structure of most original equipment manufacturers (OEMs) - in function based departments and interdisciplinary project teams - allows the development of complex systems like an automobile with the support of many area-specific experts, but also hinders a holistic system approach. That, however, is necessary to achieve the full lightweight potential of a system. System borders for example between Interior, Exterior, Hardware or Closures are "natural" interfaces that divide the complex system of an automobile and make it manageable via defined hard-points during the design process. The integration of functions and parts, however, is hindered by this strategy. One major pillar of lightweight design is the material lightweight design. Often, superior metals or composites are used to reduce the weight of a vehicle. Especially when designing with carbon fiber reinforced polymers (CFRP), a cost-efficient design becomes even more relevant due to the high material costs [1]. The permanent requirement to reduce costs leads to the platform-strategy of most OEMs [2]. Carry-over parts, used in several car models, on the one hand support the economies of scale but on the other hand limit the freedom of design for the designer. This once again complicates a holistic system approach for lightweight design via integration of function and parts.

According to Deloitte [3], for most OEMs the current zone of interest with a high degree of uncertainty and a high degree of impact are lightweight technologies and innovations. This leads to the question how a structured way of designing systems can support the above mentioned goals under the given limitations and framework.

2. METHOD

Within this research, three main areas are defined based on a deductive observation that allows such a system view with the goal of highly integrated CFRP parts. According to Ehrlenspiel 70 % of the products costs are already defined during the design and development-phase [4]. Hence, the lightweight strategies that support these first steps during the product development process (PDP) are focused. According to Maier, these strategies are material lightweight design, shape lightweight design and conceptual/functional lightweight design [5]. Henning defines the three crucial areas for lightweight design as material, geometry and function [6]. During the PDP, the doctrine to find a solution for a problem is to define the working interrelationship between the physical effect, the geometric characteristics and material characteristics [7]. Under the given framework, within the automotive industry and the deductive observation of the in general relevant areas, the applicable design tools for function integration, structural lightweight design and cost-efficient material lightweight design are adapted to foster the development of highly integrated lightweight CFRP parts.

The necessary design tools are applied to a door system and evaluated regarding their weight-saving. The first design tool is a **fiber-feasible topology optimization**, used to define the areas where CFRP with its anisotropic material properties is most efficient. The biggest benefit of fiber reinforced polymers is, determined by its anisotropic structure, obviously gained when the fibers lie directly in the load carrying direction. A deviation by only 15 ° reduces the relative strength for tension and compression by more than 80 % [8]. Hence, the necessity to have extensive knowledge about the load distribution in a part is huge. During the development of a car door, more than 30 load cases have to be considered. This leads to a lot of multi-axial stresses within the system, where CFRP is relatively inefficient. Hence, all branches and roots of a topology-optimized door have to be analyzed to find the areas where one load case can be considered as the main load case. The necessary carry-over parts have to be considered within this optimization, limiting the design freedom by a significant amount. The areas where CFRP is not the best solution are then evaluated, using an **objective materials selection process** aligned to the Ashby approach. It is of great importance to consider the OEMs specific requirements to define the pareto-optimal solution between weight-saving and additional costs for the

given area of the vehicle. A pairwise comparison [9] is used to support the definition of the requirements and allow an objective materials selection process. The last design tool used is the visualization of the **Product Architecture**. It matches the different life-cycle functions with the different parts and enables a function-based view onto the system [10]. According to Ziebart it is important to define what functions to consider before trying to integrate them [11]. Different steps (e.g. Assembly, Disassembly, Manufacture) during the life-cycle of a product require the fulfillment of different functions. To comprehensively rethink an existing system, it is important to start with the customer functions and to allocate the cost per function and the theoretical weight per function. The visualization of the Product Architecture allows such an allocation and enables an objective decision on how many additional costs are justified by which function integration.

Using a smart combination of these tools, including a morphological matrix, within the product development process, a highly integrated door system is developed that shows the potential for composite structures within the automotive industry.

3. KEY RESULTS

The fiber-feasible topology optimization of a door system shown in Figure 1 exposes that the area where the CFRP is most efficient is the waistrail area (highlighted red and blue), with the main load case bending. In this area, a weight-saving in comparison to the former design of up to 60 % is possible. The Product Architecture of a Bentley Continental door system shows that the function "provide style" with more than 10 kg and costs of more than 150 € is one of the most important functions that can partially be integrated. Here, the usage of CFRP can act as a "delighter" for the costumer that can justify higher costs like the visible CFRP-"racing-look", illuminated surfaces or even integrated switches and looms.

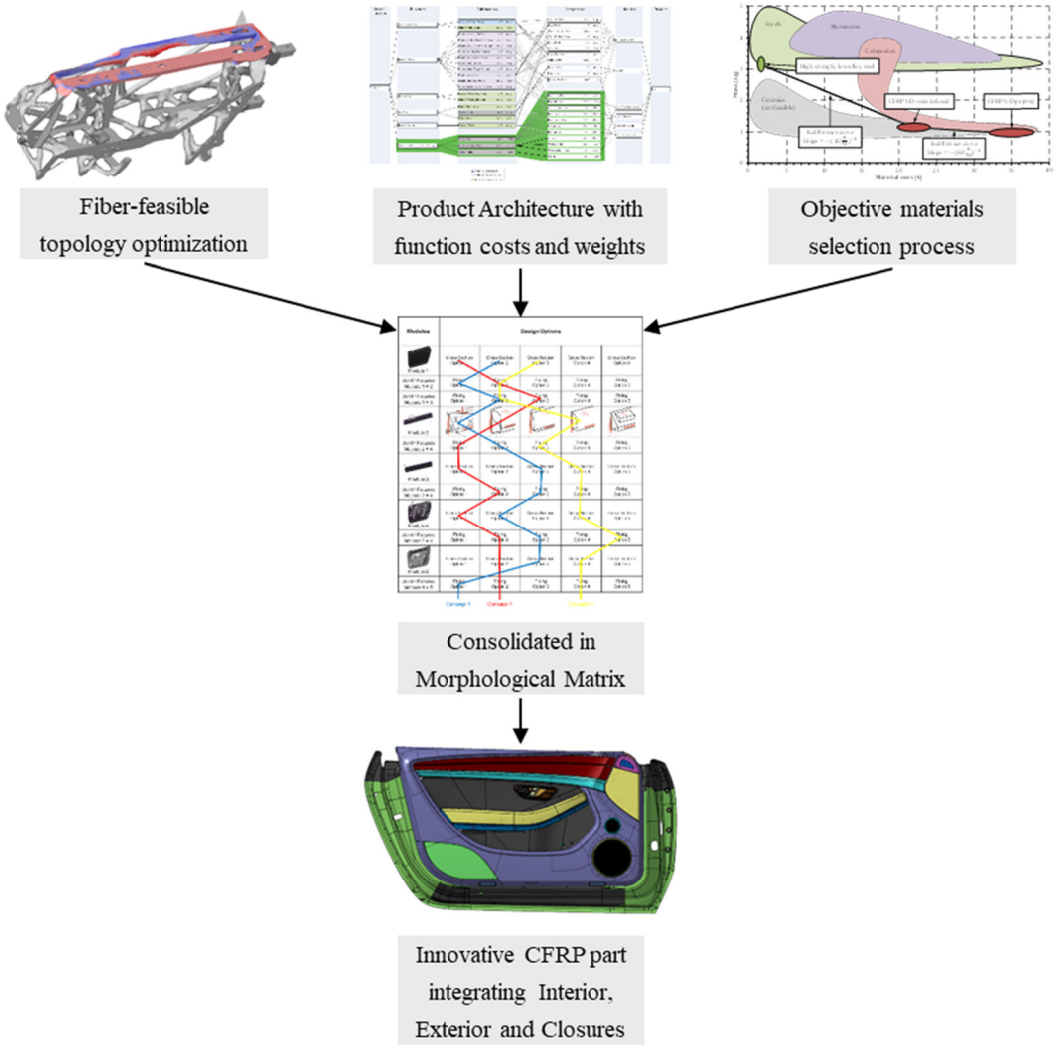

Figure 1: Three main design tools for concept design adapted and applied to a Bentley Continental door system

Including the dimensions, expected forces of the new parts and the preferences of the manufacturer into the materials selection process by Ashby, the weight-saving and the estimated costs can be shown in an Ashby chart. All

this information is then included into a Morphological Matrix where different concept designs with different fixing strategies and materials can be combined and evaluated. Under consideration of the preferences and OEM-specific requirements, a decision is made on which conceptual design should be further embodied.

In this use case, the chosen design is a highly integrated CFRP part, incorporating Interior, Exterior and Closures parts (see Figure 1, black part in lower picture). The opportunity to illuminate the pocket via optical fibers implemented into the first ply of the composite and the opportunity to integrate the window switches and seat switches into the A-surface with smart textiles offer additional potential for function integration and hence weight-saving.

4. CONCLUSION

The emerged product development process enables the designer to create highly integrated lightweight CFRP systems with a focus on innovative concepts. Therefore, three main areas within the PDP were identified by a deductive observation and then adapted to deliver a lightweight design, focusing on the integration of CFRP parts into a multi-material system. To deliver a cost-efficient design, only areas where either the load case made CFRP with its anisotropic properties the best choice of material or where the unique look of CFRP contributed to the overall style of the system were integrated. Additional functions for the costumer were also implemented and lead to some “delighters” like illuminated surfaces and integrated switches, whereby the part also served as a technology carrier. An objective selection process under consideration of the given framework and OEM-specific requirements lead to a highly integrated concept design for a door system of a Bentley Continental GT.

REFERENCES

[1] H. Schürmann, Konstruieren mit Faser-Kunststoff-Verbunden, Springer: 2007, p. 5.
[2] V. Schindler et al., Forschung für das Auto von Morgen, Springer: 2008, p. 313.
[3] N. Helbig et al., The Future of the Automotive Value Chain – 2025 and beyond, Delloitte: Issue 03/2017, p. 16.
[4] K. Ehrlenspiel et al. Kostengünstig Entwickeln und Konstruieren, Springer: 2014, p. 15.
[5] M. Maier, Entwicklung einer systematischen Vorgehensweise für den bionischen Leichtbau, Dissertation, Universität Bremen, 2015, p. 23.
[6] F. Henning et al., Handbuch Leichtbau – Methoden, Werkstoffe, Fertigung, Hanser: 2011, p. 63-67.
[7] G. Pahl et al., Engineering Design – A Systematic Approach, Springer: 2007, p. 38-41.
[8] V.I. Khaliulin et al., Prospects of Applying the Tailored Fiber Placement (TFP) Technology for Manufacture of Composite Aircraft Parts, Izvestiya VUZ, Aviatsionnaya Tekhnika, 2015; No. 4: p. 127–132.
[9] W. Beitz et al., Konstruktionslehre – Methoden und Anwendungen erfolgreicher Produktentwicklung, Springer: 2013, p. 388.
[10] J. Göpfer et al., Modulare Produktentwicklung leistet mehr - Warum Produktarchitektur und Projektorganisation gemeinsam gestaltet werden müssen, Harvard Business Manager: 2000; Vol. 3: p. 1-17.
[11] J. R. Ziebart, Ein konstruktionsmethodischer Ansatz zur Funktionsintegration, Dissertation, TU Braunschweig, Verlag Dr. Hut: Bericht Nr. 83, 2012, p. 4-5.

EXTENDED TARGET WEIGHING APPROACH – A SYSTEM LIGTHWEIGHT DESIGN APPROACH FOR NEW PRODUCT GENERATIONS

Sven Revfi[1], Albert Albers[1], Jan Holoch[1] and Markus Spadinger[1]
[1]Karlsruhe Institute of Technology (KIT) - IPEK – Institute of Product Engineering, Germany. Email address: {sven.revfi, albert.albers, jan.holoch, markus.spadinger}@kit.edu

1. EXTENDED TARGET WEIGHING APPROACH (ETWA)

The "Extended Target Weighing Approach" (ETWA) [1] describes a holistic, cross-subsystem, function-based lightweight design method – in the context of system lightweight design – to identify and evaluate lightweight design potentials in the concept phase of product development. It systematically extends the existing "Target Weighing Approach" (TWA) as introduced by Albers [2] and Wagner [3] in order to balance the crucial factors for lightweight design: mass, CO2-emission and cost. Fig. 1 shows the workflow of the ETWA.

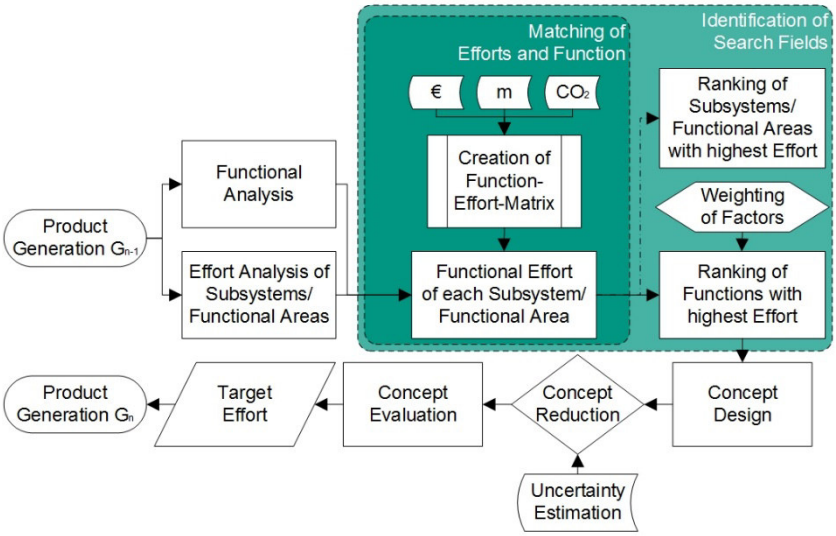

Fig. 1: Workflow of the Extended Target Weighing Approach

Ideally, the starting point for ETWA is a reference product whose mass has to be optimized. Afterwards a functional analysis is conducted and the functions fulfilled by the reference product are determined. Perpendicular to that, the effort of each subsystem meaning its mass, CO2-emissions and costs is gathered. Thereafter, the percentage contribution of each subsystem to the fulfilment of the functions is quantified in the so called Function-Effort-Matrix (see Fig. 2).

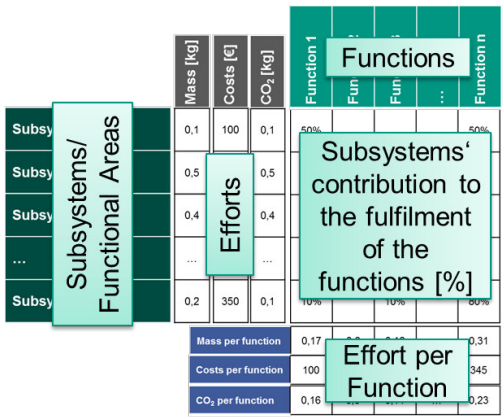

Fig. 2: Function-Effort-Matrix [4]

The identified functions are plotted on the horizontal axis, while each of the subsystems and its effort is listed on the vertical axis. This results in the effort per function and is used to identify "heavy" functions with lightweight design potential by means of evaluation methods such as function portfolio (see Fig. 3). In order to be able to take the strategic orientation of a company into account, the ETWA allows the factors mass, CO2-emissions and costs to be weighted with business specific weighting factors.

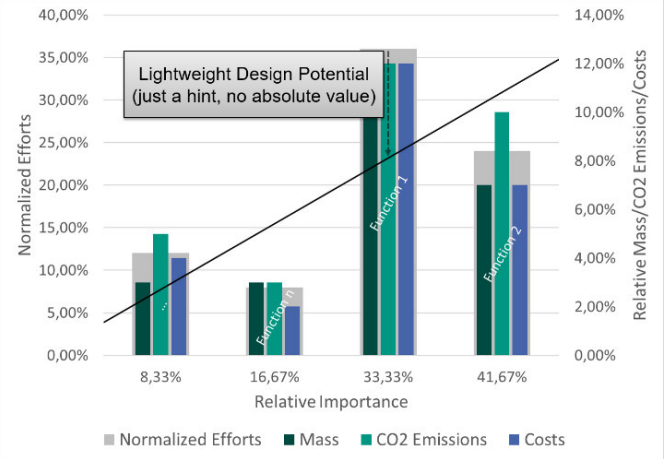

Fig. 3: Function portfolio [3]

For each of these identified functions, new concept ideas are generated using different lightweight design strategies. To evaluate the new concept ideas, a sensitivity analysis is performed by using the Function-Effort-Matrix in the opposite direction. As a result, it is possible to determine the influence on the weight, CO2-emissions and costs directly in the Function-Effort-Matrix.

In addition, new concept ideas are evaluated with regard to technological uncertainties due to a company-internal lack of information when using new technologies. Therefore, the influencing factors Impact, Carryover Variation Share, Reference Product – Technology and Reference Product – Application Scenario are examined and visualized in a spider diagram.

The following paragraph describes the determination of each effort (mass, CO2-emissions and costs) of a subsystem. Furthermore, the business specific weighting factors that allow strategic positioning when developing new concept ideas are discussed.

2. WEIGHTING OF FACTORS MASS, CO2-EMISSIONS AND COSTS

In order to generate the Function-Effort-Matrix, the effort of each subsystem must be identified. To determine the mass, either each subsystem can be weighed or its CAD data can be used. Since new concept ideas are initially designed on the computer, their mass cannot be assessed by weighing. For this reason and to ensure comparability of the new concept ideas with the reference product, the mass is determined using CAD data. Therefore, the volume is specified and multiplied by its density. This results in the mass in kilograms for each subsystem.

The CO2-emissions are determined with the aid of a life cycle assessment (LCA). The LCA is an iterative analysis method for the assessment and modelling of the environmental impacts of products and materials over their entire life cycle (“cradle to grave”). Therefore, the LCA takes the production, the use phase and the recycling/disposal into account. The workflow of the LCA consists of the following four steps: Goal and Scope, Inventory, Impact assessment and Interpretation. First, the system boundary including the functional unit, the goal and the purpose of the LCA are defined. The functional unit describes the reference value to which the results of the impact assessment are related. ETWA uses the CO2-emission in $kg_{CO2\text{-}eq}$ for this purpose. Afterwards, all input and output flows must be recorded within the defined system boundary. This results in the complete mass and energy balances describing discharges from the environment as well as emissions and waste into the environment. Then, possible environmental impacts are quantified on the basis of the inventory. The impact-oriented CML2001 method is used for this purpose. This method summarizes the potential environmental impacts of certain substances in so called impact categories (e.g. human toxicity, acidification, resource consumption or GWP). Since ETWA examines the impact on global warming, only the impact category GWP is required. The result of the impact assessment is a value in $kg_{CO2\text{-}eq}$ that includes all emissions that contribute to global warming. Finally, the results are interpreted. To do so, in addition to drawing conclusions, the following questions need to be clarified: Which life cycle phase has the greatest impact on the GWP? Which flows are the most important? [5]

The costs of each subsystem are calculated based on the guidelines of the purchased subsystems according to the greenfield approach taking the current economics and commercials into account. This so called bottom-up calculation is based on the design of an existing product but with an independent vertical integration. In order to avoid competitive conflicts, this confidential data is standardized in percentages. In comparison to the LCA, the greenfield approach only considers the production phase, as this has the greatest influence on costs.

After the effort of each subsystem has been determined, the question is, how to evaluate the generated data. At this point it is remarked that the mass is included both in the calculation of costs and in the calculation of CO2-emissions.

However, the description of the underlying calculation models for costs and the LCA in the paragraph above has shown that the mass only partly contributes to the other factors. Both in the costs and in the CO2-emissions, many other mass independent influencing variables are considered, which is why the authors assume three independent factors, that can be weighted among themselves. In order to allow business specific trade-offs as well as strategic positioning a weighting of factors is introduced in the ETWA before ranking the functions with the highest effort. Different approaches are conceivable for this. However, in order to ensure intuitive applicability, a linear approach was chosen, as for example proposed by Ashby [6] in his material selection in order to minimize mass while taking costs and CO2-emissions into account.

Equation 1 shows the chosen linear approach. The effort (mass, CO2-emissions and costs) of each subsystem are represented by m, $CO2$ and $€$. The corresponding weighting factors are illustrated by w_m, w_{CO2} and $w_€$. Equation 2 applies to the summation of the weighting factors.

$$E = w_m \cdot m + w_{CO2} \cdot CO2 + w_€ \cdot € \tag{1}$$

$$w_m + w_{CO2} + w_€ = 1 \tag{2}$$

3. CONCLUSION

In order to respect economic and ecological aspects in lightweight design, the lightweight design method "Extended Target Weighing Approach" (ETWA) has been developed. It systematically takes the factors mass, CO2-emissions and costs into account. When having a closer look at the calculation of these factors, it has been shown that they can be considered as independent for the method. This allows a business specific weighting of factors so that methodological supported, individual designs can be created. Choosing a linear approach helps using the weighting intuitively.

4. ACKNOWLEDGMENTS

This project has received funding from the European Union's Horizon 2020 research and innovation programme.

REFERENCES

[1] Albers, A. et al., "*Extended Target Weighing Approach - Identification of lightweight design potential for new product generations"*, International Conference on Engineering Design (ICED), 2017; 367-376.

[2] Albers, A. et al., "*Target Weighing – A New Approach for Conceptual Lightweight Design in Early Phases of Complex Systems Development"*, International Conference on Engineering Design (ICED), 2013; 301-310.

[3] Wagner, D., *Methodengestützte Entwicklung eines elektrischen Energiespeichers zur Erschließung von Leichtbaupotenzialen als Beitrag zur Produktgenerationsentwicklung*, Karlsruhe Institute of Technology (KIT), Department of Mechanical Engineering, Forschungsberichte des IPEK - Institute of Product Engineering, ISSN 1615-8113, 2015.

[4] Albers, A. et al., "*Synergy Effects by using SysML Models for the Lightweight Design Method "Extended Target Weighing Approach""*, CIRP Design Conference, 2018; Volume 70: 434–439.

[5] Eberle U. et al., *Die Ökobilanz*, Ökopol – Institute for Environmental Strategies, 2015.

[6] Sirisalee P. et al., *Advanced Engineering Materials*, WILEY-VCH Verlag GmbH & Co. KGaA, 2004; 84-92.

Symposium *Lightweight Design in Product Development 2018* (LWD-PD18)
Zurich, Switzerland, 14th–15th June 2018

ROBUST DESIGN OF A MORPHING AIRCRAFT WING

J. Achleitner[1], K. Rohde-Brandenburger[2], M. Hornung[3] and M. Zimmermann[1]
[1]TUM – Laboratory for Product Development and Lightweight Design, Germany. johannes.achleitner@tum.de
[2] DLR - Institute of Aerodynamics and Flow Technology, Germany. kai.rohde-brandenburger@dlr.de
[3] TUM - Institute of Aircraft Design, Germany. mirko.hornung@tum.de

1. INTRODUCTION

In this paper a contribution to airfoil design for a morphing wing sailplane with particular focus on robustness by a top-down approach is presented. Basic idea of the morphing wing concept is to change the contour of the wings leading edge regarding thickness distribution and camber. The concept is depicted in Fig. 1, showing the undeformed airfoil in high speed and the morphed airfoil in low speed configuration. The concept also includes a conventional camber changing flap. Sailplanes operate in a wide range of speeds and associated lift coefficients that change due to angle of attack. During climb in thermal upwinds, low speeds and high lift coefficients are necessary. By contrast, during cruise, high speeds and low lift coefficients are desired. The aerodynamic designers objective is to create a sailplane that reaches the highest possible average speed in given meteorological conditions by reducing drag both in high lift and low lift range. Airfoils are designed to obtain the best compromise between low speed and high speed performance. By introducing a morphing leading edge of the front 40% portion of the airfoil, this compromise can be alleviated. Weinzierl [1] showed that the maximum lift coefficient of a laminar airfoil with camber changing flap can be increased by 20% with a morphing droop-nose, which can be used to decrease wing area and increase wing loading by the same percentage. This leads to reduced induced drag and wetted surface, thus reducing overall drag and increasing performance.

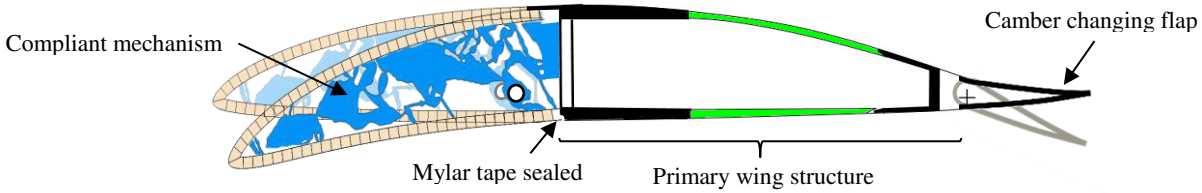

Fig. 1: Airfoil in undeformed and morphed state with primary structure, compliant mechanism and camber changing flap

Unfortunately, the performance of modern laminar airfoils is very sensitive to small contour deviations. This is especially the case when considering a morphing airfoil in high lift configuration. Little perturbations of the airfoil shape can be supercritical, causing unfavorable changes in the flow pattern, eventually leading to earlier laminar to turbulent transition or flow separation associated with a significant loss of lift and/or increase of drag. The undeformed shape can be manufactured very precisely by laminating in negative molds. In the current concept, the required deformation for morphing the wing shape is intended to be accomplished by compliant mechanisms, which are distributed span-wise approximately every half meter. It cannot be guaranteed that the desired shape can be precisely realized by the actuation mechanism over the whole wing surface. Thus, an airfoil having a morphed target shape which is robust to small contour deviations is highly favorable.

2. AIRFOIL OPTIMIZATION

The base airfoil in undeformed and deformed state for the further considerations is designed by numerical airfoil optimization. The undeformed and morphed airfoil shape is parametrized utilizing the “shape function / class function” methodology (CST) proposed by Kulfan and Bussoletti [2]. The contour line of the undeformed airfoil is expressed by two separate curves for top and bottom side. Each side is parametrized independently. The top and bottom contour lines, i.e. their z-coordinates as a function of its x-coordinates, are obtained by multiplication of a class function C(ψ) with a shape function S(ψ):

$$\zeta(\psi) = C(\psi)\, S(\psi) \qquad where: \qquad \psi = \frac{x}{c} \quad and \quad \zeta = \frac{z}{c} \tag{1}$$

The class function for the undeformed airfoil top and bottom coordinates is defined as:

$$C(\psi) = \psi^{N_1}(\psi - 1)^{N_2} \qquad with \quad N_1 = 0.5 \quad and \quad N_2 = 1.0 \tag{2}$$

$N_1 = 0.5$ ensures a round leading edge with infinite slope at $\psi = 0$. For the trailing edge angle to finite at $\psi = 1$, N_2 is set as $N_2 = 1.0$. Bernstein polynomials are used as weighted shape functions. The weighting factors x_i are the design variables for the optimization problem.

$$S(\psi) = \sum_{i=0}^{n} x_i\, B_i(\psi) \qquad where: \qquad B_i(\psi) = K_i\, \psi^i (1-\psi)^{n-1} \quad and \quad K_i = \binom{i}{n} = \frac{n!}{i!\,(n-i)!} \tag{3}$$

For morphing purposes, the upper and lower contour lines of the airfoil are decomposed into the mean line, also known as camber line, and a thickness function. Then, morphing is performed by adding additional functions to both, the camber line and the thickness distribution. Both functions are parametrized by the CST method. Compared to the undeformed airfoil parametrization, different class functions are used. For morphing of the thickness distribution, the class function

from Eq. 2 is used, but with different exponents $N_1 = N_2 = 2.0$. The ψ coordinates are transformed to the area, where morphing is applied (Eq.4). ψ_e denominates the end of the morphing section. In this case, it was decided to morph the front 40% portion of the airfoil. Therefore, $\psi_e = 0.4$. In order to ensure a precise leading edge shape, which is important for a gentle stall behavior of the airfoil, the thickness of the leading edge part remains fixed. Consequently, the leading edge is supposed to undergo a rigid body motion only and is to be designed sufficiently stiff. At position ψ_s is the beginning of the section where the thickness distribution is changed. ψ_s is set equal to the leading edge radius.

$$\psi_t = \frac{\psi - \psi_s}{\psi_e - \psi_s} \quad and \quad \psi_c = \frac{\psi}{\psi_e} \tag{4}$$

The camber line morphing begins right at the leading edge, thus the coordinate transformation according to right part of Eq.4 is utilized. As class function, a parabola is utilized:

$$C_c = (\psi_c - 1)^{N_1} \quad with: \quad N_1 = 2.0 \tag{5}$$

An example of morphing an airfoil with the CST method is shown in Fig.2. The class functions are shown in the topmost figures. The resulting shape function is shown as a blue line in the centered figures, which is a sum of the weighted Bernstein polynomials (black lines). The resulting change in camber (left) or thickness (middle) is shown in the bottom diagram. The recomposed undeformed (black) and morphed airfoil (blue) is shown in the right image. The right bottom figure shows the decomposition of the undeformed airfoil into camber line (green) and thickness distribution (blue)

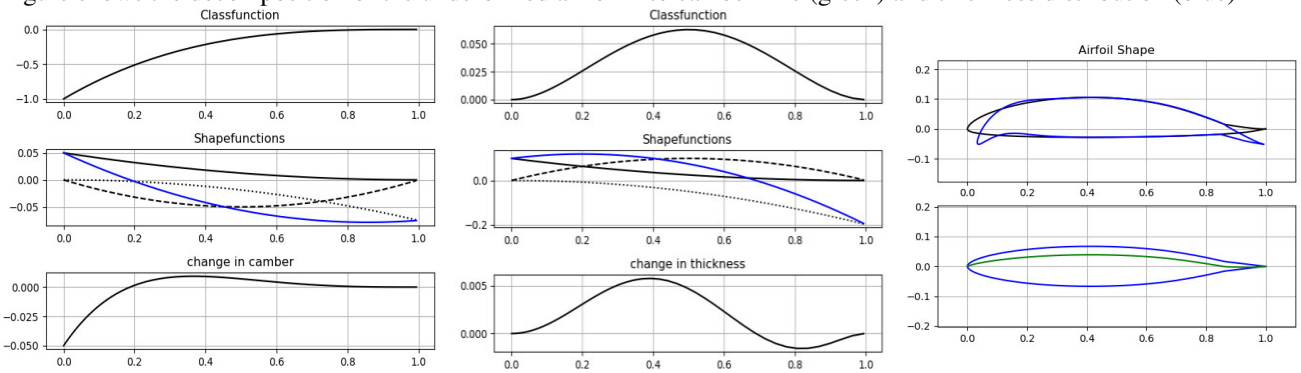

Fig. 2: Class and shape functions for (left) the camberline, (middle) the thickness distribution and (right) resulting airfoil shape

The optimization of the airfoil is performed using the so-called Subplex algorithm [3], which is a subspace line search method using a gradient free Nelder-Mead-Simplex [4] algorithm for optimization of the subdomains. As objective functionf_{obj}, the weighted sum of drag coefficients at serveral lift coefficients is used. Drag coefficients are determined by the 2D panel method with a fully coupled viscous boundary layer calculation XFOIL [5]. The design variables for optimization are the weights for the individual Bernstein polynomials x_i. For thickness and camber distribution morphing, three design variables are chosen each, $x_0 \dots x_2$used for thickness morphing and $x_3 \dots x_5$ used for camber morphing. The resulting airfoil showed superior performance compared to conventional rigid airfoils with camber changing flap.

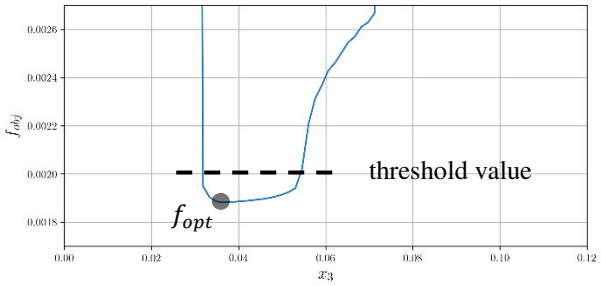

Fig. 3: Parametric study of objective function value vs. design variable x

3. ROBUST AIRFOIL DESIGN

In order to perform a first robustness analysis, a parametric study is carried out by varying one morphing design variable while holding the other five fixed at the optimum values. Fig. 3 shows the objective function value over the design variable x_3, which is the foremost design variable, determining the value of the lowering of the nose. It can be seen, that small reduction in x_3 leads to a tremendous increase in objective function value, meaning the optimization result is not robust with respect to a small reduction of nose lowering. This can occur, i.e. if the actuation system is not stiff enough to withstand the aerodynamic pressure forces. Lehar & Zimmermann [6], Zimmermann & von Hoessle [7] and Zimmermann et al. [8] suggested a classification of designs into good and bad designs and construct so-called *solution spaces*, i.e., regions of good designs. Bad designs either violate a design restriction or have a high objective function value above a threshold. Threshold is chosen to be $f_{obj} = 0.020$ (see Fig. 3), which corresponds to a less than 5% performance decrease compared to the found optimum. Fig. 4 shows an excerpt of the results of a Monte Carlo simulation by varying

a combination of two design variables while holding the others fixed at the optimum values. The colors represent good (green) and bad (red) design variables. The optimum found by the Subplex algorithm is depicted as a blue dot. It is evident that the optimum is not robust w.r.t. a variation of the design variables in many subspaces, especially in the $\{x_1, x_3\}$ subspace (top left diagram in Fig. 4). It can also be seen, that there are large spaces, where the resulting geometry is robust

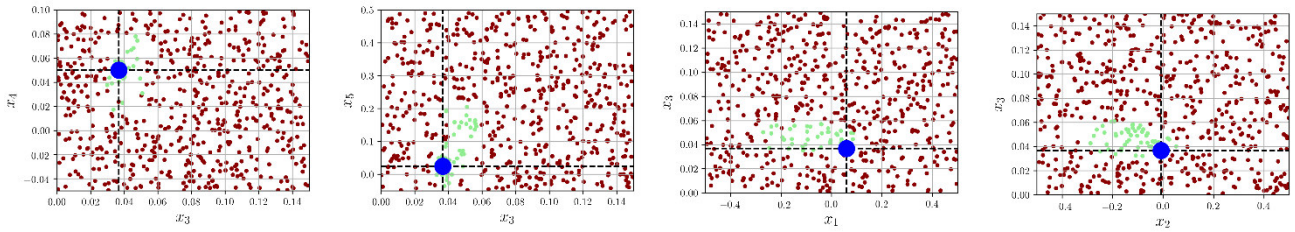

Fig. 4: Excerpt of the results of the Monte Carlo simulation

to parameter variation, at least in the 2D-subspaces. To find a robust design with a bandwidth of variation of geometry design variable as large as possible, the above study is extended. Now for each plot, the design variables which are not on the axes are not fixed at the value determined by the optimizer, but randomly varied within an interval $[x_{i,l}, x_{i,u}]$, visualized in the other diagrams as vertical and horizontal dashed lines. This represents a two-dimensional projection of a slice of finite thickness through the design space. The designer's task is to choose and update the bounding intervals of all design variables in order to find an area of good designs that is as large as possible. This area represents a solution space. The results are shown in Fig. 5. The most robust design lies in the center of each interval (black dot). Large intervals were found for each design variable with performance close to the optimum result. Note that the optimum found by the optimization algorithm (blue dot) lies outside the robust area for many sets of design variables. The new robust airfoil is shown in Fig. 6, which has an increased nose droop compared to the optimum airfoil. It should be noted, that just changing the design variable x_3 which determines the level of nose droop without adjusting the other design variables doesn't lead to a more robust design as can be seen in the third diagram of Fig.4.

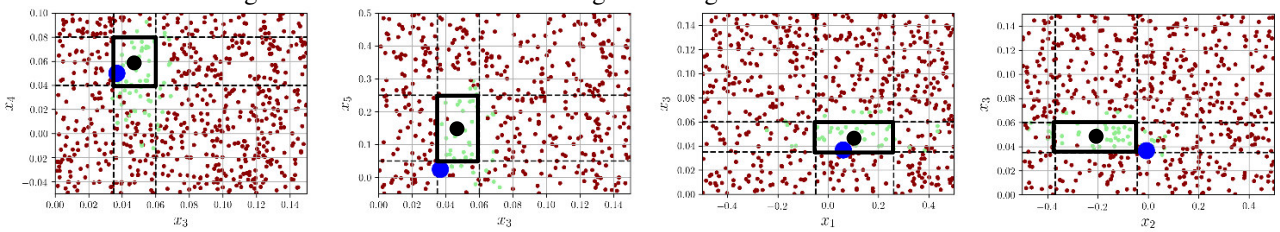

Fig. 5: Excerpt of the results of the robust design analysis

4. CONCLUSIONS

Contours of sailplane airfoils can be designed with particular focus on robustness using a quantitative top-down approach to construct solution spaces. Solution spaces are regions of good designs that are maximized. The optimum of the design problem considered is not robust, because it is close to the region of bad designs. The most robust design, e.g., with respect to structural uncertainty was identified in the middle of the computed solution space. Note that using a top-down approach, uncertainty due to variation of structural properties can be treated although no structural information was provided. This enables a decoupled and less complex development process. As to the author's knowledge, the presented method is applied for the first time in aerospace engineering.

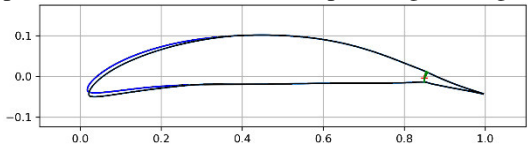

Fig. 6: Optimized airfoil (blue) vs. robust airfoil (black)

REFERENCES

[1] M. Weinzierl et al., "Highly Extensible Skin of a Variable Geometry Wing Leading Edge of a High-Performance Sailplane", *Technical Soaring*, 2015; Vol. 39, No.1: 4-9.

[2] B. M. Kulfan et al., ""Fundamental" Parametric Geometry Representations for Aircraft Component Shapes", *Int. 11th AIAA/ISSMO Multidisciplinary Analysis and Optimization Conference*, 2006

[3] T.H. Rowan, *Functional Stability Analysis of Numerical Algorithms*, Dissertation, University of Texas, Austin: 1990.

[4] M. Drela, "XFOIL: An Analysis and Design System for Low Reynolds Number Airfoils", *Low Reynolds Number Aerodynamics. Lecture Notes in Engineering*, 1989, Vol 54: 1-12.

[5] J.A. Nelder et al., "A simplex method for function minimization". Computer Journal, 1965. Vol. 7: 308–313.

[6] M. Lehar, M. Zimmermann, "An inexpensive estimate of failure probability for high-dimensional systems with uncertainty", *Structural Safety*, Vol. 36-37: 32-38.

[7] M. Zimmermann, J. von Hoessle, "Computing Solution Spaces for Robust Design", *International Journal for Numerical Methods in Engineering*, 2013, Vol. 94(3): 290-307.

[8] M. Zimmermann et al., "On the design of large systems subject to uncertainty" *J. of Eng. Design*, 2017, Vol. 28(4): 233-254

Gefördert durch:

Bundesministerium für Wirtschaft und Energie

aufgrund eines Beschlusses des Deutschen Bundestages

Symposium *Lightweight Design in Product Development 2018* (LWD-PD18)
Zurich, Switzerland, 14th–15th June 2018

A SYSTEMATIC APPROACH FOR VIBRATION REDUCTION OF LIGHTWEIGHT STRUCTURES WITH PARTICLE DAMPING

Jan Oltmann[1], Tobias S. Hartwich[1] and Dieter Krause[1]
[1]Hamburg University of Technology, Institute of Product Development and Mechanical Engineering Design, Germany.
j.oltmann@tuhh.de

1. INTRODUCTION

The reduction of vibrations or noise plays an important role for the design of many applications. Especially lightweight structures are prone to strong vibrations disturbances. Particle damping was found to be an efficient way to reduce vibrations of lightweight structures since not much weight has to be added. Particles of different shape, size or material are used to fill cavities with a certain filling ratio. Dissipation of energy occurs due to particle-to-wall and particle-to-particle collisions caused by any dynamic excitation. However, for particle damping it is difficult to define an efficient modelling technique to predict the dynamic behavior of a mechanical structure. Either simplified equivalent models or detailed simulation models but with higher computational time (e.g. using the Discrete Element Method) are used [1]. In both cases extensive experimental testing is required, due to the non-linear behavior of particle damping, depending on e.g. excitation amplitude, frequency or damper design [1,2]. But still a general validity of equivalent models is not given. Secondly, because damping mechanisms can still not be determined from specimens of smaller scales, for a valid design approach for vibration reduction it is necessary to carry out tests on the final product design, which possibly are large and complex assemblies.

In this paper a new approach to efficiently predict the influence of particle damping on lightweight structures using Frequency Based Substructuring (FBS) is presented. In this way, the consideration of particle dampers is possible without modelling its complex dynamic behavior in detail. The frequency response of the particle system - as one substructure - is determined experimentally. Finally, a hybrid frequency based assembly using test (particle cavity) and simulation (lightweight structure) results is used to determine the dynamic behavior of the entire system. Finally, in the paper a systematic approach to design particle damping using FBS is presented.

2. METHOD

The Frequency Based Substructuring (FBS) is a frequency domain method to solve linear vibration problems by decomposing a structure into several smaller parts, the so-called substructures. FBS theory was already published in the 1960s-1980s [3]. The FBS assumes that a reduced number of DoF are sufficient to describe the dynamic behaviour of a system. Each substructure can individually be characterized by its frequency response functions (FRF), that can be determined via simulation or experimental testing. This so-called experimental substructuring is one of the major advantages of this approach if experiments are carried out appropriately. Thus, real (non-linear, frequency dependant) physical effects, that cannot be modelled in an appropriate manner, can be incorporated into a frequency based assembled system response. However, only in 2006 De Klerk et al. [4] published a new systematic notation, called dual assembly, that facilitates the handling for numerical calculation. Following the dual assembly according to [4], the overall frequency response function matrix can be derived from the general equation of motion of subsystems Eq. 1 in the time domain. The interface compatibility is defined in Eq. 2 with the boolean matrix B and the equilibrium of connection forces in Eq. 3 with the Boolean localization matrix L [4].

$$\mathbf{M\ddot{u} + C\dot{u} + Ku} = \mathbf{f + g} \quad \textit{(Local Equilibrium)} \tag{1}$$

$$\mathbf{Bu} = \mathbf{0} \quad \textit{(Interface compatibility)} \tag{2}$$

$$\mathbf{L}^T\mathbf{g} = \mathbf{0} \quad \textit{(Equilibrium of connecting forces)} \tag{3}$$

With the Structural Impedance Matrix

$$\mathbf{Z}(j\omega) \triangleq -\omega^2\mathbf{M} + j\omega\mathbf{C} + \mathbf{K}$$

the transformation to the frequency domain is carried out to

$$\mathbf{Z}(\mathrm{w})\mathbf{u}(j\omega) = \mathbf{f}(\omega) + \mathbf{g}(\omega) \tag{4}$$

$$\mathbf{Bu}(\omega) = \mathbf{0} \tag{5}$$

$$\mathbf{L^T g}(\omega) = \mathbf{0.} \tag{6}$$

Introducing the Lagrange Mutliplier $\boldsymbol{\lambda}$ such that $\mathbf{g} = -\mathbf{B}^T\boldsymbol{\lambda}$, one gets the so-called dual assembly [see Source] in matrix form as following.

$$\begin{bmatrix} \mathbf{Z} & \mathbf{B}^T \\ \mathbf{B} & \mathbf{0} \end{bmatrix} \begin{bmatrix} \mathbf{u} \\ \boldsymbol{\lambda} \end{bmatrix} = \begin{bmatrix} \mathbf{f} \\ \mathbf{0} \end{bmatrix} \tag{7}$$

The Lagrange Mutliplier λ respectively represents the internal connection forces. Solving the first equation for u with $\mathbf{Z}^{-1} = \mathbf{Y}$ yields

$$\mathbf{u} = \mathbf{Y}(\mathbf{f} - \mathbf{B}^T\boldsymbol{\lambda}) \tag{8}$$

Inserting Eq.8 in Eq. 7 one finds

$$\mathbf{B}(\mathbf{Yf} - \mathbf{YB}^T\boldsymbol{\lambda}) = \mathbf{0} \tag{9}$$

$$\Rightarrow \boldsymbol{\lambda} = (\mathbf{BYB}^T)^{-1}\mathbf{BYf}$$

Which leads to the Overall Transfer Function Matrix $\mathbf{Y}(\omega)$

$$\mathbf{u} = \underbrace{(\mathbf{Y} - \mathbf{YB}^T(\mathbf{BYB}^T)^{-1}\mathbf{BY})}_{\mathbf{Y}(\omega)}\mathbf{f} \tag{10}$$

Using the FBS approach the particle damping is predicted for the described sandwich structure and shall also be applied to lager structures, where trial an error testing is not possible. In this way, the consideration of particle dampers is possible without modelling its complex dynamic behavior in detail. The frequency response of the particle system - as one substructure - is determined experimentally. Finally, a hybrid frequency based assembly using test (particle cavity) and simulation (lightweight structure) results is used to determine the dynamic behavior of the entire system. With this first step, the design of particle dampers is already facilitated because a reduced number and smaller tests are needed to determine a damper design. Furthermore, the application to different structures and especially the optimization, e.g. application area, filling ratio etc. is possible dependent on the determined particle damper FRFs. Here the results of the first optimization runs are presented. Based on the dual assembly (Eq. 10) the acceleration transmissibility can be determined. Moreover, the FBS-approach is used to set up an optimization in order to minimize the maximum transmissibility with respect to the position of the particle damper, the choice of the damper and the combination of position and choice of the damper with a weight optimization to compensate the weight gain of the particle material.

3. EXPERIMENTAL TESTING

Vibration tests are carried out within a frequency range of 5 - 25 Hz. A sandwich panel design is chosen in order to have the first resonance frequency within the frequency range. The investigated material is a typical aircraft interior sandwich panel consisting of glass fibre fabric reinforced phenolic resin prepreg face sheets (PHG600-68-50) and a Nomex honeycomb core (cell size 3.2 mm, density 48 kg/m³). The particle damper consists of a plastic cavity of different sizes with equidistant Ø 4 mm holes, 26 mm deep. It is filled with sand to 50 % filling ratio with 0.1-0.4 µm particle size.

The vibration testing is carried out as impedance sweep tests with constant acceleration on a hydraulic shaker. Two kinds of tests are carried out as depicted in Fig. 1. On the one hand the clamped sandwich panel structure with and without particle damper as well as the single particle damper are investigated.

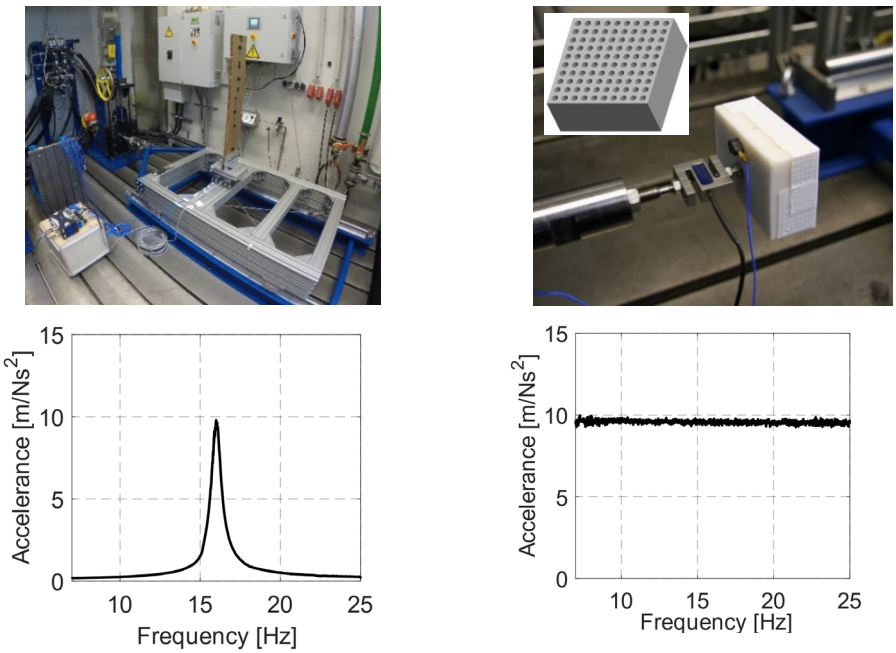

Fig. 1: Experimental Set-Up for vibration testing of sandwich panel (a) and particle damper (b) substructures; Substructure FRF of the Panel (c) and the particle damper (d) [2]

For the clamped panel, the acceleration is measured as input and output signal by triaxial ICP acceleration sensors. The excitation is a constant acceleration of 0.35 g measured on the fixture at the bottom of the panel as input signal. The

acceleration output is measured at the top of the panel. The excitation load is also measured at the fixture by a 5kN 6D load cell. The results are evaluated in the frequency domain for the out of plane direction of the panel. A structural damping of 1.44 % is calculated based on the measured acceleration transmissibility using the half power bandwidth method for the simulation of the panel substructure.

The experimental determination of the FRF of the particle damper is also depicted in Fig. 1. The interface load is measured by a 1D-100N load cell and the acceleration is measured with a lightweight (0.8 g) 50g-ICP acceleration sensor. As acceleration a 1 g excitation was chosen to have sufficient movement of the particles. Increasing the excitation level did not induce particularly higher particle loads. The substructure FRF of the panel and of the particle damper are depicted in the following figure. For a more detailed analysis it is referred to [2].

4. RESULTS AND DISCUSSION

The results of the FBS-optimization are depicted in Fig. 2 and Table 1. To compare it to experimental data three different test results are presented, to show that simply increasing the number of layers does not shift the resonance frequency out of range. Furthermore, the test result with empty particle cavity is shown to prove that there is only a slight influence due to the pure weight increase. The optimization is carried out with the genetic solver in Matlab with the objective to minimize weight and amplification. As constraints the composite layer thickness and a minimum amplification are defined. The different optimization settings are described in Fig. 2 The results show a good agreement with the for this simple example obvious optimum solution at the top of the panel with one layer, see test result for a panel with PD and 1 prepreg layer in Fig. 2.

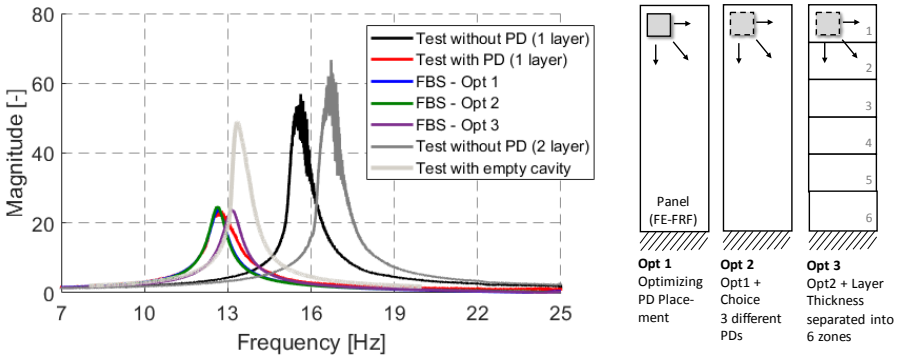

Fig. 2: Test and optimization results of particle damped honeycomb panel compared to reference structures

Table 1: Test and optimization results compared to reference structures with respect to weight

	Test				FBS-Optimization		
	1 layer	2 layer	1 Layer with empty cavity	1 Layer plus particle damping	Opt 1	Opt 2	Opt 3
Frequency [Hz]	15,9	16,4	13,5	12,9	12,7	12,7	13,1
Transmissibility	57,2	63,7	52.2	27,5	22,6	22,6	22,0
Mass [g]	467	709	537	561	539	536	508

5. CONCLUSION AND OUTLOOK

A new way to predict particle damping is presented based on frequency based substructuring approach. Furthermore, the approach is used to optimize the placement, the choice of a damper and the composite layer thickness of a typical aircraft sandwich panel to reduce the weight gain. However, the modelling approach is based on linear equations and therefore the precision of the approximation still has to be checked on different examples. In the next steps different design parameters like filling ratio and area of application shall be studied. Finally, a design of experiments, can be used to enhance the optimization approach in case of large non-linearities, where the coupled systems serves as sampling point for a response surface in areas where the linear approach is not suitable anymore.

REFERENCES

[1] C. X. Wong et al., "*Energy dissipation prediction of particle dampers",* J. o. Sound and Vibration, Vol. 319, 1-2 (2009), pp. 91–118.

[2] J. Oltmann et al., "*Design of Particle Dampers for Lightweight Structures Using Frequency Based Substructuring",* In: Int. Conf. on Noise and Vibration Engineering (ISMA), Leuven, Belgium (2018). (accepted for publishing)

[3] B. Jetmundsen et al., "*Generalized Frequency Domain Substructure Synthesis",* J. o. the American Helicopter Society, Vol. 33, No. 1 (1988), pp. 55–65.

[4] D. de Klerk et al., "*The Frequency Based Substructuring (FBS) Method Reformulated According to the Dual Domain Decomposition Method",* In: Proc. of the XXIV International Modal Analysis Conference (IMAC), St. Louis, MO (2006).

STRUCTURAL SELF-ASSEMBLED POSITIVES ELECTRODES FOR MULTIFUNCTIONAL COMPOSITE MATERIALS.

Karl Bouton[1], Dan Zenkert[2] and Göran Lindbergh[3].
[1] Department of Aeronautical and Vehicle Engineering, KTH Royal Institute of Technology, Sweden, bouton@kth.se
[1] Department of Aeronautical and Vehicle Engineering, KTH Royal Institute of Technology, Sweden, danz@kth.se
[1] Department of Chemical Engineering, KTH Royal Institute of Technology, Sweden, gnli@kth.se

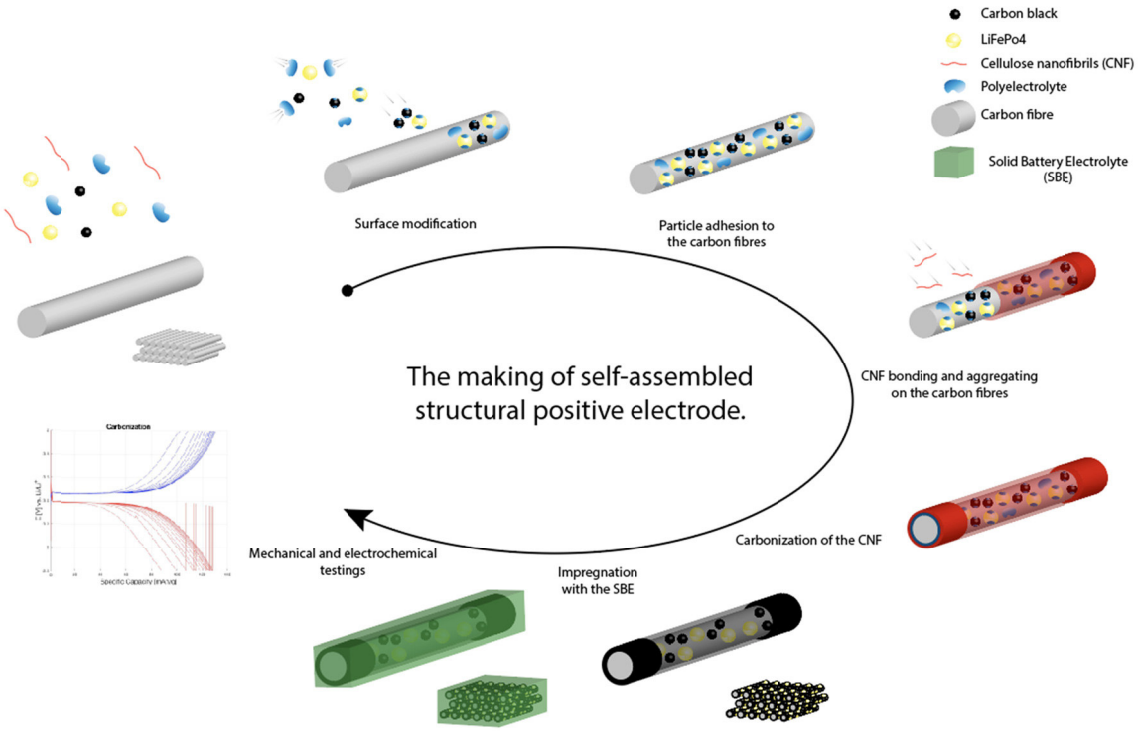

1. INTRODUCTION

The growing interest of the automotive and aeronautical industries for electric vehicles has motivated the development of new structural composite materials, showing energy storage capabilities. These multifunctional composite materials are expected to have a battery function and to carry a mechanical load at the same time. Thus, this kind of multifunctional material could lead to lighter vehicles and aircrafts.

Batteries consist of cells in which a negative electrode, a positive electrode and a liquid electrolyte enable electrochemical reactions (Fig 1.). In the same way, structural batteries are solid-state batteries made of carbon fibres-based electrodes separated by a solid battery electrolyte (SBE). While ordinary carbon fibre tows are used for the negative electrode, the carbon fibres used for the positive side have to be grafted with lithium particles ($LiFePo_4$ in this study), in order to enable electrochemical reactions. $LiFePo_4$ is a very common lithium source and has first been described by Professor John B. Goodenough's research group in the late 90's. In this work, structural positive electrodes have been prepared using an original method, a self-assembly process, and a coating containing $LiFePo_4$ particles have been deposited.

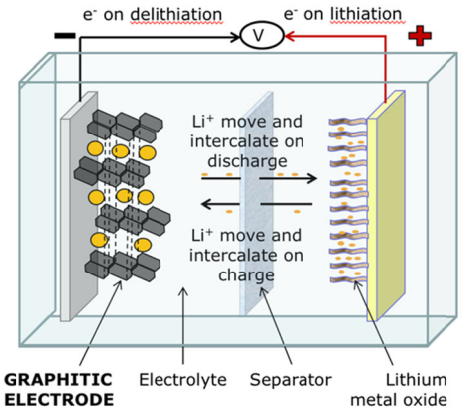

Fig1. Lithium ion battery.

2. SELF-ASSEMBLY PROCESS

The self-assembly process described below is usually used for the growth of nano or micro thin film coating. The deposition can be carried out by spray-coating or by dip-coating. In addition, in this study, cellulose nanofibrils are used as bonding agents. These cellulose nanofibrils are bio-sourced and derives from wood. As a consequence, the use of this material opens new possibilities to make multifunctional composite materials out of sustainable resources.

The substrate used for the self-assembly process is a 12K spread tow of IMS65 carbon fibres. The self-assembly process consists of a first surface preparation of this spread tow and a surface modification of the $LiFePO_4$ particles, using a cationic polyelectrolyte (a positively charged polymer). Then, the samples are dipped into an aqueous solution containing the modified lithium particles. These modified particles bond with the carbon fibres due to the positive charges brought by the polyelectrolyte. The second step consists in dipping the samples in an aqueous solution of cellulose nanofibrils (CNF). The CNF bond and aggregate around the lithium particles, due to electrostatic interactions, creating a gel. The process can be repeated several times depending on the expected coating thickness. Then, the gel is let for drying under air, at ambient temperature. During the drying, the gel turns into a stiff coating containing lithium particles bonded together with CNF's and showing a uniform thickness. However, at this point, the samples cannot be considered as electrodes.

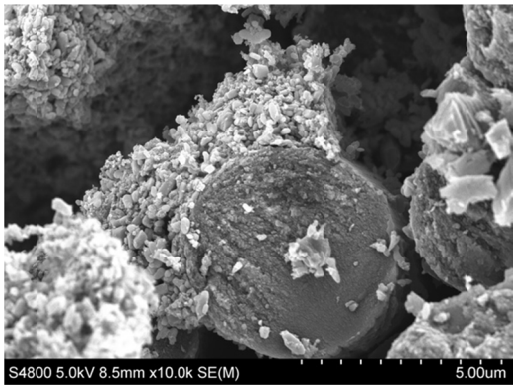

Fig. 2. SEM picture of a carbon fibre coated with LiFePO4 and carbon black particles.

3. POSITIVE ELECTRODES

The next step consists in making structural positive electrodes out of the coated samples presented previously (Fig. 2). With this aim in mind, one must think about removing all the insulating components (CNF and polyelectrolyte) and creating an electrically conductive network between the lithium particles and the carbon fibres. Indeed, lithium particles have to be electrically connected to the carbon fibres in order to enable the circulation of the electrons in the circuit, between the two electrodes. The solution is the carbonisation of the cellulose nanofibrils turning them into an electrically conductive carbon network. In addition, the insulating polyelectrolyte used during the self-assembly is totally burned off during the carbonization process, leaving no insulating component.

In order to characterize the electrochemical properties of the carbonised samples, the resulting positive electrodes have been soaked with a liquid electrolyte and galvanostatic cyclings have been carried out versus lithium metal. As a result, the samples have cycled in a stable way (Fig. 3) and showed a specific capacity of more than 100mAh/g (the maximum reachable specific capacity is about 150mAh/g). However, this measurement lacks accuracy due the complicated $LiFePo_4$ mass assessment and the future work will put the emphasis on this issue. In addition, the same work will be conducted with the thermoset Solid Battery Electrolyte (SBE) developed at KTH [1].

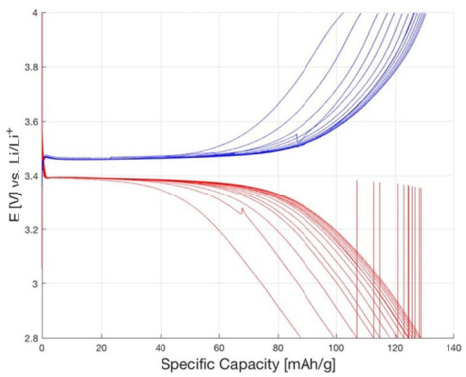

Fig. 3. Galvanostatic cycling of a coated carbon fibres spread tow.

REFERENCES

[1] N. Irhner et al., J. Mater. Chem. A, 2017, 5, 25652
[2] Asp, L. E. et al., Plast. Rubber Compos., 2013, 42, 1–7

Symposium *Lightweight Design in Product Development 2018* (LWD-PD18)
Zurich, Switzerland, 14th–15th June 2018

SMART MATERIAL BASED VARIABLE CONNECTIVITY FOR SHAPE-ADAPTABLE SANDWICH PANELS

Oleg Testoni[1], Andrea Bergamini[2] and Paolo Ermanni[3]
[1] CMASLab, IDMF, D-MAVT, ETH Zurich, Switzerland. testonio@ethz.ch
[2] Acoustics/Noise Control, Department of Mobility, Energy & Environment, Empa, Switzerland. Andrea.Bergamini@empa.ch
[3] CMASLab, IDMF, D-MAVT, ETH Zurich, Switzerland. permanni@ethz.ch

1. INTRODUCTION

This work presents and discusses novel structural concepts for lightweight, shape-adaptable, sandwich panels deploying smart material based variable internal connectivity. As illustrated in the requirement triangle introduced by Campanile in [1], shape-adaptable, lightweight structures suffer from a recurrent problem: on one side, they have to provide sufficient compliance in order to modify its shape; on the other side, they have to be stiff enough to carry operational loads without undergoing excessive deformations. Besides these opposing specifications, the lightweight requirements has also to be met.

In this work, we treat the case of a shape-adaptable, sandwich panel with a truss core and try to overcome the problem of the conflicting requirements applying the concept of smart material based mechanical switch. The latter is namely a mechanical connection between different structural elements based on smart materials that can be activated or deactivated on demand. This concept enables us to modify the internal arrangement of a structure and to increase temporarily its compliance in order to foster shape-adaptation. We expect that further developments of this concept can lead to significant advances towards applications, such as aircraft and/or automotive panels, where the introduction of adaptability and multi-functionality can increase efficiency and performance.

Smart variable connections can be implemented in a composite sandwich panel on three levels: at the interface between core and skin, within the skin and within the core. In this work, we focus on the connectivity of the truss core, investigating the design potential of the integration of smart material based mechanical switches.

2. SMART CONNECTIVITY IN A TRUSS CORE

Having as a reference a sandwich panel with truss core, we imagined substituting the trusses of the core with extendable structures able to be extended or contracted with little force and to hold the new shape thanks to smart materials. A similar concept would allow for a temporary increase in the compliance of the core when actuated, while keeping a predefined stiffness when not. In this way, it would determine a precious advantage for shape-adaptation. Three concepts based on three different smart materials were investigated: the first concept was based on Electro Bonded Laminates (EBL), the second one on Dielectric Elastomer Actuators (DEA), and the third one on Shape Memory Alloys (SMA).

EBL-based mechanical switch

In this concept, the trusses of the core of the sandwich panel would be replaced by smart elements containing an electro-mechanical switch based on EBLs. In order to allow for a significant change in stiffness, we integrated in these smart elements a central region characterized by a two different load paths, which can be selected by activating or deactivating the EBL. The latter is embedded within a host structure and is composed of a thin aluminum lamina and two electrodes glued on the host structure. The lamina itself acts as electrode and overtakes the majority of the force acting on the core element when the EBL is activated. Taking Fig. 1 as a reference, the lamina is glued to the right side of the host structure, while its other extremity is free to slide back and forth in an appositively designed pocket in the left side of the host structure. In this pocket, the end of the lamina is embedded between two layers of dielectric material, which are in turn enclosed by two metallic electrodes directly glued on the host structure to form the EBL. In this way, when the EBL is not activated, the aluminum lamina is free to slide back and forth in the pocket without carry any force; the compliant region of the host structure would, therefore, take up the loads and determine the stiffness of the entire element. On the other hand, when the EBL is activated, the aluminum lamina adheres to the walls of the pocket, taking up the majority of the load and increasing noticeably the overall stiffness.

A prototype was fabricated and tested. The host structure was 3D printed in PLA with the FDM printer Ultimaker 2+. The aluminum lamina was cut out from a 50 µm thick foil, while the electrodes were realized attaching aluminum tape Amucor (4702) from Holland Shielding Systems on the host structure. This resulted in total contact surface of 4 cm^2. As dielectric material we used a 25 µm thick Kapton foil. Tensile tests were performed to characterize the behavior of the EBL switch. All tests were performed in displacement-controlled mode at a speed of 20 mm/min on the universal testing machine Zwick/Roell Z005 AllroundLine. Each measurement was repeated 5 times at 0 V and 2000 V. The high voltage power supply model PS350 from Stanford Research System. Inc. was used to apply the voltage. The test carried out on the EBL-based mechanical switch showed high consistency, as at each voltage all different measurements

returned almost the same values. As expected, at 2000 V the clamping force of the switch was higher than at 0 V, resulting in a maximum difference in clamping force achieved by the system of about 1.15 N. This means that the maximum shear force transferred by the EBL amounts to 2.8 kPa.

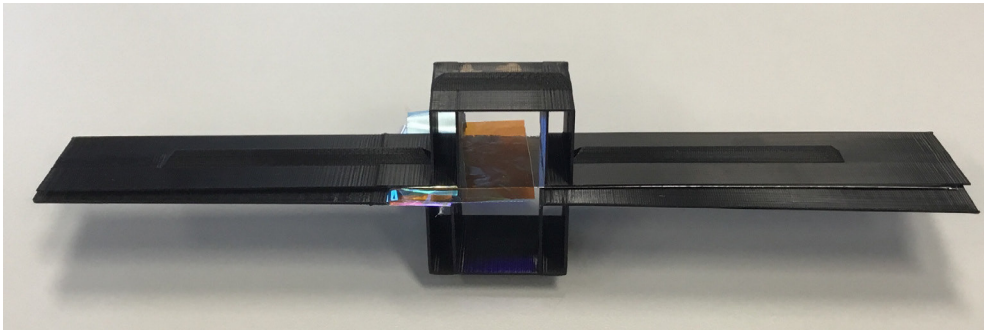

Fig. 1: EBL-based mechanical switch used in the experiments.

DEA-based mechanical switch

The second concept investigated replaces the core trusses with two small hollow cylinders with a clamping system based on DEAs. This concept recalls the idea presented by Onoda [2], who conceived a system composed of two hollow elements clamped one inside the other, where the inner element contains a piezo stack. By making the piezo stack expand or contract, Onoda managed to control the friction force between the two cylinders and to vary the stiffness of the system.

In our concept, we substitute the piezo stack with a DEA, whose much higher strain enables us not only to control the friction, but also to clamp or unclamp the two halves of the switch. The DEA is controlled through a voltage: when no voltage is applied, the DEA is compressed inside the inner element, preventing the relative displacement of the two halves. On the other hand, when a voltage is applied, the DEA contracts, reducing the stress on the walls of the inner element and releasing the clamping.

A DEA-based switch was manufactured for testing. The hollow structures were 3D printed in PLA using the FDM printer Ultimaker 2+ and designed to apply a precompression of 2 mm to the DEA. The latter was a silicon based DEA supplied by Compliant Transducer Systems GmbH and had size 16 x 16 x 22 mm^3. In order to characterize the behavior of the switch, we carried out tensile tests with the universal testing machine Zwick/Roell Z005 AllroundLine. All measurements were performed in displacement-controlled mode at a speed of 20 mm/min and repeated 5 times. The DEA was actuated at a nominal voltage of 1400 V, as indicated by the manufacturer. The voltage was applied with the high voltage power supply model PS350 from Stanford Research System. Inc. The carried out measurements showed high consistency and returned that a difference in clamping force of about 30 N is achievable with a precompression of 2 mm.

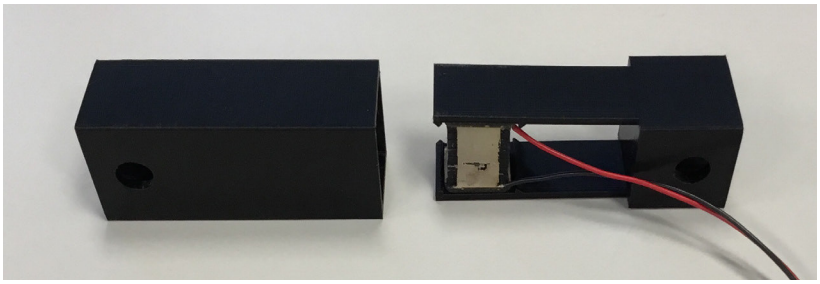

Fig. 2: DEA-based mechanical switch used in the experiments.

SMA-based mechanical switch

We conceived two concepts of mechanical switches based on SMAs. In a similar way to the DEA-based switch presented above, these are made up of two elements able to slide one inside the other, which can be clamped or unclamped on demand. In this specific case, the variable connection is actuated by SMA wires, whose contraction deforms the particular geometry of the inner element, determining an increase or a reduction of the clamping force, respectively.

For this concept, two versions were derived. The first version was designed in a way that, when the SMA wires are not activated, the two halves of the switch are free to move one inside the other. The activation of the SMA wires makes the deformable part of the inner element expand in vertical direction. In this way, it enters in contact with the inner walls of the outer part and clamps the two halves together. On the other hand, in the second version the two halves are normally clamped and the SMA wires are used to release the clamping.

Both versions were 3D printed in PLA with the FDM printer Ultimaker 2+. The SMA wires used were Ni–Ti wires with a diameter of 0.63mm. The two versions of the SMA-based mechanical switch were tested. The SMA wires were

connected to the DC power supply E3631A from Keysight and a current of 2 A was applied. This heated the SMA wires up to the temperature, where the austenite-martensite phase transformation takes place and the material contracts. The measurements carried out on the first version of the SMA-based mechanical switch showed a force difference between on- and off-state of about 15 N, whilst for the second version the force difference was about 8.5 N.

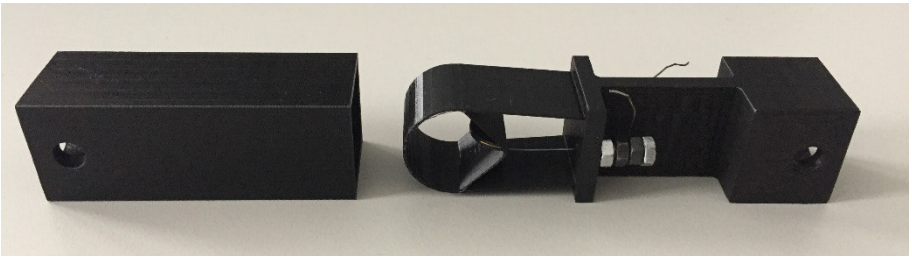

Fig. 3: SMA mechanical switch used in the experiments.

3. CONCLUSIONS

Based on the results of the tests carried out and on the experienced gained while designing and manufacturing the prototype of the mechanical switches presented, the following conclusions were drawn.

EBL-based mechanical switch

We verified the working principle of the EBL-based mechanical switch. Nevertheless, the maximum transferred force measured resulted one order of magnitude lower than what expected. Despite being a very lightweight solution, this concept shows the drawbacks of EBLs already highlighted by Di Lillo [3], suffering from charge injection and being very sensitive towards air gaps and misalignments of the electrodes. For this reason, a high precision in the manufacturing may not being sufficient for a proper functioning of the switch, as torsional moments and bending loads may lead to out-of-plane deformations of the switch and misalign the electrodes.

DEA-based mechanical switch

The DEA-based mechanical switch showed the best performance among the switch concepts tested, achieving a difference in clamping force of 30 N. Being mainly made out of silicone, DEA are lightweight, easy to integrate in a switch and can be controlled simply via an electrical input [4]. The main limitation comes from the size of the DEA, as it determines the maximum contraction and the maximum force that can be achieved. This prevents de facto their use in small structures, if high displacements or high forces are required.

SMA-based mechanical switch

The SMA-based mechanical switches are also very interesting concepts, as they showed the potential to achieve relatively high blocking force differences, while keeping a low weight. The large deformations that SMA wires can achieve and the high forces that they can generate make SMA well suited for mechanical switches. Furthermore, SMA wires can be easily integrated in small structures. Nevertheless, SMA wired require to be restretched after every actuation cycle: a specific system has, therefore, to be designed and integrated in the switch. Another drawback is the heat generated by the actuation of the wires, which has to be dissipated quickly in order to reduce the duration of the actuation cycle. Nevertheless, these two points can be solved with an appropriate design, making this solution attractive for the implementation in real panels.

REFERENCES

[1] Campanile LF. Adaptive structures: engineering applications. Chichester, West Sussex: JohnWiley , 2007

[2] Onoda et al., “Vibration Suppression by Variable-Stiffness Members”, *AIAA Journal*, no. 6, June 1991; volume 29.

[3] Di Lillo et al., “Tuning the mechanical behaviour of structural elements by electric fields”, *Appl. Phys. Lett.*, 102, 224106 (2013).

[4] Giousouf et al., “Dielectric elastomer actuators used for pneumatic valve technology”, *Smart Mater. Struct.,* 22 (2013) 104010 (6pp).

Symposium *Lightweight Design in Product Development 2018* (LWD-PD18)
Zurich, Switzerland, 14th–15th June 2018

ADJUSTABLE IMPEDANCE ELEMENTS FOR TESTING AND VALIDATION OF SYSTEM COMPONENTS

Emil Heyden[1], Andreas Lindenmann[2], Jan Oltmann[1], Tim Bruchmüller[2], Dieter Krause[1], Sven Matthiesen[2]
[1] Hamburg University of Technology (TUHH),
PKT - Institute of Product Development and Mechanical Engineering Design
Denickestr. 17, 21073 Hamburg, Germany
e-mails: emil.heyden@tuhh.de; j.oltmann@tuhh.de; krause@tuhh.de
[2] Karlsruhe Institute of Technology (KIT),
IPEK - Institute for Product Engineering
Kaiserstr. 10, 76131 Karlsruhe, Germany
e-mails: andreas.lindenmann@kit.edu; tim.bruchmueller@kit.edu; sven.matthiesen@kit.edu

1. INTRODUCTION

To continuously certify a design in the product development process, the validation is an essential step [1, 2]. The mechanical boundary conditions of systems under dynamic loads must be carefully modelled in order to receive utilizable results and to realistically reproduce the system's operation environment [3, 4]. These boundary conditions are represented by the interface elements between the structure and its environment. To replace this environment in a test rig, the interface elements must provide the same dynamic boundary conditions, such as stiffness and damping, as the lightweight structure's environment interface [3, 4].

Two systems, which show sensitivity to interface dynamics are lightweight aircraft interior systems and power tools [3, 4]. State of the art in validation of models for aircraft interiors is to design connections like joints and fixtures as stiff as possible, to neglect their dynamic influence. These discrepancies in interface properties can lead to deviations in the system behavior between the real system and the test system. To avoid those deviations, it is possible to design the connection elements individually for each test case, which leads to extensive experimental testing. Power tools are systems, which show a high degree of interactions with adjacent systems like the user and the environment. Due to the elastic and highly damped interaction with the human arm system, power tools cannot be clamped stiffly to test benches. Matthiesen shows that the user influences the function of the power tool and therefore has to be modelled in test bench experiments [5].

Interface elements with adjustable stiffness and damping can tackle these deficiencies. This contribution aims at the approach to develop Adjustable Impedance Elements (AIEs). An AIE is a machine element consisting of an Adjustable Stiffness Element (ASE) and an Adjustable Damping Element (ADE). An exemplary AIE, namely the AIE Uno, developed by Product Development Group Zurich is given in Figure 1. The AIE Uno consists of an Adjustable Stiffness Mechanism (ASM) and an Adjustable Damping Mechanism (ADM) [6]. With the use of AIEs as test bench interfaces it is possible to adjust the dynamic properties of the test system, this enables more realistic tests and decrease the amount of testing.

Fig. 1: AIE Uno consisting of an Adjustable Stiffness Mechanism (ASM) and an Adjustable Damping Mechanism (ADM) [6]

The AIProVE (Adjustable Impedance Elements for Product Validation in Compliant Environments) project, funded by DFG and SNF, aims to develop AIEs for dynamic test rigs. This contribution is part of the AIProVE project at the pd|z (Product Development Group Zurich at ETH Zurich – Univ.-Prof. Dr.-Ing. Mirko Meboldt), IPEK (Institute of Product Engineering at Karlsruhe Institute of Technology – Univ.-Prof. Dr.-Ing. Sven Matthiesen) and PKT (Institute for Product Development and Mechanical Engineering Design at TUHH -Univ.-Prof. Dr.-Ing. Dieter Krause).

2. CURRENT STATE OF ADJUSTABLE IMPEDANCE ELEMENT DEVELOPMENT

The issues described show the necessity for the use of AIEs. So far, in research a large variety of different ASEs and ADEs have been investigated. However, little research addressed the combination of both elements into AIEs. The working elements can be subdivided into active and passive elements. Active elements, which are implement in closed loop control systems and are not suited for high frequency applications. Therefore, the focus of this project is on passive systems. The following section will give a brief introduction in ASEs and ADEs. An extensive overview is given by van Ham et al. [7], Tagliamonte et al. [8] and Vanderborght et al. [9].

Most ASE working principles are based on elastic deformation. As a brief excerpt, the adjustment of stiffness properties can be achieved by pretensioning antagonistic springs with nonlinear characteristic, configuration change of springs, change of spring angles or biaxial loading of elastomer foam. Besides elastic deformation other technologies like for instance magnetostrictive or piezoelectric transducers have been investigated. The different working principles show individual restrictions in their application. The majority of ADEs are working based on one of the following working principles: fluid friction, dry friction, eddy current or magnetorheological fluid. The adjustment of fluid and dry damping is usually still realized mechanically. Eddy current and magnetorheological fluid dampers adjust the damping by changing the magnetically field. Similar to ASEs the different working principles of ADEs show limitations in their suitability for AIE use, like for example nonlinear behavior in dry friction or the dependence on large relative velocities in eddy current principles.

With Adjustable Impedance Elements in system testing and validation, mechanical interface properties can be created more accurate. Furthermore, the quick and easy adjustment of interface stiffness and damping can enable and accelerate new findings for product development. The current state of development of AIEs is limited to very specialized applications of either ASEs or ADEs and only a few mechanisms combine both principles. However, known AIEs with adjustable stiffness and damping are not widely available and do not meet the demands of the aircraft interior and power tool test environment.

3. REQUIREMENTS ON ADJUSTABLE IMPEDANCE ELEMENTS

In order to develop AIEs, which are suitable for aircraft interior and power tool testing requirements on the AIE have to be derived from the application and test scenarios.

Aircraft interior testing is one test scenario which is studied at the Hexapod test rig at the TUHH (Figure 2 a)). The dynamic behavior of the system depends significantly on the connection properties between the lightweight structure and its environment [3]. To replace this environment in a test rig, the connection elements must provide the same dynamic boundary conditions as the lightweight structure's environment interface [4]. Joints and fixtures are two types of connection elements for aircraft interiors. The dynamic behavior of aircraft interior is highly affected by different environments such as joint type, loading, excitation frequency, airframe position [4]. In aircraft interior testing at the Hexapod test rig high loads with low frequency can be observed, which imposes a requirement on AIEs that cannot be met yet. Usually these connection elements are designed as stiff as possible to neglect their influence. This leads inevitably to deviations, since the impedance of the test rig is different from that of the system's operation environment. To avoid these deviations and create realistic boundary conditions, the connection elements have to be designed individually for each test case. The influence of a new design is not exactly known beforehand, which makes experimental testing even more extensive. Connection elements with adjustable stiffness and damping could lead to more realistic evaluation of lightweight structures and to less extensive experimental testing [3].

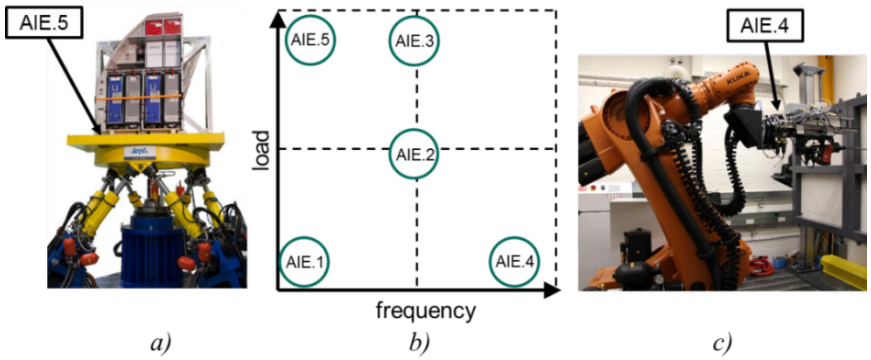

Fig. 2: Variety of AIE prototypes for different application scenarios defined by level of load and level of frequency.

In the validation of power tools technically relevant surrounding systems are the user and the environment [3]. The interactions between the power tool and the user have been subject of research for many years. A significant amount of research focuses on the influence of the power tool on the user and possible health-related consequences that result from the vibration exposure on the human hand-arm system. However, research has shown that the user has an influence on the power tool's function [5]. Due to the heterogeneous nature of the human body the user influence can scatter greatly

and is therefore a factor of uncertainty in product development and validation. In order to model the passive user influence (vibrational properties) the so-called mechanical driving point impedance is used, which is a complex frequency-based description of the hand-arm dynamics [10]. From the knowledge of the mechanical impedance, simulation models as well as mechanical hand-arm models can be derived. With mechanical hand-arm models power tools can be validated in a reproducible test environment without neglecting or modeling the user influence inaccurately. However, the mechanical impedance and thus the derived models are greatly affected by influencing factors like for instance the direction of vibration excitation on the hand or the body posture. Existing simulation and mechanical hand-arm models are therefore being only valid for one specific application, hand-arm system and power tool and often show the need for a lightweight design due to small dynamic masses in hand-arm vibration. Furthermore, a challenge in hand-arm model development for power tool testing are small forces with high frequency, which can cause inaccuracies in model behavior due to nonlinearities (e.g. static-dynamic transition in dry friction). Therefore, an aim of current research is the development of lightweight hand-arm models with adjustable model parameters (e.g. stiffness, damping) with the use of AIEs (Figure 2 c)).

These two validation environments show the need for AIEs in different testing environments to make testing more realistic and therefore is combined in a joint research project between the mentioned institutions.

4. DEVELOPMENT STRATEGY OF ADJUSTABLE IMPEDANCE ELEMENTS FOR DYNAMIC TESTING

This chapter will summarize and describe the steps in developing a set of AIEs for implementation on test benches. In Figure. 3 a short overview is given, to illustrate the work packages.

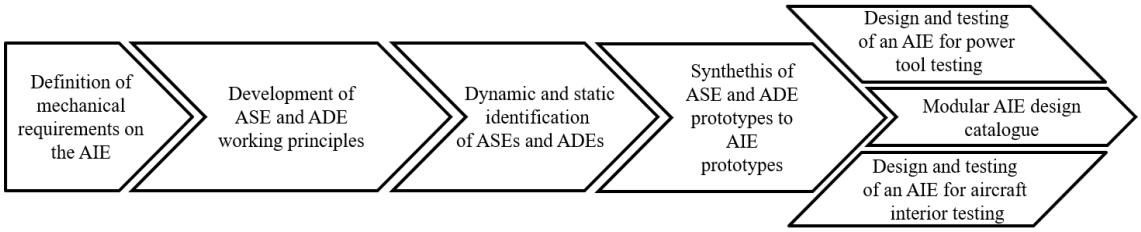

Fig. 3: Development strategy of AIEs for dynamic testing.

At first the technical requirements in terms of maximum loads and frequencies for the AIEs will be determined. Considering the requirements at total of four ASEs and four ADEs will be developed. Validation has to be a continuous process [1, 2] and therefore is conducted at each step in the development process by comparing the prototypes performance with the requirements. Since not all working principles of ASEs and ADEs are compatible a synthesis into AIE prototypes will be conducted, which results in five functional prototypes for the different application scenarios (Figure 2 b)). In order to demonstrate the capabilities of AIEs two prototypes will be implemented in existing test benches for aircraft interior and power tool testing. For both application scenarios different requirements have to be fulfilled. The performance of the AIE for high forces and low frequencies is studied at the at the Hexapod test rig at the PKT (AIE. 5 in Figure 2 b)) whereas the AIE for low forces and high frequencies is tested in the power tool test lab at the IPEK (AIE. 4 in Figure 2 b)). In the end of the project, the results will be summarized and guidelines for designing and dimensioning AIEs will be released in a modular design catalogue in order to support scientists researching AIEs as well as scientists requiring specific AIEs for their work. Furthermore, by findings through test bench experiments with the two advanced AIEs new guidelines for aircraft interior and power tool tests will be developed based on the possibility to use AIEs.

REFERENCES

[1] Lindenmann, U., “Handbuch Produktentwicklung”, *Münchner Hansa,* 2016, p. 541-569
[2] Albers, A., “Five Hypotheses about Engineering Processes and their Consequences”, *Proceedings of the TMCE,* 2010
[3] Bruchmueller, T. et al., “An Adjustable Impedance Element – System Requirements and Design Approach”, *26. DfX-Symposium*, 2015.
[4] Seemann, R. et al., “FE-Modelling Guidelines for the Dimensioning of Aircraft Cabin Interior Un-der Stationary Dynamic Loads”, *29th Congress of the International Council of Aeronautical Sciences (ICAS)*, 2014.
[5] Matthiesen, S. et al., “Der Mensch als zentrales Teilsystem in Wechselwirkung mit handgehaltenen Geräten- ein problemorientierter Ansatz zur Untersuchung dieser Schnittstelle”, *25. DfX-Symposium,* 2014
[6] Stuecheli, M. et al., “Work Density Analysis of an Adjustable Stiffness Mechanism”, *IEEE Int. Conf. Robot.Autom,* 2016, 2322: p. 91-106
[7] van Ham, R. et al., “Compliant actuator designs”, *IEEE Robot. Automat. Mag,* 2009; 16(3): p. 81-94
[8] Tagliamonte, N. et al., “Double actuation architectures for rendering variable impedance in compliant robots”, *Mechatronics,* 2012; 22(8): p. 1187-1203
[9] Vanderborght, B. et al., “Variable impedance actuators: A review”, *Robotics and Autonomous Systems,* 2013; 61(21): p. 1601-1614
[10] Matthiesen, S. et al., “Anforderungen an ein Messsystem zur Ermittlung der Rotationsimpedanz von Hand-Arm Systemen”, *7. VDI-Tagung Humanschwingungen,* 2018, 2322: p. 91-106

Symposium *Lightweight Design in Product Development 2018* (LWD-PD18)
Zurich, Switzerland, 14th–15th June 2018

OPTIMIZATION OF HONEYCOMB SANDWICH STRUCTURES JOINTS WITH ADDITIVELY MANUFACTURED CORES

Johann Schwenke[1] and Dieter Krause[1]
[1] Hamburg University of Technology (TUHH)
Institute of Product Development and Mechanical Engineering Design (PKT),Germany.
johann.schwenke@tuhh.de and krause@tuhh.de

1. INTRODUCTION

Honeycomb sandwich structures are often used for aircraft cabin interior, such as galleys, lavatories or partitions, because of their excellent weight specific material properties. Weak spots are the load introduction points, since the honeycomb core cannot absorb the local forces respectively introduce them properly into the thin top layers. Therefore, local reinforcements, so-called inserts, are used, which are usually glued into cutouts in the core [1], [2]. In the manufacturing process, a distinction is made whether the insert is bonded during the production of the sandwich panel (hot bonded) or is installed after the production of the sandwich panel (cold bonded) [3], [4], [5].

In the development and optimization of the insert joints, the diameters of the cylindrical inserts or the surrounding potting compound are often varied to increase the pull-out strength [6]. If higher strengths are required hard tissue blocks need to be used. This further increases the mass of the structure. Due to the large number of inserts in the aircraft cabin there is a high potential for targeted weight reduction.

2. OPTIMIZATION

One way to reduce the structural weight while maintaining the same functionality is to optimize the topology of the inserts starting from the original design space and manufacture them using 3D printing. By virtue of cavaties in the inner structure instead of full material it is possible to reduce the weight of the insert or to increase the diameter without increasing the weight. Another option is to change the common cylindrical shape of the insert to a more complex geometry, for example a star shape. These modifications change the distribution of the mass and the shape of the interface to the surrounding honeycomb core structure. The goal is to increase the surface of the interface without increasing the weight or to use the same surface of the interface by reducing the weight.

Besides the possibility to optimize the inserts additive manufacturing also allows to optimize the global core structure. Under the keyword hierarchical honeycombs there are plenty examples in the literature, where additively manufactured core structures are derived and tested instead of the classic honeycomb cores [7], [8], [9], [10], [11].

New optimization approach

An even higher potential to reduce weight offers a new design procedure which contemporaneous integrates the insert more directly into the core structure. The ultimate goal is to combine the both approaches, which means that the global core structure and the local core structure at the load introduction points is optimized an additively manufactured. For the moment the focus is on the local load-path optimization at the load introduction point. For the global structure a conventional honeycomb structure with a constant cell size is used. Oltmann et al. showed that an adaptive core, where the diameter of the honeycomb cells decrease in direction of the load introduction point, increase the weight specific stiffness and strength [12]. Schwenke et al. used different numerical optimization methods to receive a load-path optimized design and showed how initial and boundary conditions influence the design [13].

The aim of this paper is to present how numerical optimization especially topology optimization and new design possibilities through additive manufacturing can be used for structural improvements of the load introduction into honeycomb sandwich structures (Figure 1).

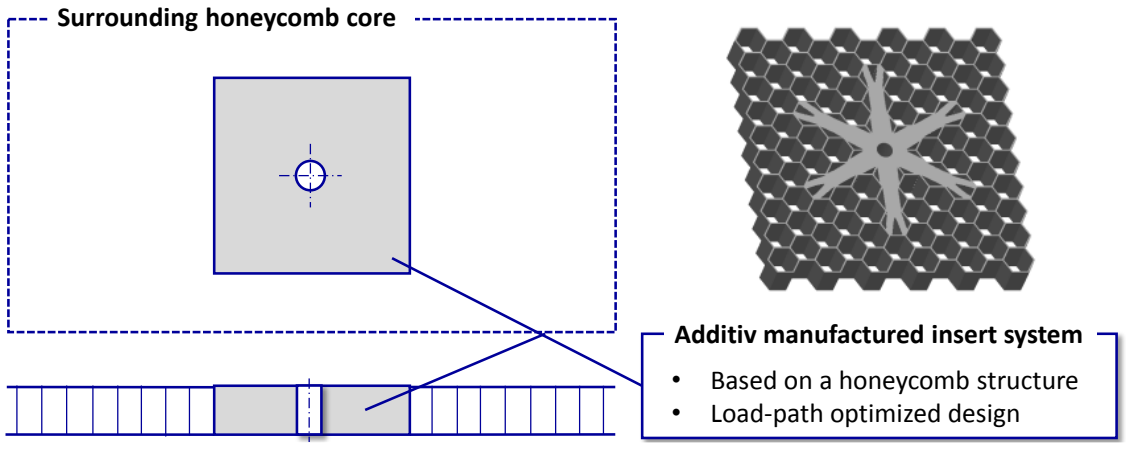

Figure 1: Additive manufactured insert system

Therefore, optimizations of an insert system under in-plane and out-of-plane loads are performed and analyzed. The most important initial and boundary conditions are summarized and the influence of different test conditions between simple standard tests and real life applications are discussed. Furthermore it will be shown how the additive manufactured insert system based on a honeycomb structure and a load-path optimized design (Figure 1) can be expanded to an additive manufactured insert system with multiple load introduction points (Figure 3). The aim of the paper is also to point out which particular aspects have to be taken into account to transfer the results to larger panel structures and which challenges arise when several side-by-side inserts are optimized simultaneously.

3. INITIAL AND BOUNDARY CONDITION

The influence of the most important initial and boundary conditions for numerical optimizations are summarized in Figure 2.

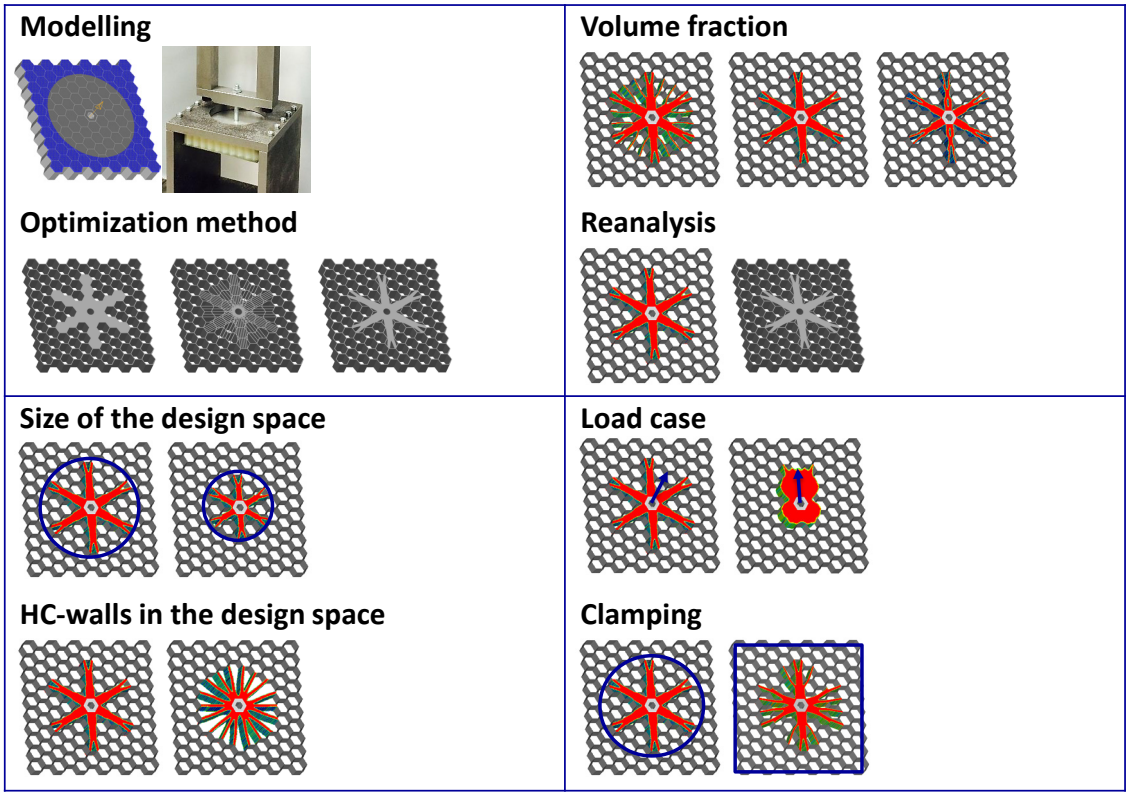

Figure 2: Influence of initial and boundary conditions

It is obvious that the modelling and the chosen optimization method have an influence on the optimization result. Furthermore a change of the size and structure of the design space will lead to different designs. Also the chosen optimization method itself has some decisive boundary conditions for example the remaining volume proportion after a topology optimization, or the simple fact that a reanalysis of the optimization result is necessary to derive a final design. Furthermore, the test conditions like the applied load and the clamping have an influence on the result. These both aspects will be discussed in the next section in more detail. With the pull-out test and the shear test as described in the handbook of insert construction there exist quasi standard test methods for insert in sandwich structure [14].

Load case

The two most important load cases for inserts in sandwich structures are out of plane load and in-plane load which are tested via a pull-out test respectively a shear-test. For the considered use case the pull-out test is more important than the shear test because under in-plane load the forces can be direct introduced into the facesheets, which are in this case parallel to the direction of the load. In real life application there is rarely a pure in- or out of plane load direction instead there is most time a combination of both load case.

The test results show that it is more important to optimize the structure in a pull-out test, because the derived design performs quite well under shear load. Especially when a symmetrical insert should be use, there is almost no difference between the designs from a combined load direction compared to the result from a pull-out test. There is some additional potential, if the exact direction of force is considered during the optimization and through additive manufacturing the production of such individualized insert is possible. One occurring problem is to validate such a design with the simple standard test another is the higher complexity of the manufacturing process, because in this case the orientation of the insert plays a very important role.

Clamping

Additionally, the shape of the clamping has an impact on the optimization result. The derived design varies if the clamping of the standard test is changed. For example is the design derived from a pull-out test with a circular hole and a pull-out test with a square shape totally different (Figure 2). In real life applications there does not exist a clamping around the insert the panel is only connected at some point to other panels or parts. Therefore, an optimization with the real test conditions is very expensive, but necessary to derive a load-path optimized design. If the additive manufactured insert system is extended to multiple nearby load introduction points so that it becomes advantageous to optimize them simultaneously. The emerging problem is that the design space becomes bigger than the opening in the standard pull-out test and the optimization results are not applicable anymore.

Multiple Inserts

In Figure 3 a first load-path optimized design for an additive manufactured insert system is shown which is based on a honeycomb structure and has multiple load introduction points whose positions are flexible.

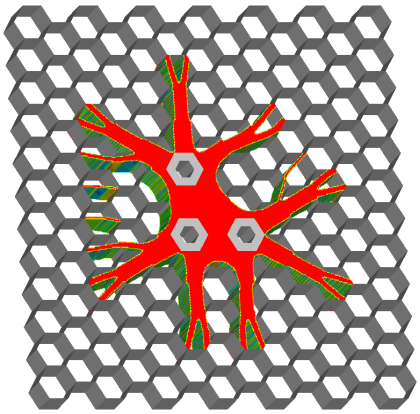

Figure 3: Insert system with multiple load introduction points

The problem is that there are no real standard tests for inserts and the common test are too far away from real life applications, so that they are not suitable for an optimization of the insert. The challenge is therefore to derive and define a test especially for multiple insert concepts. Requirements are that it should be possible to carry out the test with little effort, but consider nevertheless the installation situation, the load directions, symmetry conditions and multiple load-introduction points to ensure that the insert is not only optimized for the standard test but also for the actual application.

REFERENCES

[1] Bitzer, T.: „Honeycomb Technology: Materials, Design, Manufacturing, Applications and Testing", Chapman & Hall, London, 1997.

[2] Zenkert, D.: „The Handbook of Sandwich Construction", Engineering Materials Advisory Services Ltd., Worcestershire, 1997.

[3] Lim, J. W. and Lee, D. G.: „Development of the hybrid insert for composite sandwich satellite structures", in: Composites Part A: Applied Science and Manufacturing, Volume 42, Issue 8, 2011, p. 1040-1048.

[4] Bianchi, G., Aglietti, G. p. and Richardson, G.: „Static performance of hot bonded and cold bonded inserts in honeycomb panels", in: Journal of Sandwich Structures and Materials, Volume 12, 2010, p. 59-82.

[5] Thomsen, O. T.: „Sandwich plates with 'through-the-thickness' and 'fully potted' inserts: evaluation of differences in structural performance", in: Composite Structures, Volume 40, Issue 2, 1998, p. 159-174.

[6] Raghu, N., Battley, M. and Southward, T.: „Strength variability of inserts in sandwich panels", 8th International Conference on Sandwich Structures ICSS, 2008.

[7] Mousanezhad, D., Ebrahimi, H., Haghpanah, B., Ghosh, R., Ajdari, A., Hamouda, A.M.S. and Vaziri, A.: „Spiderweb honeycombs", in: International Journal of Solids and Structures, Volume 66, 2015, p. 218–227.

[8] Sun, Y., Wang, B., Pugno, N., Wang, B. and Ding, Q.: „In-plane stiffness of the anisotropic multifunctional hierarchical honeycombs", in: Composite Structures, Volume 131, 2015, p. 616–624.

[9] Taylor, C. M., Smith, C. W., Miller, W. and Evans, K. E.: „Functional grading in hierarchical honeycombs: Density specific elastic performance", in: Composite Structures, Volume 94, Issue 8, 2012, p. 2296–2305.

[10] Ajdari, A., Jahromi, B. H., Papadopoulos, J., Nayeb-Hashemi, H. and Vaziri, A.: „Hierarchical honeycombs with tailorable properties", in: International Journal of Solids and Structures, Volume 49, Issue 11-12, 2012, p. 1413–1419.

[11] Oftadeh, R., Haghpanah, B., Vella, D., Boudaoud, A. and Vaziri, A.: „Optimal Fractal-Like Hierarchical Honeycombs", in: Physical Review Letters, Volume 113, Issue 10, 2014.

[12] Oltmann, J., Seemann R., Spallek, J. and Krause, D.: „Additively Manufactured Components for Structural Applications in Aircraft Interior – Two Case Studies", 27. DfX-Symposium, Institute of Product Development and Mechanical Engineering Design, Hamburg University of Technology, 2016.

[13] Schwenke, J., Oltmann, J. and Krause, D.: „Optimierung der Verbindungsstellen von Sandwichstrukturen mit additiv gefertigtem Kern", 28. DfX-Symposium, Institute of Product Development and Mechanical Engineering Design, Hamburg University of Technology, 2017.

[14] ESA Requirements and Standards Division: „Space Engineering: Insert design handbook", ECSS, Noordwijk, 2011.

Symposium *Lightweight Design in Product Development 2018* (LWD-PD18)
Zurich, Switzerland, 14th–15th June 2018

DESIGN AUTOMATION FOR ADDITIVE MANUFACTURING APPLIED TO BRANCHED FLUID FLOW STRUCTURES

Manuel Biedermann[1], Manuel Schoen[1] and Mirko Meboldt[1]
[1]Product Development Group Zurich (pd|z), ETH Zurich, Switzerland, manuel.biedermann@mavt.ethz.ch

1. INTRODUCTION

Additive manufacturing (AM) offers a large degree of design freedom but requires a deep understanding regarding design, process and material characteristics [1]. To increase the accessibility for valuable AM applications, design automation aims at capturing the required know-how and implementing the design generation for recurring tasks. In the field of design optimization and design for AM (DfAM), many methods follow this basic idea such as topology optimization or automated generation of lattices for lightweight designs [2, 3]. However, with the rise of novel AM applications an automated design approach may also be extended to many other disciplines, applications and design principles in addition to pure lightweight structures. This work presents a procedure for automating the generation of branched flow structures used for fluid distribution between a source and multiple points. The approach first constructs the topology of a branched network applying a heuristic rule. It then optimizes its shape utilizing optimality criteria for branching angles and pipe diameters. After providing background information on the optimality criteria in section 2, the work presents the method with a simple example in section 3. The work discusses the method in the context of design automation for AM in section 4 and concludes with a summary and outlook in section 5.

2. OPTIMALITY CRITERIA FOR FLUID BRANCHING

Branched flow structures occur in natural and technical systems for the distribution of a fluid from a source to multiple end-points under a minimized pressure loss or required pump power [4, 5]. Fig. 1 (A) highlights the advantage of using a branched flow structure for the example of distributing a fluid from a source S on a circle center to N end-points P_j with index j lying on the circle. For the case of N = 24, three different pipe networks with equal volume are depicted. A simple solution is to use N radial pipes without branches (bifurcation level B = 0) to connect source and end-points, which requires pump power W_{radial}. As illustrated in Fig. 1 (A) the pump power W can be greatly reduced using a branched flow network of pipes (B = 2 or B = 3). In comparison to the radial configuration (B = 0), the fluid flow is bundled in pipes with a larger diameter and not guided in separate pipes with a smaller diameter.

The topology of a branched fluid network is described through the connectivity between source S, end-points P_j and the utilized branching points. As shown in Fig. 1 (B) the shape of a network may be defined through the angles (γ_i, ψ_i, ϕ_i) at every branch with index i and the diameter of D_e of each pipe segment with index e. Given the fluid properties, optimality criteria can be derived for an optimized network shape with Y branches that minimizes the required pump power [6, 7]. These optimality criteria are generic and applicable for arbitrary positionings of source S and end-points P_j. In case of laminar flow, the relation between the optimized channel diameter D_e and the mass flow rate $\dot{m}_e$ through channel e follows $D_e \sim \dot{m}_e^{1/3}$. If the flow splits equally at a branch, the relation between the diameter D_1 of the dividing branch with flow rate $\dot{m}_1$ and the diameter D_2 of the two resulting sub-branches with flow rate $\dot{m}_2 = ½\,\dot{m}_1$ is $D_1/D_2 = 2^{1/3}$. For turbulent flow in rough channels the corresponding expressions are $D_e \sim \dot{m}^{3/7}$ and $D_1/D_2 = 2^{3/7}$. Regarding the angles at each bifurcation, it is shown that $\gamma_i \sim 75°$ and $\psi_i \sim \phi_i \sim 142.5°$ require minimal pump power for laminar flow, whereas $\gamma_i \sim 50°$ and $\psi_i \sim \phi_i \sim 155°$ represent optimized angles for turbulent flow in rough pipes.

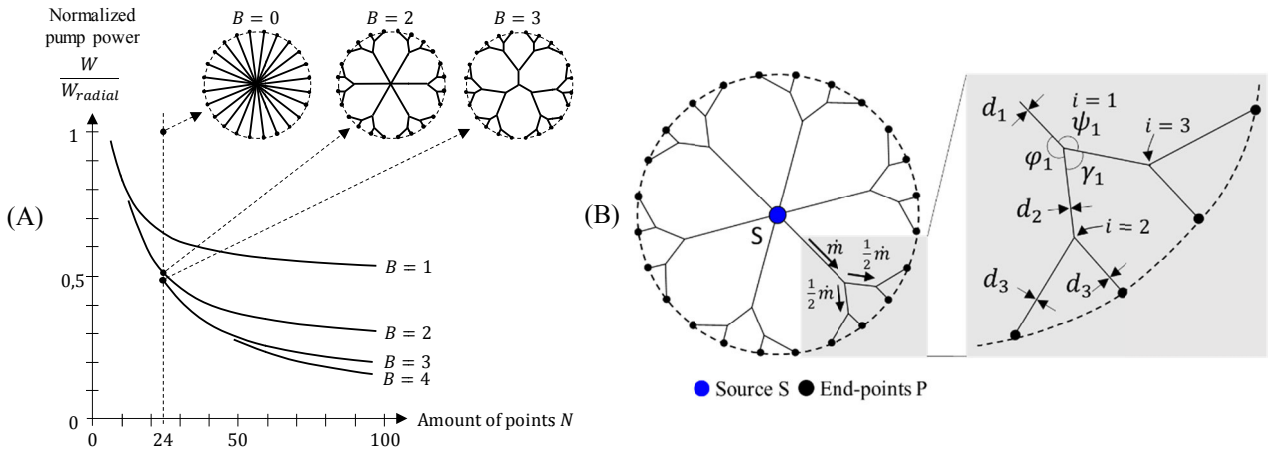

Fig. 1: (A): Comparison of required pump power W for fluid network with radial pipes (branching level B=0, W_{radial}) and branched flow structure (B = 2, B = 3) for the supply to N end-points; (B): Visualization of design parameters (branching angles γ_i, ψ_i, ϕ_i and pipe diameters D_e) used to define optimality criteria for branched flow networks

3. METHOD FOR AUTOMATED DESIGN OF BRANCHED FLUID FLOW STRUCUTRES

The previous section highlights the advantage of using branched flow structures for distributing a fluid under minimized pressure drop or required pump power. The corresponding complex flow networks can be constructed employing the described optimality criteria. To simplify and accelerate the generation of such structures, the basic idea of the presented method is to implement these design principles as an automated design procedure. The individual steps of the method are depicted in Fig. 2 and outlined in the following.

Initial step (1) begins with the specification of the input requirements for the flow distribution task. A user defines the position of source S from which fluid is required to be distributed to a set of end-points P_j. Other specifications include an objective function (e.g. required pump power), a bounding box area A, and fluid properties (e.g. mass flow rate, pipe diameter at source or end-points, laminar or turbulent flow, wall roughness). Fig. 2 visualizes the setup for a simple example using a single source S and five end-points P_j.

Given the position of fluid source S and end-points P_j, step (2) generates an initial topology or layout of the branched flow network. In general, numerous topologies are possible for a given set of end-points P_j. The idea of this method is to generate a topology through a heuristic rule employing Y branches. Different implementations are possible for a heuristic rule. The utilized heuristic rule starts with the end-point P_1 furthest away from the source S, identifies its closest neighbor P_2 and sets a branching point P_{12} in the direction of source S for the formation of a Y branch. This procedure is repeated for the remaining set of points P_j including branching point P_{12} but excluding points P_1 and P_2. Fig. 2 shows the initial layout for the example consisting of four Y branches.

The initial topology defines the basic connectivity of a pipe network for the distribution of the fluid. However, since it is created with a heuristic rule, it does not yet represent an optimized layout. For this purpose, step (3) applies the optimality criteria described in section 2 to define optimized diameters D_e for each pipe and adjust the angles (γi, ψi, ϕi) at each branch. The angles at each branching point are modified applying an iterative procedure, in which the difference between actual angle and prescribed angle is used to move the corresponding branching point. This iterative form-finding procedure leads to an optimized shape of the flow network. For a certain layout, measures such as required pump power or pressure drop can be calculated through analytical formula. In Fig. 2 the adapted layout is shown together with the initial layout depicted with dashed lines.

Based on the optimized layout and derived pipe diameters, step (4) generates the corresponding 3D fluid geometry. The solidification may be achieved using NURBS (Non-uniform rational B-Splines) surfaces or meshes. To further analyze the flow distribution network a computational fluid dynamics (CFD) analysis may be employed in step (5) to fine-tune the shape of the branches, analyze turbulence effects at branches and examine the flow uniformity at the outlets of the end-points. As mentioned in step (2), multiple solutions are possible for the network topology. Depending on the implementation, steps (2) to (5) may thus be repeated for different layouts employing an evolutionary algorithm. The outcome in step (6) represents an optimized, branched fluid structure.

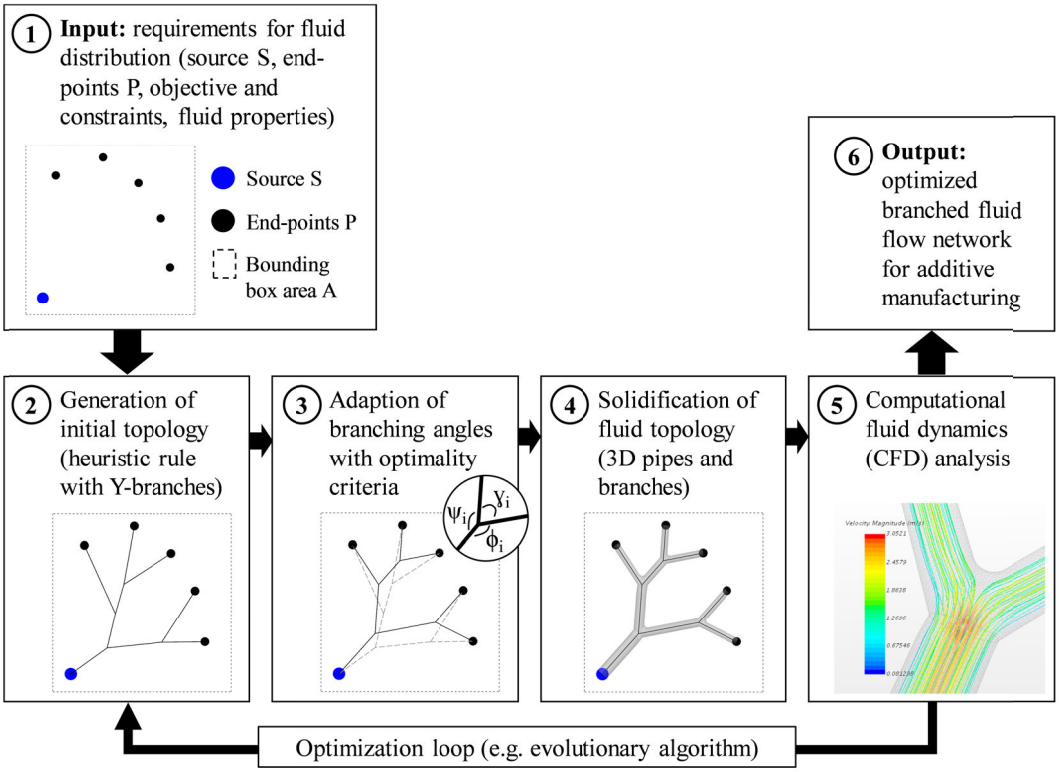

Fig. 2: Method for automated design of branched fluid flow structures

4. DISCUSSION

The described method makes it possible generate branched flow structures for fluid distribution. It is not limited to a plane layout of source and end-points but works also for three-dimensional configurations. As the method is based on a parametric approach, it avoids manual steps such as the reconstruction of a CAD model, which may, for instance, be required for fluid topology optimization. AM processes such as selective laser sintering (SLS) allow fabricating such structures without the need for support structures. For processes such as selective laser melting (SLM) the shape of pipes may be adjusted to elliptical or droplet-shaped cross sections to avoid support structures depending on the chosen build direction. Specific AM manufacturability constraints are yet to be incorporated into the method.

Employing optimality criteria has the advantage that prior knowledge regarding the design solution is used to optimize an initial topology through a simple, iterative scheme. However, the optimized layout usually represents only a local optimum and is strongly dependent on the initial topology and corresponding heuristic rule. Applying an evolutionary algorithm offers the possibility to examine and compare different topologies (local optima) but may lead to an increased computational effort, especially for a larger number of end-points. To further analyze these trade-offs, the method needs to be validated with more complex applications.

The distribution of a fluid flow from a source to multiple end-points represents a frequently required and recurring design task. As parts are usually exposed to multiple requirements from different disciplines, the presented method may be combined with design tools for the generation of lightweight structures. For example, given an optimized fluid distribution network, a structural optimization may be used to cover the fluid network with an optimized, load-carrying material distribution [8].

In a broader context the automated design generation for complex AM structures offers many potentials. By letting a user specify inputs on a high function-driven level, novice CAD users are enabled to create complex structures for AM whereas the design process is accelerated for advanced users. As a result, design automation for AM makes it possible to increase the accessibility for valuable AM applications. Combining such automated design approaches for different design tasks and disciplines offers the possibility to enable users create complex, multi-physics applications for AM.

5. SUMMARY AND OUTLOOK

AM allows fabricating complex structures with a high level of complexity regarding shape, material and functionality. To improve the accessibility for complex and valuable AM applications, it is beneficial to automate the underlying know-how and design process for recurring tasks. As an example, this work presents a method for the generation of branched flow structures. Based on the discussion the method can be further improved regarding several aspects such as employed heuristic rule for topology definition, incorporation of AM manufacturability, evaluation of computational efficiency as well as validation through more complex examples. With the rise of novel AM applications, an automated design procedure seems promising for many different disciplines and design tasks. Possible future directions of research may identify other recurring design tasks, optimality criteria and design principles, useful design patterns and novel mechanisms for AM that can be made easily accessible through an automated design approach.

REFERENCES

[1] D.W. Rosen, “Research supporting principles for design for additive manufacturing”, *Virt. and Phys. Prototyping*, 2014; 9: pp. 225-232.

[2] Y. Tang et al., “A survey of the design methods for additive manufacturing to improve functional performance”, *Rapid Prototyping J.*, 2016; 22: pp. 569-590.

[3] D.W. Rosen, “A review of synthesis methods for additive manufacturing”, *Virt. and Phys. Prototyping*, 2016; 11: pp. 305-317.

[4] V. Fleury et al., *Branching in Nature*, Springer Berlin Heidelberg: 2001.

[5] A. Bejan et al., “Constructal theory of generation of configuration in nature and engineering”, *J. Appl. Phys.,* 2006; 100: 041301, pp. 1-27

[6] L. Gosselin et al., “Tree networks for minimal pumping power”, *Int. J. of. Th. Sci.,* 2005; 44: p. 53-63.

[7] L. Gosselin et al., “Emergence of asymmetry in constructal tree flow networks”, *J. Appl. Phys.,* 2005; 98: p. 9-16.

[8] T. Kamps et al., “Design approach for additive manufacturing employing Constructal Theory for point-to-circle flows”, *Additive Manufacturing*, 2018; 20: p. 111-118.

Symposium *Lightweight Design in Product Development 2018* (LWD-PD18)
Zurich, Switzerland, 14th–15th June 2018

AN EFFICIENT SIZE AND SHAPE OPTIMIZATION OF ADDITIVELY MANUFACTURED LATTICE STRUCTURES SUBJECT TO STRESS AND BUCKLING CONSTRAINTS[1]

Jonas Schwart[2], Kristina Shea[2] and Tino Stanković[2]

[1] This is a conference presentation based on Schwarz, Jonas, et al. *Structural and Multidisciplinary Optimization* (2018): 1-14. https://doi.org/10.1007/s00158-017-1885-z.

[2]Engineering Design and Computing Laboratory, Dept. of Mechanical and Process Engineering, Swiss Federal Institute of Technology (ETH Zürich)
*Corresponding author: schwarjo@ethz.ch

1. ABSTRACT

Additive Manufacturing (AM) offers great capabilities to design complex parts and products that are performance optimized and customized. However, for designers this is highly challenging due to the vast design space of new possible geometries that can be realized using AM. In response to this, the presented research focuses on the development of efficient computational methods and tools for generative design of AM lattice structures; structures that were previously too complex to fabricate but now can be realized using AM. Lattice structures have advantageous strength to weight ratio, they can carry load efficiently and have favorable energy absorption properties, making them interesting for both academia and industry. In the first step of this research an approach for optimization of discrete AM lattice structures using Sequential Linear Programming (SLP) to simultaneously solve a size and shape optimization problem subject to local stress and Euler buckling is proposed. The approach produces the solution incrementally, providing a valid design vector at each iteration step using a first order Taylor expansion for the nodal movement and the buckling constraint. The results show that the proposed approach produces optimized designs that are either close or identical to the solutions obtained by the non-linear problem formulation while significantly decreasing the computational time.

2. INTRODUCTION

An increased interest in structural optimization is observed in the recent decade mostly in response to the advancement in digital fabrication and Additive Manufacturing (AM). Of particular interest in this context are computational approaches for the synthesis of optimized designs that are completely or at least partially realized by a truss structure as a governing design principle. To capitalize on the newly emerged design freedom enabled through AM technologies, challenging structural optimization problems are introduced [2], which to be solved efficiently require a methodological approach through the integration of mathematical programming methods with the engineering design process [3,4,5]. In response to these challenges, the focus of this work is on the extension of Sequential Linear Programming (SLP) for size and shape optimization of discrete truss structures subject to yield stress and local Euler buckling constraints. To both, address the computational efficiency of the method and account for real world engineering tasks.

4. METHOD

The overall approach in this work considers an iterative method where the size and shape optimization problem is solved by an approximation using a linearized size and shape sub-problem solutions as shown in Fig 1. The superscript 0 emphasizes that the corresponding vector is constant during the current optimization step k with its values based on the previous optimization step *k*-1. The output of the linearized sub-problem is valid only in the vicinity of the point at which the linearization is applied, i.e. ($\mathbf{a}^0$, $\mathbf{q}^0$, $\mathbf{x}^0$). Providing that the change in design variables is sufficiently small, the overall solution is obtained by means of simple update of member sizes $\mathbf{a}^0 = \mathbf{a}$ and nodal coordinates as $\mathbf{x}^0 = \mathbf{y} + \mathbf{x}^0$ at the end of each sub-problem solution step.

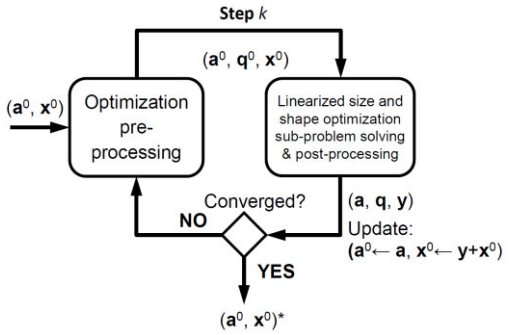

Fig. 1: Flow diagram of the method

The non-linear size and shape optimization problem formulation that will serve as a basis for the SLP approach proposed in this work is given as follows:

$$\min_{\mathbf{a},\mathbf{q},\mathbf{y}} V = \mathbf{l}(\mathbf{y})^{\mathrm{T}}\mathbf{a} \tag{1a}$$

$$\text{s.t. } \mathbf{A}(\mathbf{y})\mathbf{q} = -\mathbf{f} \tag{1b}$$

$$-\sigma_y \mathbf{a} \leq \mathbf{q} \leq \sigma_y \mathbf{a} \tag{1c}$$

$$\mathbf{q} \geq s\frac{\mathbf{a}^2}{\mathbf{l}(\mathbf{y})^2} \tag{1d}$$

Where the design variables are the vector of cross-sectional areas $\mathbf{a}$, the member forces $\mathbf{q}$ and the shift of the nodal positions in each spatial coordinates $\mathbf{y}$ from the initial nodal positions $\mathbf{x}$. The objective is to minimize the volume V of the structure. Vectors $\mathbf{l}$ and $\mathbf{a}$ denote of the lengths and cross-sectional areas of the members. The equilibrium constraint in Eq. (1b) contains the cosine-connectivity matrix $\mathbf{A}$, the member forces $\mathbf{q}$ as well as the external load vector $\mathbf{f}$. The stress constraint in Eq. (1c) contains the yield stress σ_y. The buckling constraint in Eq. (1d) contains s, which substitutes for material and cross-sectional properties. Using a first order Taylor expansion the objective function and all the constraints are linearized to conform to a linear and convex optimization problem, which can be solved efficiently by established linear-programming algorithms [6,7]:

$$\min_{\mathbf{a},\mathbf{q},\mathbf{y}} V = \mathbf{a}^{\mathrm{T}}\mathbf{l}^0 - \mathbf{a}^{0\mathrm{T}}\mathbf{A}\mathbf{y} \tag{2a}$$

$$\text{s.t. } \mathbf{A}\mathbf{q} + \mathbf{J}_{\mathrm{Aq}}\mathbf{y} = -\mathbf{f} \tag{2b}$$

$$-\sigma_y \mathbf{a} \leq \mathbf{q} \leq \sigma_y \mathbf{a} \tag{2c}$$

$$q_i \geq \frac{-\mathrm{sa}_i^0\left(2\mathrm{a_i l_i^0} + \mathrm{a_i^0}\left(\mathrm{l_i^0} - 2\mathrm{l_i}\right)\right)}{l_i^{0\,3}} \;\forall i: a_i \leq a_i^{cr} \tag{2d}$$

$$\mathbf{l}^0 - \mathbf{A}^T\mathbf{y} \geq l^{\min} \tag{2e}$$

$$-\Delta_{\mathrm{Step}}^{\max} \leq \mathbf{y} \leq \Delta_{\mathrm{Step}}^{\max} \tag{2f}$$

$$\mathbf{a} \geq \mathrm{a}^{\min} \tag{2g}$$

However, the overall approach is sequential, and might lead to a local optima. To reduce the amount of iterations needed, the linearization point is improved in the pre-processing step by matching the exact buckling constraints. For further details refer to [1].

5. RESULTS AND DISCUSSION

In this section, the performance of the proposed method is benchmarked against a series of published problems of increasing size against different established methods. For detailed comparison, see Table 1 and [1].

Table 1: Overview of all optimization results and running times of the different example problems

	Nodes in ground structure	Connectivity	# nodes	# members	Local buckling constraints	Layout optimization		LP size & shape optimization		NLP size & shape optimization	
						V [mm^3]	t [s]	V [mm^3]	t [s]	V [mm^3]	t [s]
Hemp's cantilever	7 × 4	1st degree	28	81	No	5.000	0.6	4.388	19.3	4.396	172.76
	7 × 4	Full degree	28	378	No	4.611	0.4	4.376	20.7	4.390	1182
	25 × 13	1st degree	325	1188	No	5.000	0.9	4.354	127.7	4.372	5721
	25 × 13	Full degree	325	52650	No	4.365	93	4.336	11574	4.338	48923[a]
L-Hinge	4 × 2 × 5	1st degree	28	112	No	3.100	0.6	2.709	8.3	2.712	33.2
	4 × 2 × 5	1st degree	28	112	Yes	5.881	2.1	4.731	26.6	4.731	63.0
L-Bracket	12 × 12 × 4	1st degree	480	2836	Yes	37280.2	24.7	29828	1677.1	30026.8	5428.3[a]

[a]Denotes optimizations which did not converged after the maximum number of iterations

Fig. 2 shows the computational time of the proposed method against a Layout only and a NLP problem formulation. It shows that the proposed method improves on the objective function as good as the NLP problem formulation, while being around 1-2 magnitudes faster on a standard desktop computer.

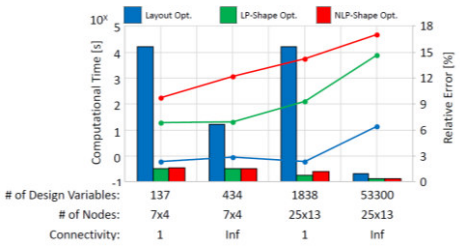

Fig. 2 Hemp's cantilever benchmark for layout, size and shape optimization for different initial ground structures compared against the computational time (lines) and the relative error (bars).

Fig. 3 and Fig. 4 show the resulting structures with and without buckling constraints. It shows that the buckling constraints play an important role in the outcome of the optimized results. Fig. 5 shows the continuously analyzed optimized result. It shows that the structure is generally fully stressed, but some stress concentrations occur on the joints and sharp edges, which is a limitation of the proposed method and generally of discrete optimization.

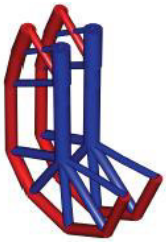

Fig. 3: Shape optimized L-Hinge without buckling constraints $V^* = 2.709$

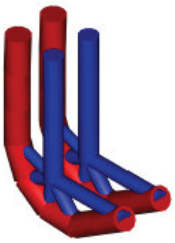

Fig. 4: Shape optimized L-Hinge with buckling constraints $V^* = 4.731$

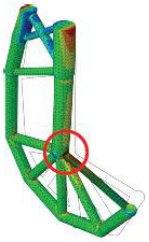

Fig. 5: Linear elastic analysis of Fig. 3

Fig. 6 shows the convergence history of the L-Bracket example with the maximum constraint violation as a bar plot. As the step size is reduced, the method converges and all constraints are fulfilled in the final solution. Fig. 7 shows the location of the cross sectional areas of the element length of 10mm against the member force. The stress and buckling constraints are indicated as lines. It shows that the proposed method drives the solution to the constraint boundary.

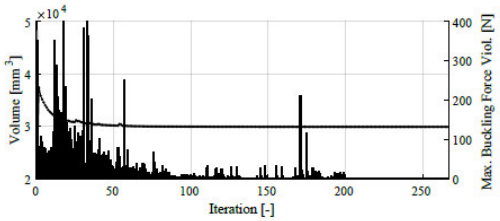

Fig. 6: L-Bracket example convergence history (line with dots, left axis) and buckling constraint violation (bars, right axis)

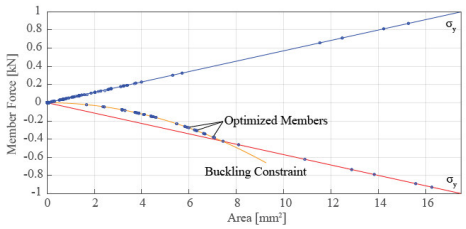

Fig. 7: Buckling and stress constraint satisfaction of the layout only optimized L-Bracket example shown for a member length of l=10mm

6. DISCUSSION AND CONCULSION

This work proposes an explicit SLP problem formulation for simultaneous size and shape optimization of truss structures subject to stress and local buckling constraints. The handling of local buckling constraints involves a post-processing step with projection of the sub-problem solutions to the exact local buckling constraint. In comparison to layout optimization methods the method excels when low-density initial ground structures are considered. The comparison with the exact non-linear problem formulation solution shows that the proposed size and shape optimization method performs extremely well producing results within 1% boundary. This is achieved with significant time savings.

REFERENCES

[1] Schwarz, Jonas, et al. "Efficient size and shape optimization of truss structures subject to stress and local buckling constraints using sequential linear programming." Structural and Multidisciplinary Optimization (2018): 1-14.

[2] Rosen, David W. "A review of synthesis methods for additive manufacturing." Virtual and Physical Prototyping 11.4 (2016): 305-317.

[3] Schmit, Lucien A. "Structural design by systematic synthesis." Proc. of Second Conference on Electronic Computation ASCE, New York. 1960.

[4] Kocvara, Michal, and Jochem Zowe. "How to optimize mechanical structures simultaneously with respect to topology and geometry." Proceedings of the first World Congress of Structural and Multidisciplinary Optimization (edited by N. Olhoff and GIN Rozvany). Vol. 23. 1995.

[5] Achtziger, Wolfgang. "On simultaneous optimization of truss geometry and topology." Structural and Multidisciplinary Optimization 33.4-5 (2007): 285-304.

[6] ApS M (2015) The MOSEK optimization toolbox for MATLAB manual. Version 7.1 (Revision 28).

[7] Grant M, Boyd S (2014) CVX: Matlab software for disciplined convex programming, version 2.1.

Symposium *Lightweight Design in Product Development 2018* (LWD-PD18)
Zurich, Switzerland, 14th–15th June 2018

AN APPROACH TO DESIGN FUNCTIONALLY GRADED MATERIALS USING ADDITIVE MANUFACTURING

T. Ehlers[1], R. B. Lippert[2] and R. Lachmayer[3]
[1]Institute of Product Development, Germany. ehlers@ipeg.uni-hannover.de
[2]Institute of Product Development, Germany. lippert@ipeg.uni-hannover.de
[3]Institute of Product Development, Germany. lachmayer@ipeg.uni-hannover.de

1. INTRODUCTION

A possibility to design lightweight components is the application of additive manufacturing, because a high degree of design freedom is given. Thus, structural components can be adapted to the loading conditions precisely. In order to design such a load-adapted component with low mass, e.g. internal structures can be used. By adjusting parameters, such as diameters or wall thicknesses, the structure can be adapted locally. However, restrictions coming from the process have to be taken into account which limit the possibilities for a precise adaptation. For example, maximum overhangs or downskin angles have to be considered.

Against this background, an approach is to design Functionally Graded Materials (FGM) and to manipulate the process as well as material parameters accordingly. Thus, structural components with locally different properties can be manufactured. For example, the laser power, the laser beam diameter or the hatch distance can be manipulated in the manufacturing process. Another possibility is to change the powder composition by processing multi-materials.

The article characterizes the major potentials and applications for FGM using Selective Laser Melting (SLM). Here, the processing of metals in SLM is considered. Furthermore, the fundamentals to manufacture FGM are discussed and summarized by defining influence factors. Based on this investigation, different possibilities to simulate FGM are compared and proofed by simulating a demonstrator. The results are evaluated in terms of manufacturability with regard to an experimental setup.

2. STATE OF RESEARCH

Local adaptation of components using Selective Laser Melting

Related to the high design freedom, an economical and technically useful application using SLM is especially given for complicated geometries, which contain cavities or free-form structures and thus cannot be manufactured using conventional technologies [1, 2]. The design freedom enables the realization of weight-optimized components, which can be manufactured with high material utilization and operate efficiently in the product life cycle [3, 4].

Against this background a local adaption of a component is possible by using internal structures (e.g. lattice structures) [5]. Compared to solid geometries, a high rigidity with simultaneous low amount of material can be reached [6]. However, the CAD file has to be modified with a high design effort. Accordingly, a suitable design space has to be determined to introduce internal structures [6 - 8]. Previous investigations using a pedal crank as demonstrator have shown, that a weight reduction of about 60% can be reached in comparison to conventional manufacturing solutions (shown in Fig. 1) [6, 7]. In doing so, the design process is subjected by limitations of the in-process. The design process as well as relevant design guidelines for internal structures are shown in [6].

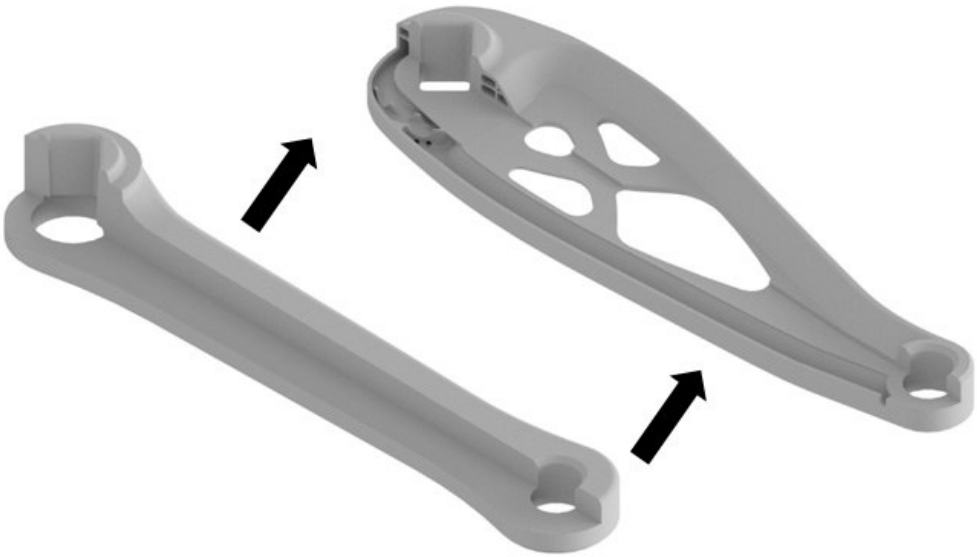

Fig. 1: Initial model of a pedal crank (left) and the optimized model (right)

Functionally Graded Materials in Additive Manufacturing

An alternative to adapting a component to the loading conditions is the application of FGM, which are defined as the locally continuous adaptation of the component properties to different requirements from the product life cycle [9]. FGM can be adjusted locally and continuously either by manipulating process parameters or by varying the material composition. As depicted in Fig. 2, FGM enable a high adaptability of a component. Furthermore, a distinction has to be made comparing mono as well as multi-material. A multi-material is characterized by the combination of two (or more) materials with a transition zone [10].

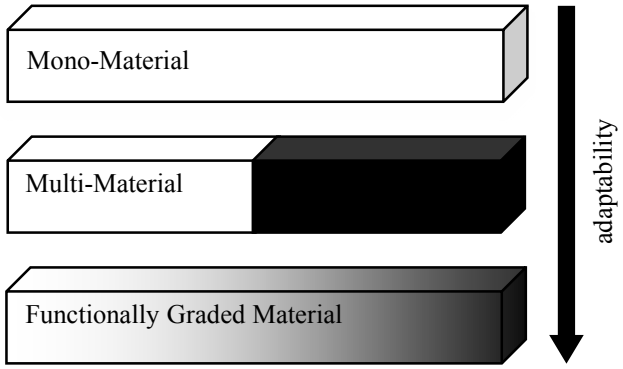

Fig. 2: Illustration of a Mono-Material, Multi-Material and a Functionally Graded Material

The capacities of FGM are already known but can only be realized with great effort using conventional manufacturing processes. Through the application of SLM, a precise control of FGM is possible in theory, because every voxel can be manufactured with different characteristics. Against this background, *Weisheit et al.* [11] described studies on the preparation and testing of FGM for injection and die casting tools by laser deposition welding. Here, the FGM properties were realized by the variation of the material composition. The major disadvantage of laser deposition welding is the lower accuracy. On the other hand a good mixing of materials is possible.

Design of Functionally Graded Materials for Selective Laser Melting

To improve the accuracy of the FGM, Selective Laser Melting can be used. In doing so, the benefit of a high degree of detail can be enabled by extending the standard process through a unit for material deposition. A major challenge is the design and simulation of FGM in order to fit the capacity of the in-process. Against this background, *Burlayenko et al.* describes a finite element algorithms for modeling FGM by a layered construction of homogeneous elements. These elements are assigned different material properties using individual layers. An alternative to shorten the simulation time is the assignment of the FGM properties by the formation of Gaussian quadratures over the element surfaces [12].

3. AN APPROACH TO SIMULATE FUNCTIONALLY GRADED MATERIALS

In this work, the simulation of FGM are investigated for a bending beam under static load using the software ‘Ansys Workbench v. 18.2’. In the approach a local material composition should be realized. Therefore, the material properties are changed using an artificial temperature. This approach was chosen, because in Ansys Workbench the young’s modulus can be adjusted according to the temperature, modifying the values in category ‘technical data’. The gradient of the young’s modulus is chosen to be linear. For this purpose, a young’s modulus $E_{initial}$ = 71 GPa for 20 °C is defined as the initial state. In the final state, a young’s modulus of E_{end} = 210 GPa for 40 °C is defined. In between, the values are linearly interpolated. The procedure is identical for determining the temperature-dependent density as well as the poisson's ratio.

To demonstrate the approach, steel and aluminum are selected as examples. The properties, which are used for the simulation, are summarized in Table 1. The isotropic coefficient of thermal expansion was deactivated so as not to distort the result. Furthermore, isotropic material properties are assumed, which have same properties in all spatial directions.

Table 1: Material parameters for the simulation

temperature	material	density ρ [kg/m^3]	young‘s modulus E [GPa]	poisson's ratio υ[-]
$T_{initial}$	aluminum	2700	71	0.35
$T_{initial} < T < T_{end}$	interpolation			
T_{end}	steel	7850	210	0.3

In the first step, the static simulation for a homogeneous beam under flexural load of aluminum is solved. The resulting stresses are read out at each node n and correlated with a temperature $T(n)$ Eq. 1 in order to adapt the material properties listed in Table 1 in a further simulation as a function of the stresses occurring in the component.

$$T(n) = m \cdot \sigma(n) + b \qquad \text{with: } m = \frac{T_{end} - T_{initial}}{\sigma_{max} - \sigma_{min}}; \qquad b = T_{end} - m \cdot \sigma_{max} \tag{1}$$

Subsequently, in the next simulation, the node temperatures are applied in addition to the static loads in order to adapt the young‘s modulus to the stresses. The high stresses areas are assigned a high young‘s modulus. The continuous course of the young‘s modulus over the bar is shown in Fig. 3.

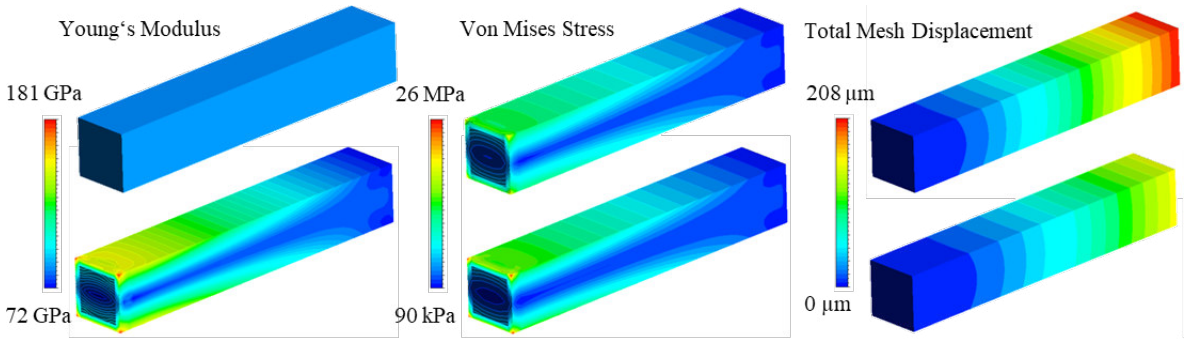

Fig. 3: Simulation results from the mono material beam (top) and FGM beam (below)

Due to the FGM properties, the maximum deformation could be reduced from 208 µm to 149 µm. The Von Mises equivalent stress increases from 21 MPa to 27 MPa. The mass increases from 2.41 kg to 2.75 kg. This corresponds to a weight increase of about 13%. In a next step, the component can be optimized so that the deformations correspond to the initial model and weight can be reduced by changing the topology. Accordingly, the lower stress areas of structural components can be replaced with softer, lower density materials to save weight. Compared to recesses or internal structures, the advantage is that no notches in the component arise which influence the stress distribution.

4. CONCLUSION

A field of application for FGM are structural components under static and dynamic load. Especially for highly stressed components, an added value can be generated. Thus, the material composition can be adapted to the occurring stress distribution. The focus is on optimizing the force flow and reducing the mass. In contrast to conventional hardening, an almost arbitrary profile of hardness or strength can be achieved by a gradual transition from a tough core material to a high strength material in the surface areas, which can be realized e.g. in form of a spatial mathematical function on the component volume. Furthermore, FGM can improve fracture toughness and creep resistance by incorporating crack stops (according to [8]). Another point is to set the material damping over the material composition. Potentials can be found anywhere where stresses have to be reduced, stress distribution or thermal properties have to be improved as well as a higher fracture toughness has to be achieved. At the same time, FGM can be used as a wear and corrosion protection layer of tools in die casting or to modify chemical, mechanical, magnetic and electrical material properties. In particular, the lightweight design can benefit from FGM.

In this article, internal structures and FGM were discussed as design elements for a local adaption of structural components using additive manufacturing. Particular attention was paid to the potentials, fields of application and possibilities for simulation of FGM.

REFERENCES

[1] R. Hague et al., “Design opportunities with rapid manufacturing”, *Assembly Automation,* 2003; Vol. 23 (4): p. 346 – 356, ISSN: 0144-5154

[2] R. Hagl, “*Das 3D-Druck-Kompendium: Leitfaden für Unternehmer, Berater und Innovationstreiber*”, Springer Gabler, 2005, ISBN 978-3-658-07046-5

[3] C. Emmelmann et al., “Laser Additive Manufacturing and Bionics: Redefining Lightweight Design”, *Physics Procedia 12,* 2011, p. 364 - 368, ISSN: 1875-3892

[4] J. Ohlsen et al., “Funktiontsintegrierte, bionisch optimierte Fahrzeugleichtbaustruktur in flexibler Fertigung”, *Automobiltechnische Zeitschrift (ATZ),* 2015, ISSN: 0001-2785

[5] S. Teufelhart, “Geometrie- und belastungsgerechte Optimierung von Leichtbaustrukturen für die additive Fertigung”, *Seminarbericht: Additive Fertigung,* 2012

[6] R. B. Lippert, “*Restriktionsgerechtes Gestalten gewichtsoptimierter Strukturbauteile für das Selektive Laserstrahlschmelzen*”, TEWISS – Technik und Wissen GmbH Verlag, 2018, ISBN: 978-3-95900-197-7

[7] R. Lachmayer et al., “*Additive Manufacturing Quantifiziert - Visionäre Anwendungen und Stand der Technik*”, Springer Vieweg Verlag, 2017, ISBN: 978-3-662-54112-8

[8] H. A. Richard, “*Additive Fertigung von Bauteilen und Strukturen*”, Springer Vieweg Verlag, 2017, ISBN: 978-3-658-17779-9

[9] S. Yin et al., “Hybrid additive manufacturing of Al-Ti6Al4V functionally graded materials with selective laser melting and cold spraying”, *Journal of Materials Processing Tech. 255*, p. 650–65

[10] R. Siqueira et al., “Development of a topology optimization method for tailored forming multi-material design”, *24th ABCM International Congress of Mechanical Engineering December 3-8,* 2017

[11] A. Weisheit et al., “Multifunktionale Gradientenwerkstoffe für den Werkzeugbau”, *Abschlussbericht: BMBF-Vorhaben, FK: 03N5045*, 2006
[12] V. N. Burlayenko et al., “Modelling functionally graded materials in heat transfer and thermal stress analysis by means of graded finite elements”, *Applied Mathematical Modelling,* 2017, Vol 45, ISSN 0307-904X

INDIVIDUALIZED AND SUSTAINABLE LIGHTWEIGHT STRUCTURES FROM ADDITIVE MANUFACTURING AND CARBON FIBER PATCHED COMPOSITES

R. Kussmaul[1], M. Biedermann[2], J. Jónasson[1], M. Zogg[3], C. Klahn[3], M. Meboldt[2], P. Ermanni[1]
[1]Laboratory of Composite Materials and Adaptive Structures, ETH Zurich, Switzerland, kralph@ethz.ch
[2]Product Development Group Zurich, ETH Zurich, Switzerland, manuel.biedermann@mavt.ethz.ch
[3]Inspire AG, Technoparkstrasse 1, 8005 Zurich, Switzerland, zogg@inspire.ethz.ch

1. INTRODUCTION

Combining additive manufacturing (AM) with carbon fiber reinforced polymer (CFRP) patched composites unlocks potentials in the realization of individualized lightweight structures. In this work a digital process chain for the efficient design of such structures is developed. Two arising design opportunities are investigated for a biomedical application. First is the geometrical individualization of a composite structure using AM cores. These cores consist of a thin shape-giving shell which is filled with removable filling material and thus able to withstand autoclave process conditions. Second is the load-bearing structure individualization employing the fiber patch placement method. The design opportunities are demonstrated using the example of an exoskeleton hip structure [1]. The results are compared to a state-of-the-art aluminum hip component.

The overall design process for the individualized component is illustrated in Fig. 1. Starting point is an initial parametric CAD model of the structure. Secondly, the patient's geometry is captured using 3D scanning. The next step employs the patient's data to adapt a parametric CAD model to the individual body shape. The geometry model is then combined with the results of a multibody simulation for patient-specific load estimation in order to generate a finite element model of the structure. In the next step, numerical optimization is applied to determine optimized fiber reinforcements applied in addition to a fixed base laminate. The fiber reinforcement architecture from the optimization is then transformed to a patched laminate layup.

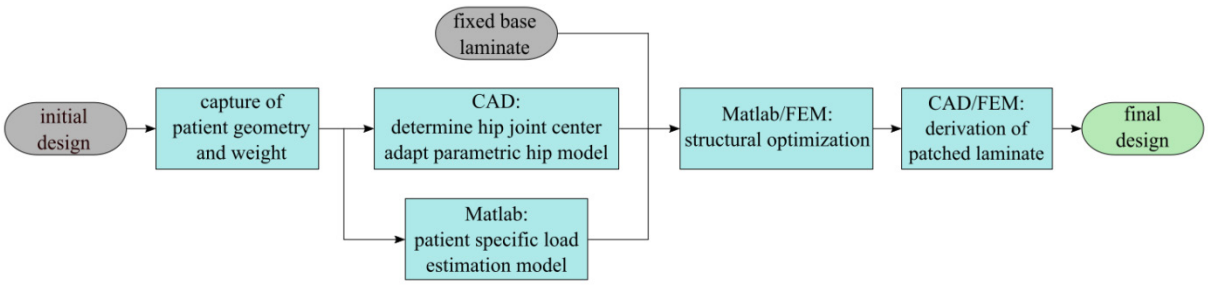

Fig. 1: Design process for individualized AM-CFRP exoskeleton hip component

2. DESIGN-ASSISTED MANUFACTURING APPROACH

The novel exoskeleton hip is fabricated using additive manufacturing and autoclave carbon fiber prepregs. The complexity-for-free principle of AM and the excellent mass-specific properties of CFRP allow for the creation of a highly integrated lightweight structure [2]. The exoskeleton hip is mainly subjected to bending and torsional loads. It is thus designed as a closed shell structure as seen in Fig. 2, which allows for the part to sustain the bending loads predominately through membrane stresses in the thin CFRP skin.

2.1. AM core design

The principle idea for the manufacturing of an individualized CFRP hip component relies on a core as seen in Fig. 2, which is additively manufactured for each specific pilot. In general, such a core may remain inside the final part or may be removed after manufacturing. This work uses an AM core that consists of a thin hull, which serves as a shape-giving male tooling element for the prepreg layup. Selective Laser Sintering (SLS) is employed to fabricate the hull from PA12 with a thickness of 1.6 mm. As the AM core is very thin, it would not be able to withstand autoclave process conditions. Hence, prior to processing, the core is filled with common salt (sodium chloride) through an opening on its top. After filling, the opening is closed with a threaded plug. The core can be re-opened after curing to remove the salt. In order to simplify manufacturing, the core is also able to hold and position the required metal load introduction elements and inserts through integrated form fits until the co-cured interface with the CFRP is established. To remove accessible sections of the core after processing, the core features a set of breaking lines with a reduced thickness of 0.8 mm. That way, the core can be broken into small fragments and removed after the curing process. Support leashes are printed on the inside of the AM core surface. These support leashes can be accessed via the opening on the top side of the hip. They allow generating the mechanical force required to rupture the core along the breaking lines. After the core is divided into small pieces, it can be removed through the top hole. Thus, the lightweight potential of the structure is increased. The final hip and its components are shown in Fig. 2b).

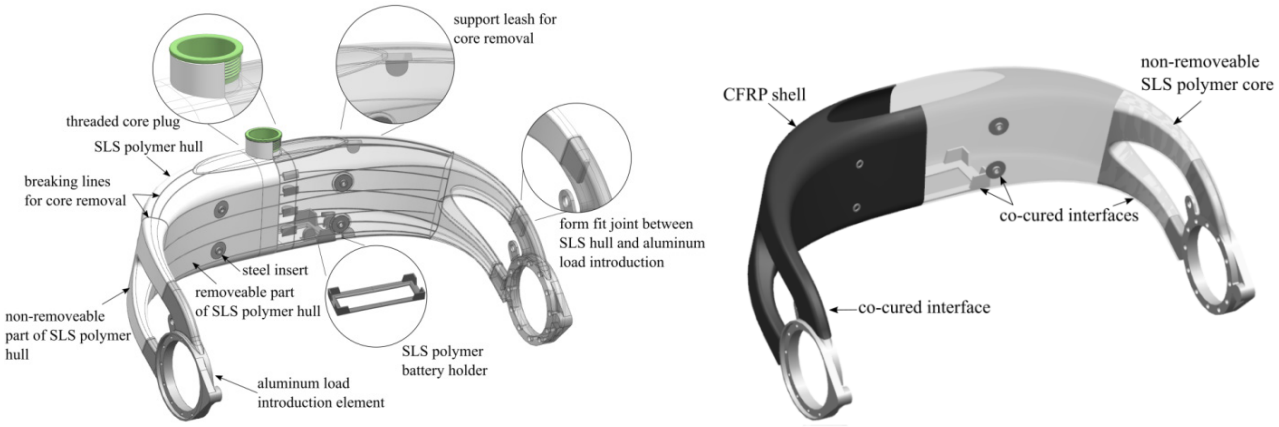

Fig. 2: a) Concept of core design and b) final exoskeleton hip component. The SLS core is partially removed in order to increase lightweight potential. The right half side of the hip is shown transparent.

3. GEOMETRICAL INDIVIDUALIZATION

Geometrical individualization of a lightweight CFRP structure is a valuable design opportunity arising from the combination with additive manufacturing.

First step for the individualization of the structure is capturing the patient's geometry. Devices such as a Microsoft Kinect Sensor are employed to capture a body surface with a precision in the 1 mm range, which is sufficient for individualizing the exoskeleton hip. As illustrated in Fig. 3a), paraplegic patients are scanned hanging in an upright position using a standing vest. Prior to scanning, marker points are attached to the patient on three anatomical landmarks: the left and right anterior superior iliac spine on the sides of the human hip as well as the posterior superior iliac spine on the back side of the human hip. Fig. 3b) shows two body scans with attached marker points.

In the second step, the parametric CAD model is adapted. For a given pilot the 3D-scanned body geometry is imported and orientated to a global coordinate frame. As Fig. 3c) shows, the scanned marker points at the hip spines are used to estimate the hip joint centers through a predictive method [3]. Their connection defines the axis of rotation of the hip drive motors and thus of the position of the hip component. The contour of the exoskeleton hip follows the outer body surface with a specified offset. To automatically adapt the structure to a certain 3D scan, support points are utilized. These points are created by intersecting the scanned body with a predefined set of lines originating from the center of the exoskeleton hip. The support points that result from a specific scan are used to update the CAD design in a parametric manner including high-level features such as splines and loft functions.

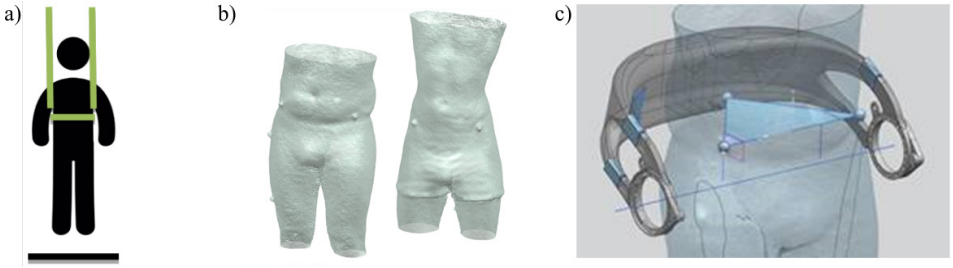

Fig. 3: a) Setup for patient scanning, b) 3D-scanned body surfaces with marker points, c) estimation of hip joint center using marker points

4. LOAD-BEARING STRUCTURE INDIVIDUALIZATION

Individualization of the load-carrying structure is the second promising design opportunity. It arises from the utilization of the so-called fiber patch placement method.

The exoskeleton hip component consists of a quasi-isotropic continuous base laminate, which is designed to sustain the loads created by a 5th percentile female user (47.2 kg weight, 1.52 m height [4]) without structural failure. The targeted patient for this study however is an 85 kg male user, yielding increased torsional and bending moments on the hip by 65 % and 80 %, respectively. The base laminate will not suffice to take the increased loads, hence local patch reinforcements applied. Reinforcement contours are obtained by applying an efficient optimization algorithm for stiffness and strength of composite structures [5]. The optimization routine selectively switches the initial zero thicknesses of potential reinforcement plies to multitudes of the single ply thickness value using sensitivity information. The results suggest placing reinforcements with seven layers in 0° and one layer in 90° direction. As Fig. 4a) shows, major reinforcement areas are covering almost the complete top surface. At the bottom hip surface mainly the rearwards region is reinforced. In a next step, the obtained reinforcement contours are mimicked by fiber patches. The patches have rectangular shape and a fixed width of 20 mm; their lengths can be varied to 20, 40 and 60 mm. The fiber patches are placed

to match the intended reinforcement contours and fiber angles as closely as possible as can be seen in Fig. 4b). In order to patch-reinforce the individualized hip, 196 patches of length 60 mm, 36 patches of 40 mm length and 20 patches of 20 mm length are required.

Patched laminates suffer a loss of stiffness compared to continuous laminates. A novel mechanical model based on shear-lag approximation of interlaminar stresses is used to calculate the stiffness loss of the present combination of continuous and patched laminate layers. Additionally, the stress concentrations due to interrupted fibers are computed. Consequently, the modulus of the patched laminate is reduced by 8.88 % and a maximum stress concentration factor of 1.59 is considered.

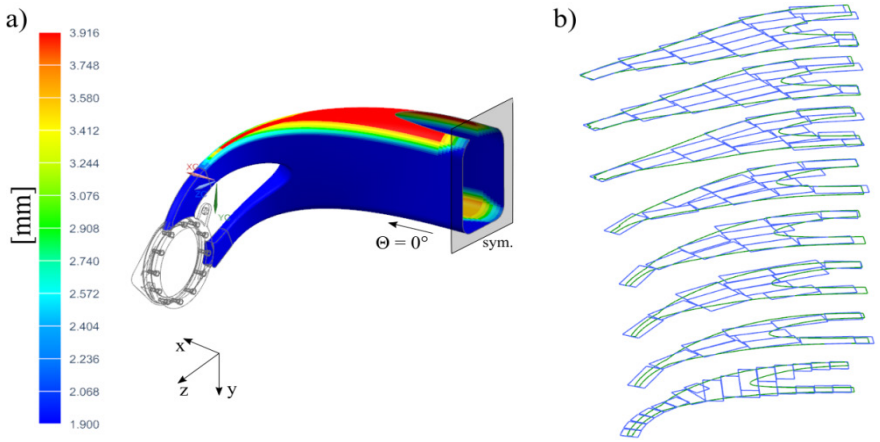

Fig. 4: a) Total laminate thickness, b) eight layers of upper hip patch reinforcements: optimal reinforcement contours are colored in green, physical rectangular fiber patched are shown in blue color.

5. RESULTS

Fig. 5a) compares the mass of the aluminum reference with the AM-CFRP hip. In the novel hip design, significant mass reduction is achieved due to the load-tailored CFRP shell and a redesign of the load introduction elements. A total mass saving of 57 % is obtained. Fig. 5b) compares the number of parts of the two versions. The highly integral AM-CFRP design comprises of 10 parts, yielding a reduction of 77 %.

The switch of the patient from a 5th percentile female to a 85 kg heavy male results in an increased torsional moment by +80.1 % and an increased bending moment by +64.8 %. Optimization results indicate that this load increase can be compensated by an additional +20.5 % laminate mass. Additionally, nesting optimization results show that for the patch reinforcements 7.9 % of raw material is cutoff waste, while for continuous fiber reinforcements 42.5 % of the material is wasted.

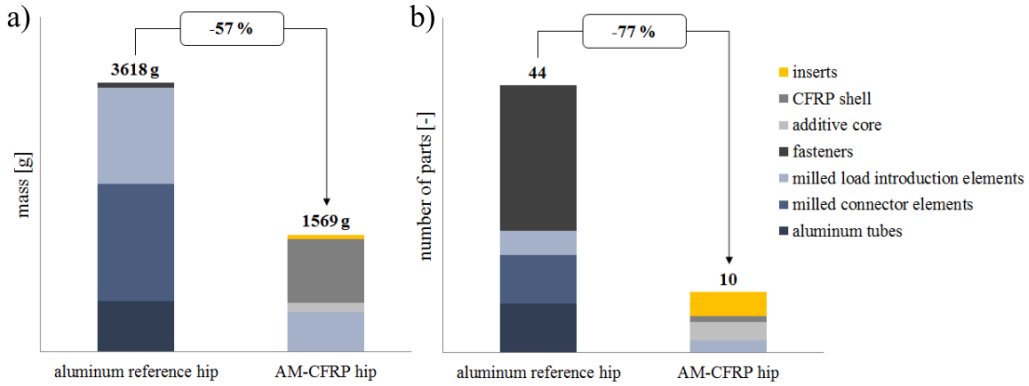

Figure 5: a) Comparison of mass and b) number of parts for reference and AM-CFRP hip

REFERENCES

[1] Esquenazi, A., Talaty, M. and Jayaraman, A. Powered exoskeletons for walking assistance in persons with central nervous system injuries: a narrative review. PM&R, 9.1:46-62, 2017.

[2] Türk DA, Kussmaul R, et al. (2016) Additive manufacturing with composites for integrated aircraft structures. Journal of Advanced Materials, 3:55–69.

[3] Bell, A. L., Pedersen, D. R., & Brand, R. A. (1990). A comparison of the accuracy of several hip center location prediction methods. Journal of biomechanics, 23(6), 617-621.

[4] Kimpara, H., Lee, J. B., Yang, K. H., & King, A. I. (2005). Development of a three-dimensional finite element chest model for the 5th percentile female. Stapp car crash journal, 49, 251.

[5] Kussmaul, R., Zogg, M., et al. (2018). An optimality criteria-based algorithm for efficient design optimization of laminated composites using concurrent resizing and scaling. Struct Mul Opt, 1-16.

Symposium *Lightweight Design in Product Development 2018* (LWD-PD18)
Zurich, Switzerland, 14th–15th June 2018

IMPREGNATION ANALYSIS OF COMPRESSION MOULDING OF THERMOPLASTIC COMPOSITES MADE FROM HYBRID TEXTILES BY THICKNESS ASSESSMENT AND OPTICAL ANALYSIS METHODS

Maximilian Koerdt[1], Oliver Focke[2] and Axel S. Herrmann[1]
[1]Faserinstitut Bremen e.V., Germany. koerdt@faserinstitut.de
[2]MAPEX Center for Materials and Processes - Bremen University, Germany. focke@uni-bremen.de

1. INTRODUCTION

Hybrid textiles contain reinforcement fibres and thermoplastic fibres in a pre-mixed arrangement. They offer the great advantage of drapability and allow a complex arrangement of reinforcement fibres, combined with fast consolidation processes. This paper illustrates different approaches to analyse the process of impregnation. In the presented work, different approaches for analysing phenomena occurring during impregnation of thermoplastic composites are investigated. In detail, the change of thickness during impregnation as well as flow-phenomena, visualised by computer-tomography on one hand, and a glass tooling on the other hand, are discussed.

2. MATERIAL

A hybrid non-crimp fabric (NCF), containing Carbon- and PEEK-multifilaments, is processed in a thermoforming step (see figure 1). The ply-wise deposition of the fibres assures a homogeneous and regular distribution of both fibre materials. However impregnation distances are relatively high in ranges of 125 µm. Due to spreading, an even distribution of the carbon fibres was achieved, combined with fibre volume contents of 60%. Consolidation takes place due to parallel application of an external pressure and temperatures up to 400°C.

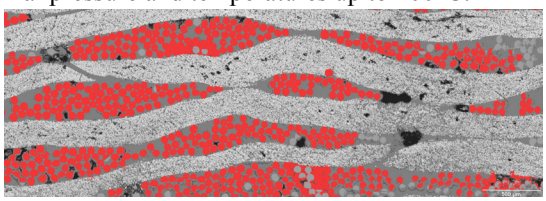

Fig. 1: Cross-Section of hybrid NCF prior impregnation (PEEK-fibres dyed in red)

3. METHODS - GLASS TOOLING

An objective of the process analysis is to examine the interactions between fibres, polymer fluid. A glass tooling allows an online insight into an impregnation process, showing effects of fibre rearrangement during impregnation.

To realise a visual insight into the process of impregnation, a die-edge compression mould with a one-side glass cover was developed. To decrease the required process temperature, fibres from polyamide-6 with identical design substituted the PEEK-fibres. A special challenge was to design the glass-cover, so that it resists compression pressures up to 3 MPa combined with process temperatures up to 300°C. A safety factor of 2.2 thus lead to a 60 mm thick block of borosilicate glass.

The setup did not give insight into the impregnation on meso- nor micro scale. However, macro-impregnation could be observed clearly to begin directly with melting and being complete within 1-2 minutes at 1 MPa external pressure. The carbon-rovings showed an interesting deformation during impregnation. At the beginning of impregnation, rovings were undulated, resulting from their unstretched deposition inside the preform. During impregnation however, a stretching of the fibres was observed. Furthermore, some rovings in some laminates experienced a transversal displacement, leading to gaps inside the laminate (figure 2).

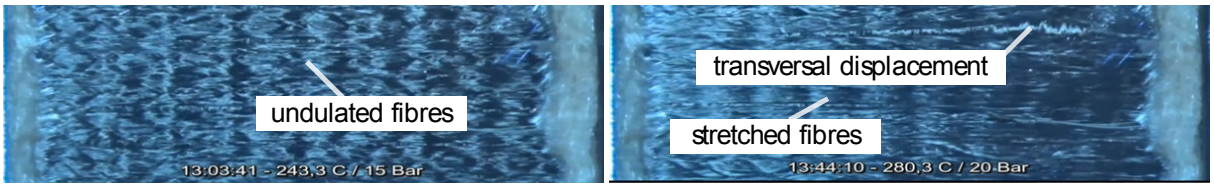

Fig. 2: Top-View of impregnation after 3 min (left) and 40 min of impregnation (right)

An explanation for the fibre-stretching is the provoked in-plane flow of the polymer to the die-edge, where the pressure drops to ambient pressure. Permeability in longitudinal direction is about one decade higher than in transverse direction due to the model of Gebart [1], so flow in longitudinal direction is more likely than transversal flow.

An explanation for the transversal flow is a slot thickness at the die-edge, which is a too large or inhomogeneously distributed. This shows the necessity to reduce the die-edge to a minimum, to minimise flow through it. Since the

transversal flow did not occur in the beginning of the impregnation process, the assumption that it was not promoted by an inhomogeneous material distribution and resulting in-plane pressure gradients, is valid.

4. METHODS - THICKNESS MEASUREMENT

Tracking the thickness of the stacking during impregnation allows drawing conclusions about the degree of impregnation. These experiments show a link between the laminate thickness and the penetration of the flow front.

To investigate the correlation of the laminate thickness and the void content, temporal thickness changes were tracked during thermoforming. For this, a glass scale unit was attached to the mould, being able to measure dimensional changes with a resolution of 1 µm. The laminates were demoulded after different impregnation times and a picture analysis delivered void contents. Both values, the local thickness and the void content, are compared in a corresponding graph. The external pressures were increased from 1.5 to 3.0 to 4.0 MPa after a third of the total impregnation time.

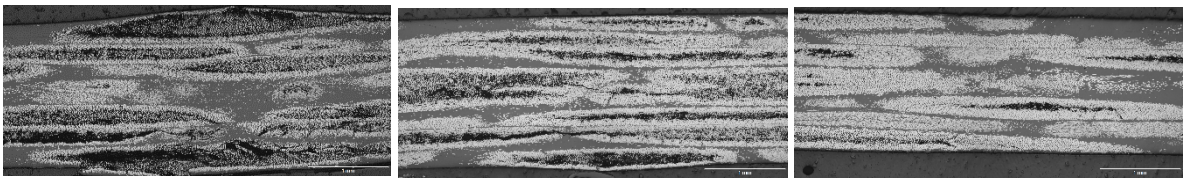

Fig. 3: Cross-Section after 5, 10 and 20 min of impregnation

The cross-sections in figure 3 show an increasing degree of impregnation of the laminates. However, a void-free laminate could not be achieved. An explanation for this are flow distances, which are too long and possibly entrapped air bubbles, creating a pressure counteracting against impregnation.

For comparing the continuously tracked thicknesses to the measured void content, both values were plotted in terms of a relative thickness. The relative thickness of 1 is supposed to be a void-free laminate and is based on the measured void-content. All three tracked laminate thicknesses are equalized after the first compression stage, thus starting at a similar relative thickness.

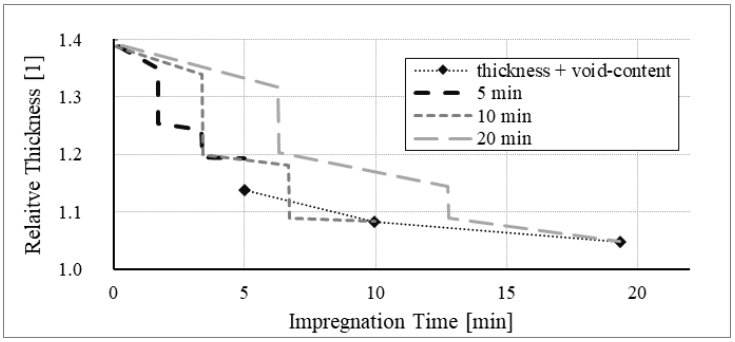

Fig. 4: Comparison of online thickness and resulting void-content with equalized start thickness

Figure 4 illustrates the correlation between thickness and void-content. For the 20 min impregnation curve, the final relative thickness is supposed to be equal to the void-content. The other related curves show a good correspondence with the associated void-content. For 5 min impregnation, a shift of 5% was observed between measured void content and the measured relative thickness. The 10 min curve delivers almost the same result as the measured void-content. Hence, a correlation is given between laminate thickness and void-content. However, for process analysis, a focus has to be laid upon equal circumstances for the artificial start point for thickness measurement.

5. METHODS - CT-TOOLING

The analysis of relevant phenomena during impregnation is of great interest to optimize the process regarding quality and efficiency. An online insight into the impregnation would thus be of special interest. Therefore, an investigation of possibilities for an online-impregnation analysis, supported by computer-tomography, was executed.

A small tooling was designed to create laminates with dimensions of 20 x 20 mm, as illustrated in figure 5. A demountable aluminium frame surrounds the cavity. Two cartridges realize temperatures up to 400°C in 5 min from room temperature, while cooling is accomplished by air channels. The unit is mounted inside a pressure unit, which can be integrated inside a Phoenix-x-ray CT (enabling minimum resolutions of 16 µm) or the Zeiss Xradia 520 Versa at MAPEX (enabling minimum resolutions of 0.7 µm).

First experiments focused on the question, if monitoring of the impregnation is possible, without opening the tooling in sequenced steps where the impregnation process is interrupted by cooling. Unfortunately, the aluminium frame showed to be disruptive (figure 5), thus it had to be removed for an improved insight. Furthermore, the upper and lower aluminium cavity created interference with the x-ray beams, so that shifted regions were observed in the pictures.

Consequently, the subsequent analysis was executed by completely demoulding the laminates from the cavity and scanning them separately.

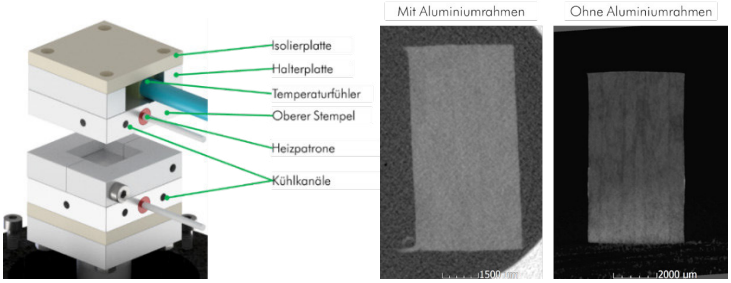

Fig. 5: Compression mould (left); CT-image of laminate cross-section with and without aluminium frame

A special interest in this work was the characteristic of voids inside the laminates during impregnation. To evaluate them, the sequential performed CT-scan of the laminates was analysed concerning the void volume and their respective dimensions in in-plane and out-of-plane direction.

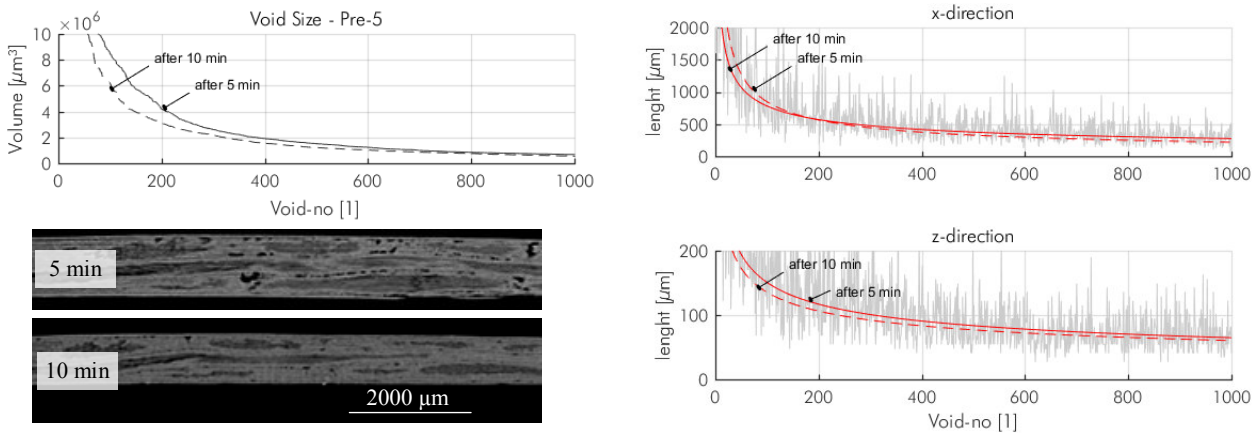

Fig. 6: Distribution of void volumes (upper left), cross-section of laminate after different impregnation-times (bottom left), projected dimensions in in-plane and out-of-plane direction (right)

The results in figure 6 show a reduction of the void volume with time, however only a small diminution, which may be a result of insufficient pressure. Nevertheless, the images clearly illustrate the penetration of the flow front. Furthermore, the CT-scan gives information about the void-sizes. It shows that in out-of-plane direction the void size is about one decade smaller, than in in-plane direction. In out-of-plane direction, the maximum void-dimensions are in the same range, as the single-ply thicknesses. However, the majority of voids is about half of the single ply thickness. In in-plane direction, most of the voids are in the range below 2 mm. Generally, the analysis shows an exponential distribution of the void dimensions.

6. CONCLUSION AND OUTLOOK

Concluding, this contribution shows possibilities for monitoring the propagation of impregnation for thermoplastic composites from hybrid textiles. The information can further be used as a source for input parameters and as verification for impregnation models, as presented in [2] or [3] for instance, as well as for boundary conditions for the development of new manufacturing processes. Measuring the thickness during thermoforming gives beneficial results to assess the degree of impregnation without great efforts. CT-analysis is a promising method to evaluate the quality of the laminate during impregnation and to deliver input parameters for impregnation models. Analysing the impregnation by a glass tooling however only gives information about effects on macro-scale.

ACKNOWLEDGEMENT

The authors thank MAPEX Center for Materials and Processes – Bremen University for supporting the presented work.

REFERENCES

[1] B.R. Gebart, “Permeability of Unidirectional Reinforcements for RTM”, *Journal of Composite Materials*, 1991, Vol. 26
[2] N Bernet et al: “An impregnation model for consolidation of thermoplastic composites made from commingled yarns”, *Journal of Composite Materials*, 1999, Vol. 33
[3] J Studer et al: “Direct thermoplastic melt impregnation of carbon fibre fabrics by injection moulding”, *ECCM 17*, 2016

Symposium *Lightweight Design in Product Development 2018* (LWD-PD18)
Zurich, Switzerland, 14th–15th June 2018

CONCEPT FOR A TAILOR-MADE VISUAL INLINE INSPECTION SYSTEM FOR FIBRE LAYUP PROCESSES DEPENDING ON MATERIAL AND PROCESS CHARACTERISTICS

Sebastian Meister[1]
[1] German Aerospace Center e.V. (DLR) -
Center for Lightweight-Production-Technology, Stade, Germany. sebastian.meister@dlr.de

1. INTRODUCTION

Fiber layup processes like Automated Fiber Placement (AFP) are state of the art technologies for the production of large scale lightweight components like wing covers or fuselages. Lukaszewicz [1] gives a detailed review of both technologies. These composite components are produced layer by layer using narrow material strips. During this material layup it is possible to generate defects e.g. wrinkles, twists, gaps, overlaps, etc. with probably a huge influence on the mechanical properties of the produced component. [2], [3] Recognizing these defects, inline quality assurance (QA) systems are part of ongoing research and industrial development. These systems are mostly inflexible in the use of different sensors and algorithms. One single system is used for every production case. For different materials and various processes, this system performs differently and possibly non-deterministic. In order to compensate this issue it is necessary to understand the relation between optical material properties and the applied sensors and algorithms.

Optical properties of individual resins and polymers as well as textiles are described in literature. [4], [5] Various composites are not part of this existing knowledge. The approach considered in this paper is based on analyzing optical properties of fiber materials and link them to the characteristics and properties of various feasible sensors and algorithms. Beyond that, the knowledge is usable for design aspects and the manipulation of component behavior. The concept provides the opportunity to characterize materials itself and the current material status based on optical properties. This offers the possibility to determine changes in chemical properties and derive statements on the manufacturing performance of a particular material. [6]

In automated quality inspection, this proposal has the potential to increase the performance of an inline QA system significantly. Using this optical properties data, it will be possible to build a tailor made inline inspection system. This system is specifically designed by knowledge and had a well-known error range. Beyond that, directly to the producibility correlated material parameters can be derived from the optical material properties.

During this work, the following scientific questions have to be answered:

- Which dependencies in optical characteristics had to be analyzed to configure a tailor-made inline QA system for a specific material?
- How do we describe layup defects by its optical characteristics?
- How robust performs an inline QA system for different materials?

2. CONCEPT

This concept paper describes an approach for the measurement and interpretation of optical material properties, with the aim to optimize production and inspection processes.

Effects

For the material analysis using optical characteristics, several influencing variables are of interest. These include electromagnetic radiation influences as well as climate ascendancies. The following effects have to be measured for a material characterization:

- Spatial reflection behavior
- Spatial scattering behavior
- Spatial transmittance behavior
- Emission ratio
- Reflection ratio
- Transmittance ratio
- Angle of polarization
- Surface texture

Material

The presented concept focusses on the analysis of resins and composites with a minimum filament gap of 5.5 µm. Being able to measure the effects mentioned above, it is necessary to consider samples with a minimum size of 20 x 20 mm and a maximum size of 100 x 100 mm. Having regard to the huge thermal influences on the materials behavior, the samples are air condition stored. Simulating a production environment, it is possible to heat the samples up to 400°C during measurement cycle.

Sensors

Achieving a deep understanding of materials behavior, the mentioned effects have to be sensed within a spectral range from 300 nm up to 3500 nm. [4], [5] Recognizing thermal influences, it is also necessary to consider information from thermal infrared region from 7.5 µm to 13 µm.

Meeting these requirements, it is reasonable to use three different types of sensors. At first a monochrome camera with a spectral resonance from 350 nm to 850 nm is applied. Measuring the thermal infrared band, a thermal imaging sensor is used. Acquiring spectral information, a radiation spectrometer with a measuring range from 300nm to 3500nm is sensible.

Lighting

In Order to use the sensors mentioned above in its entirety, a selection of a reasonable lightings is indispensable. The radiation spectrum extends from 300 nm up to 3500 nm. This includes ultra violet, visible light, Near-Infrared and infrared spectrum. Therefore the exposure rate (E) has to be greater than $E > 6000$ W/m². It is important to guarantee an illumination of the measurement sample over the entire spectral range. This is feasible in various ways. One possibility is the radiation with various discreet working, superposed radiation sources. Another option is the assignment of a broad band radiation source. Combining these approaches is also possible to induce homogeneous radiation intensity over the entire radiation spectrum. In Order to distinguish polarization effects, the use of polarization filters is also required.

Data evaluation

In Order to evaluate generated data and derive predictions for feasible sensor and algorithm configurations, the use of artificial neuronal networks (ANN) is reasonable. Using this tool, also complex correlations are obtainable and extractable.

Depending on the input parameters and the desired predictions, it is necessary to use a fully connected network with multiple layers. Input parameters are the measured optical properties. Output parameters are one or multiple sensors and algorithm combinations for a particular process and material. Keep the possibility in mind, that various combinations solve the requirements with the same performance.

Training the ANN can be carried out by using the optical material characteristics and evaluate them using defined scoring values. These performance figures are determined for each sensor with single and multiple algorithms in use. Following, the forecast for a sensor and algorithm combination is possible.

Time line

It is planned to implement the general system concept, including multiple sensors and algorithms, until Q4/2019. Optical material characterization and the linking to the corresponding sensor-algorithm behavior will be finished in Q1/2021. The validated system is ready to run in Q4/2021.

REFERENCES

[1] D. H.-J. Lukaszewicz, C. Ward and K. D. Potter, “The engineering aspects of automated prepreg layup: History, present and future,” Composites Part B: Engineering, 2012, pp. 997 – 1009.

[2] K. Potter, “Understanding the origins of defects and variability in composites manufacture,” in Conference on Composite Materials (ICCM), 2009.

[3] C. Krombholz, D. Delisle and M. Perner, “ADVANCED AUTOMATED FIBRE PLACEMENT,” in International Conference on Manufacturing Research, Cranfield, UK, 2013.

[4] Bruker Optik GmbH, “Analysis of Polymers and Plastics - Quality Control & Failure Analysis,” Bruker Optik GmbH, Ettlingen, Germany, 2015.

[5] Hitachi High-Technologies Corporation, “Measurement of Optical Characteristic of Plastic by UH4150 Spectrophotometer - An example of High Throughput measurements in the UV, Visible and Near-Infrared Regions -,” Hitachi High-Technologies Corporation.

[6] G. A. George, G. A. Cash and L. Rintoul, “Cure Monitoring of Aerospace Epoxy Resins and Prepregs by Fourier Transform Infrared Emission Spectroscopy,” in Polymer International, 1996; 41: 169-182,.

Symposium *Lightweight Design in Product Development 2018* (LWD-PD18)
Zurich, Switzerland, 14th–15th June 2018

3D-PRINTING WITH THERMOPLASTICS AND CONTINUOUS CARBON FIBER

M. Titze[1], B.T. Kletz[2] and J. Riemenschneider[3]
Institute of Composite Structures and Adaptive Systems, German Aerospace Center (DLR), Brunswick, Germany.
[1]Maik.Titze@dlr.de, [2]Bjoern.Kletz@dlr.de, [3]Johannes.Riemenschneider@dlr.de

1. INTRODUCTION

Using standard filaments and standard fibers is key to enable industrial scale 3D-printing with continuous carbon fiber reinforcement. The novel printing head for Additive Composite Structures (AddCompS™) serves this task as one element along the completely new developed process chain for continuous fiber reinforced 3D-printing. Both the AddCompS printing head and the process chain are described within this paper.

2. PRINTING HEAD DESIGN

The design of the printing head offers the opportunity to process standard fiber materials in conjunction with up to three different thermoplastics. The developed manufacturing process is based on the Fused Filament Fabrication (FFF) technology and serves the need for additive manufacturing of three dimensional, fiber reinforced, multi-material, lightweight structures. To establish a robust printing process, several innovations focus on the routing of the standard fibers as well as the thermal management of the printing head and of the generated structure.

The fiber is automatically pulled into the printing head due to its adhesion to the thermoplastic melt during the extrusion. To ensure an adequate feeding of the fiber it is essential to reduce its friction within the printing head, guard the fiber from sharp edges and prevent small bending radiuses. Another challenge is the development of a valve which allows the fiber to get in contact with the melt, but prevents the melted plastics from infiltrating the valve. This is solved by an optimized geometry of the contact zone between fiber and thermoplastic melt supported by centrally supplied compressed air along the fiber routing. The concept is outlined in Figure 1. The thermoplastic melt flow is redirected along a specially shaped needle, so that the flow is forced alongside the extrusion direction. Assisted by a low pressurization of the needle the fiber is routed into the melted plastic while preventing the melt from rising into the needle.

Besides the routing of the fiber, the thermal design of the printing head is crucial for a reliable printing process. This is assured by realizing a sharp temperature gradient between the zone of filament feeding and the melting zone. Preceding investigations using different types of conventional heatbreaks manufactured from aluminium or titanium showed unsatisfactory results. For this reason a new concept is developed and shown in Figure 1. A 1 mm to 3 mm thick calcium silicate glassfiber reinforced plate serves as thermal insulation between the cool feeding zone and the hot melting zone. The temperature gradient is further increased by an actively cooled body directly attached to the insulation plate. Long term measurements indicated a temperature of 45 °C directly above the insulation plate while the temperature of the melting zone is 220 °C. The printing head, the cooling body and the thermal insulation plate are aligned during assembly with a tool to guarantee an edge free channel for the filament routing. To also process materials like PEEK the printing head is able to provide melting temperatures of up to 450 °C. This is addressed by utilizing two cartridge heaters with a total heat power of 400 W, which also enable the system to precisely control the temperature distribution and rapidly react to changing environmental influences.

With the aim of high quality results the impregnation of the fiber as well as the adhesion of the fiber to the matrix and the thermal management of the printed structure needs to be considered. The adhesion as well as the process stability is improved by preheating the fiber before it gets in contact with the melted plastics. It is of major importance the fiber is not damaged during this process step. Other points to address are the printing bed temperature, the temperature of the preceding printed structure to properly bond the new extruded material and the general cooling of the structure to prevent internal stress concentrations or distortions. Another challenge is to prevent the fiber from being pulled out from its desired position during high speeds, sharp curvature movements or real three-dimensional trajectories. For that purpose an adaptive cooling system, which acts directly below the extrusion nozzle on the extruded material, is installed at the printing head. In dependence of the process parameters like the extrusion speed of the printing head or the movement speed and the movement history of the kinematic system, this device allows to set up customable fluid mass flows from different directions to precisely control the temperature distribution of the extruded material. This enables the manufacturing system to print sharp curves or three-dimensional structures without support while assuring an accurate placed fiber.

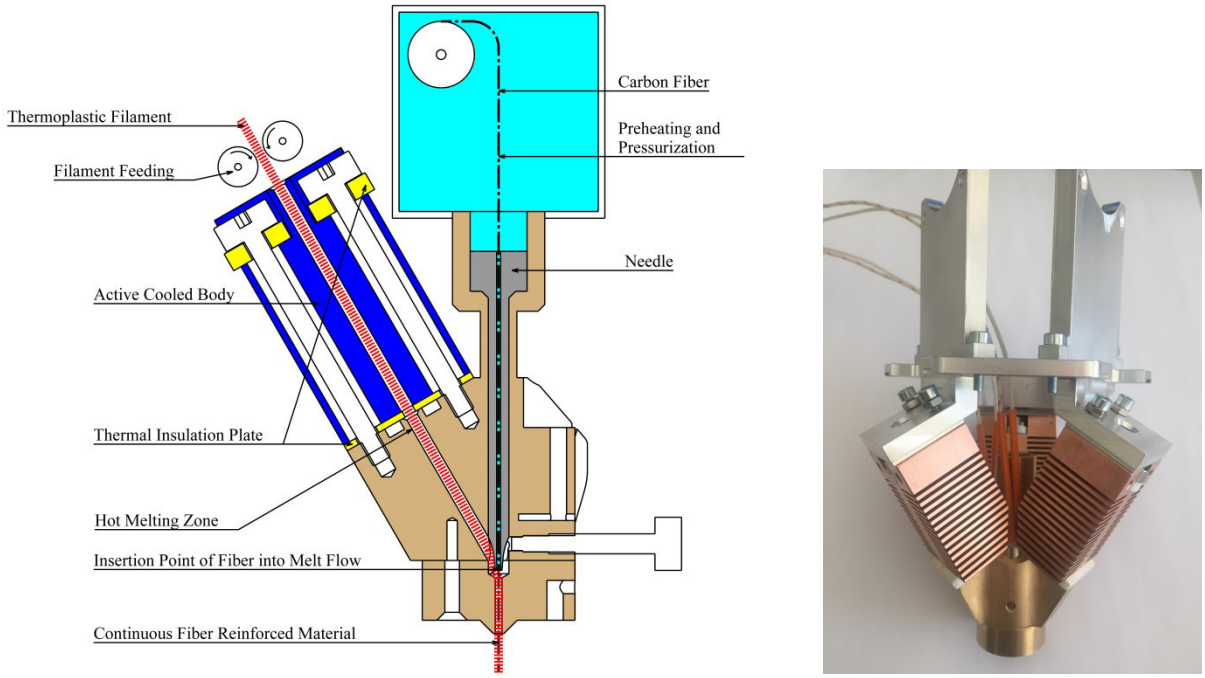

Fig. 1: Printing Head Design

3. ADDITIVE MANUFACTURING PROCESS

For a successful implementation of a process chain from a CAD model to an additive manufactured three-dimensional continuous fiber reinforced structure, it is necessary to innovate in different fields of activities. First, the printing head technology itself needs to be developed as described before. Second, there needs to be a process integration which combines the printing head technology, a kinematic system, a control system und the required sensor system. As a third point, the design methodology needs to be defined, considering the specific requirements of the printing head in conjunction with the kinematic system. Design rules have to be formulated and restrictive boundary conditions need to be known. This can only be done, if, as a fourth topic, the material development and material characterization in dependence of the process parameters are accounted. As a last fifth working area, mechanisms for an inline quality assurance during the printing process are required. This creates the potential to monitor the printing process and react dynamically to deviations. By simultaneously addressing these work areas, a robust additive manufacturing system for generating continuous fiber reinforced structures is developed.

The translation of a virtual model to a real structure demands multiple work steps. First of all the design of the CAD model needs to be done in compliance with the design methodology which is defined by the provided additive manufacturing system. Afterwards the numerical model can be compiled for its manufacturing with the kinematic system. Thus, the information of the trajectories to build the structure is stored. For that purpose a software tool is developed, capable to directly translate CATIA CAD models into G-code, to plan the path movements of the kinematic system. The current software version is able to handle structures with a three-dimensional closed polygon base layer and arbitrary thickness. The next step contains the insertion of the printing parameters according to the planned movements like nozzle temperature, filament feeding rate or adaptive cooling of specific trajectory sections. Subsequent the required fiber and thermoplastic materials are loaded into the manufacturing system. Using a central control unit, the created printing job is executed. Additionally a quality control of the generated structure is conducted.

As a first step the described process chain is used to manufacture test specimen for material characterizations as well as real three-dimensional structures. The focus is on the optimization of the printing parameters for different material combinations. This includes PLA, PC, PEI, PEEK as thermoplastics and different types of fibers like twisted yarn or standard and special coated rovings with a size from 3K up to 24K. These materials are used to print test specimen with different ply orientations to characterize them mechanically. Further surveys address cooling profiles for the adaptive cool system. Different parameter settings for the cooling of edges and for the realization of three-dimensional structures without support are explored. In addition the inline quality assurance system is developed further by collecting and evaluating process data. This is assisted by the development of numerical models to simulate critical process steps and analyze the collected process data.

4. OUTLOOK

Figure 2a indicates a sample structure fabricated using the described additive manufacturing system. It shows the ability to print high quality parts with sharp edges and continuous fiber reinforcement. Ongoing research will focus on an optimization of the printing process to improve the mechanical properties of the produced structures. An example of the effect of different printing parameters on the adhesion of the thermoplastics and the fiber is highlighted in Figure 2b. First tensile testing results based on preliminary printing parameter optimizations are drafted in Figure 2c. The preliminary results show a three times higher strength and six times higher stiffness. Also the manufacturing of real three-dimensional fiber reinforced structures is addressed in the future. Furthermore a CNC-robotic system will be used as kinematic with six degrees of freedom. The investigations will include the influence of different printing head orientations regarding the printing path as well as the limitations to print in three-dimensional space without support structures.

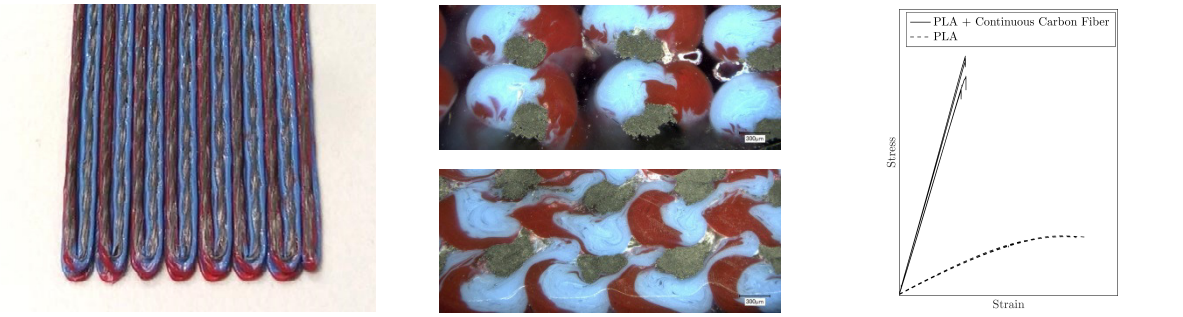

(a) Sample Structure *(b) Microscope Analyses* *(c) Tensile Test (Printed UD Structure)*

Fig. 2: Printing results achieved with AddCompS printing head

Symposium *Lightweight Design in Product Development 2018* (LWD-PD18)
Zurich, Switzerland, 14th–15th June 2018

TOASTING CFRP PARTS - CELLULAR HEATABLE TOOLING AND INFRARED THERMOGRAPHY ASSISTED PROCESS TIME STABILISATION OF FULL SCALE CFRP-PARTS IN CURING PROCESSES

H. Ucan[1], J.T. Hesse[2] and M. Kantelberg[3]
[1]German Aerospace Centre (DLR), Institute for Composite Structures and Adaptive Systems, Stade, Germany, Hakan.Ucan@dlr.de
[2]German Aerospace Centre (DLR), Institute for Composite Structures and Adaptive Systems, Stade, Germany, Jan-Timo.Hesse@dlr.de
[3] Fibretech-Composites GmbH, Bremen, Germany, Michael.Kantelberg@fibretech-composites.de

1. INTRODUCTION

The topic of lightweight plays an essential role in the development of aircraft. More and more carbon fiber reinforced plastics (CFRP) find a steady growing demand in aircraft manufacturing and are equipped in their latest generation with over 50% of the total structure weight. This development is offset by labor-intensive manufacturing processes that cause very high costs for the components. This is the reason why it is important to provide rapid and cost-effective production processes today and in the near future to counteract the striven production rate of 70 AC/month.

2. OBJECTIVES, MOTIVATION AND CONCEPT FOR TOASTING CFRP PARTS

The aim of the use of a modular heated mold in an autoclave is to shorten the process time of autoclave curing and thus to increase cost-effectiveness and productivity. Furthermore, the optimization of component quality, through more even curing, is in the foreground. In current autoclave processes, most metallic forming tools have a high thermal mass. A large part of the energy goes into the heating of the tool. Furthermore, due to the fluidic and thermodynamic conditions inside the autoclave, the components are also heated longitudinally and also from top to bottom. This leads to an inefficient autoclave process. In order to achieve a nearly ideal curing, long autoclave cycles are accepted. Due to the uneven temperature distribution within the material, high internal stresses can also occur and thus influence the mechanical properties and the quality of the component. [1] [2]

To prevent this, a new claim is made. The concept consists of several main units (see figure 1):

- Research autoclave BALU with a loading length of 20m and a loading diameter of 5,8m
- An infrared thermography system that is integrated into the autoclave loading space. Consisting of a liner drive and a water-cooled pressure vessel that allows using the system by temperatures up to 250°C and pressures up to 10 bar.
- A CFRP mold with three cellular electrical heating zones allows temperature up to 220°C
- A new and innovative control system that can communicate with the existing control and the new above mentioned units.

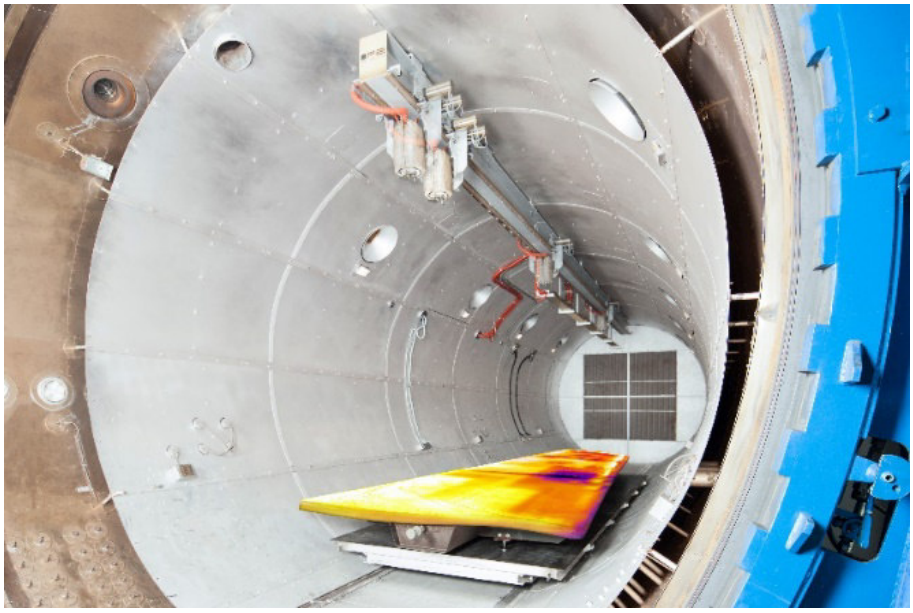

- ***Fig. 1: Concept of TOASTING CFRP parts based on infrared thermography and cellular heatable tooling***

The interaction of the components is as follows. The thermography system measures the temperature of the component surface and sends it as set point via the controller to the PLC. Here, the heating zones of the CFRP mold are regulated. Through this action the component temperature at the bottom and on the top will have nearly the same temperature. This leads to a TOASTING effect that makes the curing in the autoclave much more efficient.

3. TOASTING WING COVER - RESULTS OF THE FULL-SCALE DEMONSTRATION

The implemented new control system is validated on the basis of a full scale wing cover component. This is to show that an effective curing by means of heated tools in an autoclave is also suitable for larger structures (see figure 2).

Fig. 2: Toasting wing cover - Full-scale demonstration

All three heating zones of the CFRP mold (see figure 3) have a similar characteristic of the temperature, which follows the set point course of the cycle very closely. Compared with the same cycle without tool heating of the CFRP mold from the preliminary tests, it is possible to save significantly more than 80 minutes of process time because all temperatures - including the cold spot - reach the target temperature of 135 °C (180 C) before or with the cycle specification. At the same time, the component sees the same temperatures at all positions (front, rear, top and bottom) and is thus cured very homogeneously. Further studies show a process time saving of an average of 33% compared to conventional metal tools.
With the successful curing of the wing demonstrator it could be shown that with use of cellular heatable CFRP molds - in particular with a thermography camera inside the autoclave - the process can accelerate the process and improve the quality of the component at the same time.

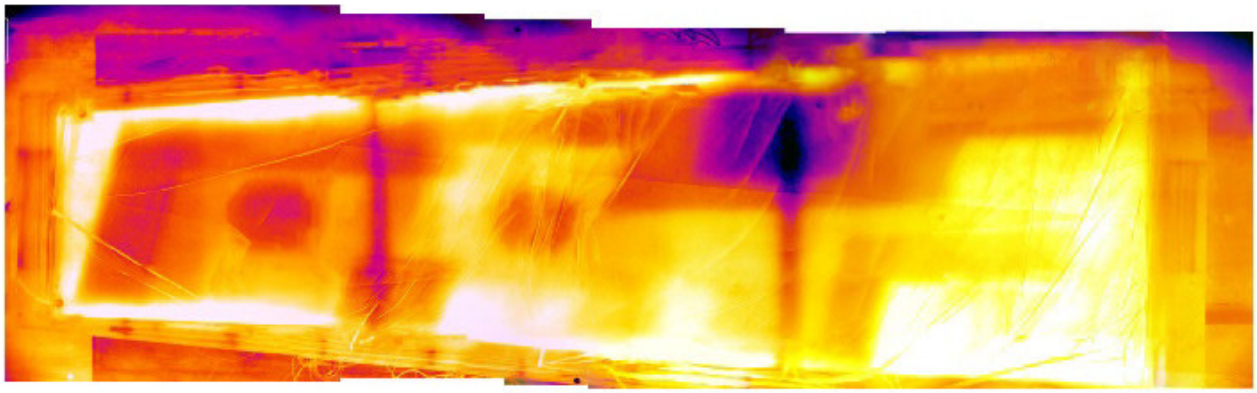

Fig. 3: Temperature distributions on the surface of the wing cover during the autoclave process

REFENCES

[1] L. Nele et al., “Autoclave cycle optimization for high performance composite parts manufacturing”, Procedia CIRP , 2016, page 57
[2] H. Schürmann, “Konstruieren mit Faser-Kunststoff-Verbunden”, Springer Verlag, 2014

Symposium *Lightweight Design in Product Development 2018* (LWD-PD18)
Zurich, Switzerland, 14th–15th June 2018

INTRALAMINAR FRACTURE IN GLASS FIBER-REINFORCED POLYMERS WITH EPOXY AND POLYURETHANE MATRICES

Davi M. Montenegro[1], Francesco Bernasconi[1], Markus Zogg[1], Matthias Gössi[2], Rafael Libanori[3], Konrad Wegener[4] and André R. Studart[3]
[1]Innovative Composite Structures, Inspire AG, CH-8005 Zurich, Switzerland, davi.montenegro@inspire.ethz.ch
[2]Corporate Research, Sika Technology AG, CH-8048 Zurich, Switzerland
[3]Complex Materials, Department of Materials, ETH Zurich, CH-8093 Zurich, Switzerland, andre.studart@mat.ethz.ch
[4]Institute of Machine-Tools and Manufacturing, Department of Mechanical and Process Engineering, ETH Zurich, CH-8092 Zurich, Switzerland

1. INTRODUCTION

The fracture toughness of laminated composite materials is a very important property for damage-tolerant design, but remains poorly understood under transverse mechanical loading conditions. In this study, the transverse intralaminar fracture in unidirectional laminates with ductile polymer matrices is investigated. The presence of a ductile matrix calls for the use of concepts of nonlinear fracture mechanics for the accurate determination of the resistance of the composite to crack propagation. Unidirectional glass fiber-reinforced polymers with a polyurethane (PU) matrix are studied and compared with a benchmark system out of epoxy (EP). The fracture toughness of these composites is evaluated through the determination of *R*-curves using single edge-notched beams (SENBs) and the *J*-integral method, whereas the underlying fracture mechanisms are investigated through *in situ* testing in a scanning electron microscope.

2. MATERIALS AND METHODS

A two-component, commercial epoxy resin under the catalog name SikaDur 300 from Sika Technology AG (T_g ~90 °C, peak value of tan δ from dynamic mechanical analyses) is used as the benchmark system. The polyurethane resin, named PU, is a two-component prototype thermoset system formulated at Sika Technology AG (T_g ~85 °C) and consists of a polyol resin and an isocyanate-based hardener.

The transverse intralaminar fracture toughness of the laminates is evaluated by measuring crack-resistance curves (*R*-curves) through the compliance method for the opening mode (mode I), as explained in [1]. With this method, several load-partial unload cycles are run and the current crack length is calculated based on the specimen's current compliance. Due to the material nonlinearity of the matrices and of the laminates, the crack-growth resistance is quantified in terms of the nonlinear strain-energy release rate, *J*, as a function of crack extension, Δa, leading to the so-called *J*-*R* curves. 30 x 5 x 2.5 mm^3-sized beams are cut out from 5 mm-thick laminate plates that are prepared by vacuum-assisted resin infusion molding with layup $[0]_{15}$. The specimens are cut such that the fiber direction is parallel to the specimens' thickness.

Additional three-point-bending tests of SENBs out of EP- and PU-GFRPs are performed inside a scanning electron microscope (SEM) with a micromechanical tester from Deben in order to identify the fracture mechanisms in the laminates. The specimens have one surface polished so as to reveal the fibers and are subsequently coated with a platinum nanolayer with thickness of ~5 nm before being placed into the SEM.

3. RESULTS

Although the raw force versus load-line-displacement (LLD) raw data do not directly quantify the fracture toughness of the materials under investigation, they do provide qualitative insights about the difference in fracture toughness. While the two matrices present partly superposing curves as shown in Fig. 1a, the EP-GFRP specimens bear only about 50–60% of the peak forces withstood by the specimens out of PU-GFRP as seen in Fig. 1b. In all systems there is initially a linear increase of the force with increasing LLD. The specimen stiffness, given by the slope of this linear relation, varied according to the difference in the initial crack length. The LLD values at which the specimens reach their peak forces are indicative of the deformability of the investigated samples. Peak values are found in the range of 0.30–0.35 mm and 0.03–0.05 mm for EP and EP-GFRP samples, respectively. By contrast, higher peak LLD values of 0.50–0.65 mm and 0.13–0.17 mm are observed for PU and PU-GFRP, respectively. With the exception of EP-GFRP, the other three material systems present a smooth transition to the nonlinear regime, during which significant damage occurs throughout the specimens. After the peak load is reached, both PU and PU-GFRP maintain higher force levels than their epoxy counterparts.

Now, crack propagation through the pure matrices is described and discussed. The results in Fig. 1c show that EP presents 10–20% higher fracture toughness at short crack extensions (< 0.05 mm), but at longer crack extensions (> 0.05 mm) the crack growth resistance of the PU matrix is up to 2.3-fold higher than that of EP. *J*-values for the epoxy polymer rise quickly at the beginning, reaching 1.0 kJ/m^2 at Δa ~ 0.05 mm. After this point the increase in *J* is slower and peaks at a value of 4.0 kJ/m^2 for crack extensions slightly shorter than 0.85 mm. The polyurethane presents similar *J*-values as epoxy for Δa ~ 0.05 mm and rises after this point with a much steeper slope, reaching 4.0 kJ/m^2 much earlier than epoxy, at a crack extension of 0.18 mm, thus characterizing higher fracture toughness. *J* continues rising with increasing crack propagation for the polyurethane, peaking at 7.0 kJ/m2 at Δa ~ 0.35 mm. For the range of crack

extensions studied, both systems present rising *R*-curves. The steeper rise in the *R*-curve of the polyurethane stems from its greater ability to develop plastic deformation as seen in static 3-point-bending tests.

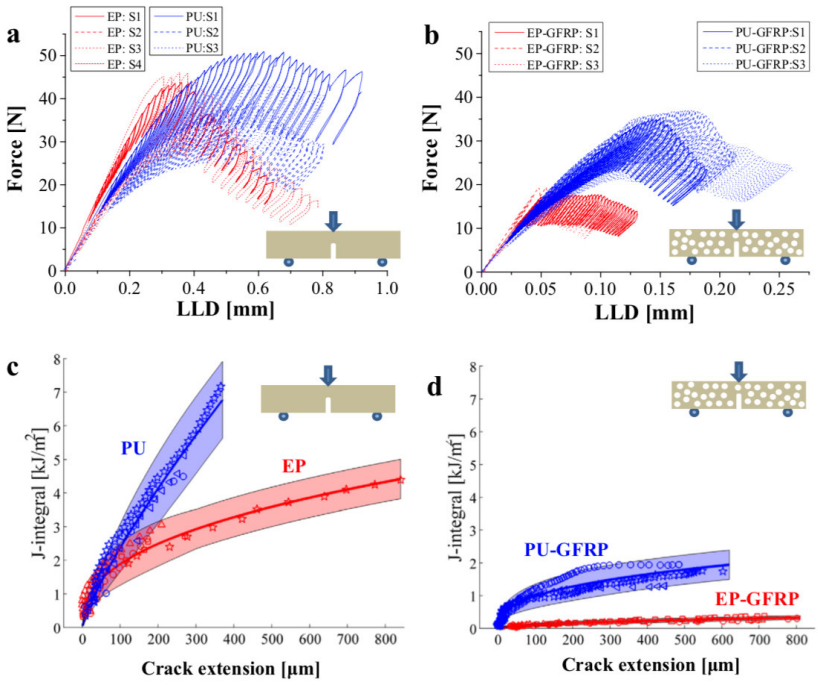

Fig. 1: (a, b) Force-LLD curves obtained in the SENB tests with (a) pure matrix and (b) laminate specimens. (c, d) Crack-resistance curves of the (c) matrices and (d) laminates. The curves in (c, d) were obtained with a least squares fitting of the function $J = C1(\Delta a + \delta)^{C2}$. The shaded areas in (c, d) are error estimations added to the fitted data and are based on the standard deviation of the single measurements and on the propagation of the experimental uncertainties.

The effect of the different fracture toughness of the polymer matrices alone on the *R*-curves of 90º GFRP layers is further investigated using an approach that has already been successfully employed to assess the crack-growth resistance of heterogeneous materials such as bone and nacre. The results in Fig. 1d show that PU-GFRP is noticeably tougher than EP-GFRP for the entire range of crack extensions covered in this study. Contrarily to the *R*-curves of the pure matrices, which differ by less than 20% for very short cracks (< 0.05 mm), the *J*-values for PU-GFRP are 100% higher than those of EP-GFRP already at crack extensions as low as a couple tenths of micrometers. Surprisingly, the PU-GFRP laminate exhibits fracture toughness as high as 1.9 kJ/m^2, which is about 6-fold higher than the maximum value presented by the EP-GFRP. The progression of the *R*-curves obtained for PU-GFRP is nonlinear, presenting a swift rise in *J* up to a crack extension of around 50 µm, at which point the laminates reach approximately 50% of their peak toughness. After crack extensions of 300 µm, most of the evaluated specimens reach about 85–90% of their maximum energy dissipation capabilities. The $J_R(\Delta a)$ curves obtained for the EP-GFRP are more reproducible than those of the PU-GFRP for crack extensions larger than 0.15 mm, which can be a result of sample-dependent interfacial properties or small variations in the local fiber volume content.

In order to better understand the origins of the distinct *R*-curve behavior of the laminates, the underlying crack propagation mechanisms leading to such fracture response are investigated through micromechanical testing with *in situ* observation in a SEM. Crack propagation in the PU-GFRPs is slower and follows a less defined pattern as compared to that in the EP-GFRPs as shown in Fig. 2. In EP-GFRPs, damage starts to develop ahead of the crack tip as a result of adhesive failure at the interfaces, as seen in Fig. 2b and 2c. These cracks run along the interfaces concurrently to the formation of interfacial voids. Such voids grow until they meet the neighboring ones through crack propagation within the matrix. Matrix cracking takes place so swiftly that it is not possible to observe crack arresting by the matrix between two neighboring interfacial cracks. A force drop of about 20% is noticed in the recorded load upon debonding of multiple interfaces at once, as seen in Fig. 2a and 2e at an LLD value of 132 lm. The damage process repeats itself for three more load-unload cycles, until another force drop of about 50% is recorded at approximately the same peak load as before and at a load-line displacement of 141 µm (see Fig. 2a). At that moment, several interfaces ahead of the initial crack tip are debonded and the total crack extension Δa reaches 900 µm, at which point the test is interrupted. These results reveal that the main fracture mechanism in EP-GFRP is fiber/matrix debonding.

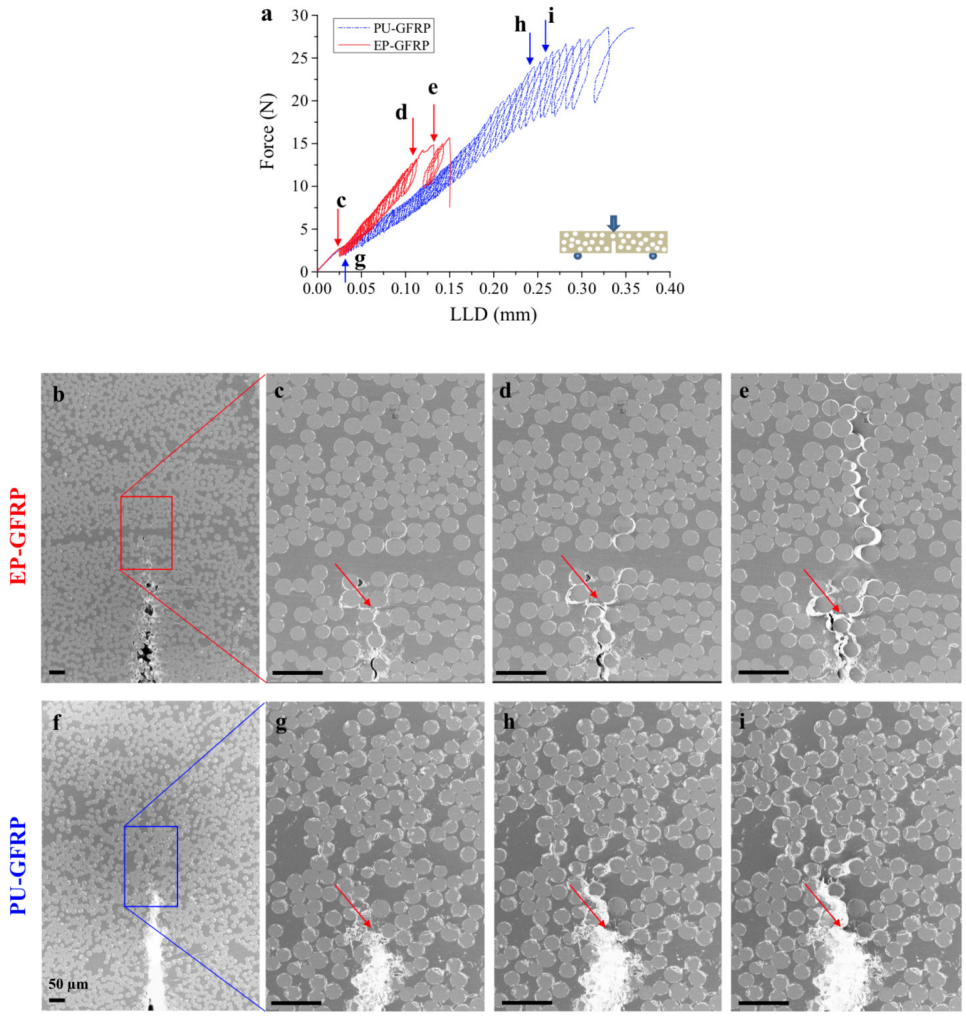

Fig. 2: (a) Force vs. load-line displacement curves for the* in situ *tests showing the moments at which pictures (b) to (i) were taken; and ('b' to 'i') sequence of scanning electron micrographs showing the crack propagation ahead of the crack tip in the EP-GFRP ('b' to 'e') and in the PU-GFRP ('f' to 'i'). The arrows point to the location of the crack tip at the start of the test. The load-line displacement in each picture is (b, f) 0 µm, (c) 25 µm (d) 108 µm, (e) 132 µm, (g) 30 µm (h) 218 µm and (i) 253 µm. Scale bar in all pictures: 50 µm.

Crack propagation in the PU-GFRP differs markedly from that in its EP counterpart, as shown in Fig. 2f–i. No pronounced signs of damage are observed until a LLD of about 100 µm, when a pre-damaged region at the crack tip starts to open, as shown in Fig. 2g. Upon separation from the fibers, the matrix develops extensive plasticity before eventual failure, characterizing cohesive failure. This suggests that crack nucleation takes place within the matrix rather than at the interface. This phenomenon is normally associated with a strong fiber/matrix adhesion and enables efficient exploitation of the resin's toughness during crack propagation. The test is finally stopped at an LLD of 360 µm since no further toughening mechanisms were noticed. At this point, the force-displacement curve had deviated from linearity for about 200 µm. These findings lead to the conclusion that the predominant fracture mechanism in PU-GFRP is cohesive failure within the matrix rather than adhesive debonding at the interfaces.

4. CONCLUSIONS

Careful analysis of the mode I transverse intralaminar fracture in unidirectional GFRPs showed that it is possible to harness the full toughening potential of the utilized matrix if the dominant failure mechanism occurs within the polymer matrix rather than at the polymer-fiber interfaces. This explains the significantly improved fracture toughness of polyurethane-matrix laminates as compared with epoxy-matrix counterparts. The matrix-dominated failure mechanism in the PU-based system, which was experimentally confirmed by micromechanical testing with *in situ* SEM observations, is very likely to stem from a stronger fiber/matrix adhesion that hindered adhesive failure at the interfaces. As a result, the fracture energies of unidirectional GFRPs with PU are up to 6-fold higher than those of the benchmark system.

REFERENCES

[1] ASTM E1820:2015 - Standard test method for measurement of fracture toughness.

Symposium *Lightweight Design in Product Development 2018* (LWD-PD18)
Zurich, Switzerland, 14th–15th June 2018

LIGHTWEIGHT POTENTIAL OF CARBON/FLAX HYBRID LAMINATES

Jonas Maria Schmid[1], Markus Zogg[2]
[1]Radiate Engineering, Switzerland. schmid@radiate.ch
[2]Inspire, Switzerland. zogg@inspire.ethz.ch

1. INTRODUCTION

Carbon fiber reinforced polymers (CFRPs) are the material of choice for highly stressed components due to their strength and stiffness properties and the resulting lightweight design potential. Classical fiber reinforced polymers (FRPs) for lightweight structures consist of synthetic fibers such as carbon fibers (CF), glass fibers or aramid fibers combined with a polymer matrix. Since the production of carbon fibers is very energy-, greenhouse gas- and cost intensive, the question arises about possibilities for the realization of more ecological and cost-efficient lightweight FRP structures. Engineers and designers need to find a trade-off between structural integrity, environmental compatibility, costs and manufacturing feasibility. One approach to make CFRP structures more energy- and cost-efficient is to reduce the carbon volume fraction and use carbon fibers partially only exactly where they are really needed and where they are structural efficient. In the remaining areas, the carbon fibers are substituted by cheaper and more environmentally friendly fibers, which reduce the overall environmental impact and the costs of the FRP structure. The combination of different fiber types in a composite is called fiber hybridization. The present assessment [1] aims to hybridize carbon and flax fibers (FF) in an interlayer configuration without reducing the mechanical FRP performance (stiffness, strength and weight) significantly. As illustrated in Figure 1, the processing and manufacturability of CF/FF hybrid laminates is investigated and the mechanical properties of pure CF-, FF- and CF/FF- hybrid laminates are characterized. Based on the results, the analytical lightweight potential of various CF/FF laminate configurations and their preferred load cases are calculated, in order to quantify the structural lightweight potential of CF/FF hybrid laminates compared to pure CF laminates and to define general design guidelines for CF/FF hybrid laminates.

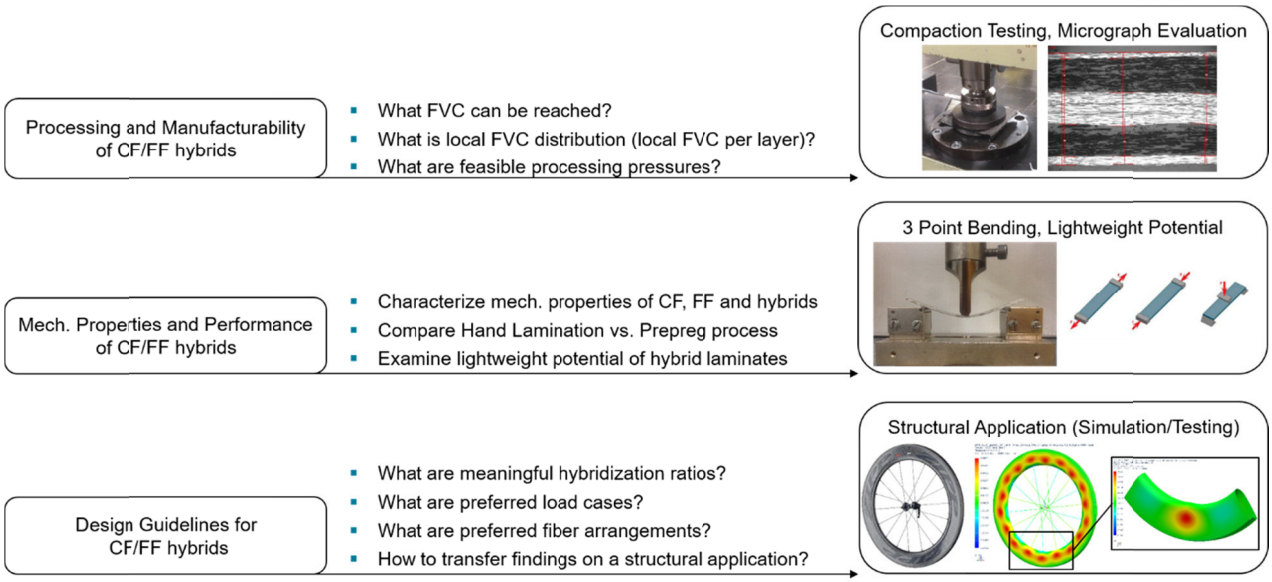

Fig. 1: Research questions and assessment methods.

2. PROCESSING AND MANUFACTURABILITY

Method

By means of compaction response testing pure CF and FF (saturated and unsaturated) are exposed to different compaction pressures. For each single fiber type, it is measured what fiber volume content (FVC) can be reached at which specific pressure. In addition, cross sections of different cured CF/FF hybrid samples are evaluated by micrograph analysis. With this technique, the local layer thicknesses and thus the local fiber volume contents in the individual CF and FF layers can be determined. By combining the results of both assessments, a statement about the manufacturability and definition of preferable processing pressures for the combined processing of CF and FF can be made.

Results

From the compaction response it can be seen, that flax FVC is up to 30% lower than carbon FVC at low compaction pressures (0.5-1bar). As shown in Figure 2, a strong dependency of flax fiber compaction capability and the applied pressure is observed, resulting in a low FVC deviation of 10% between carbon and flax for high pressures (10-20bar).

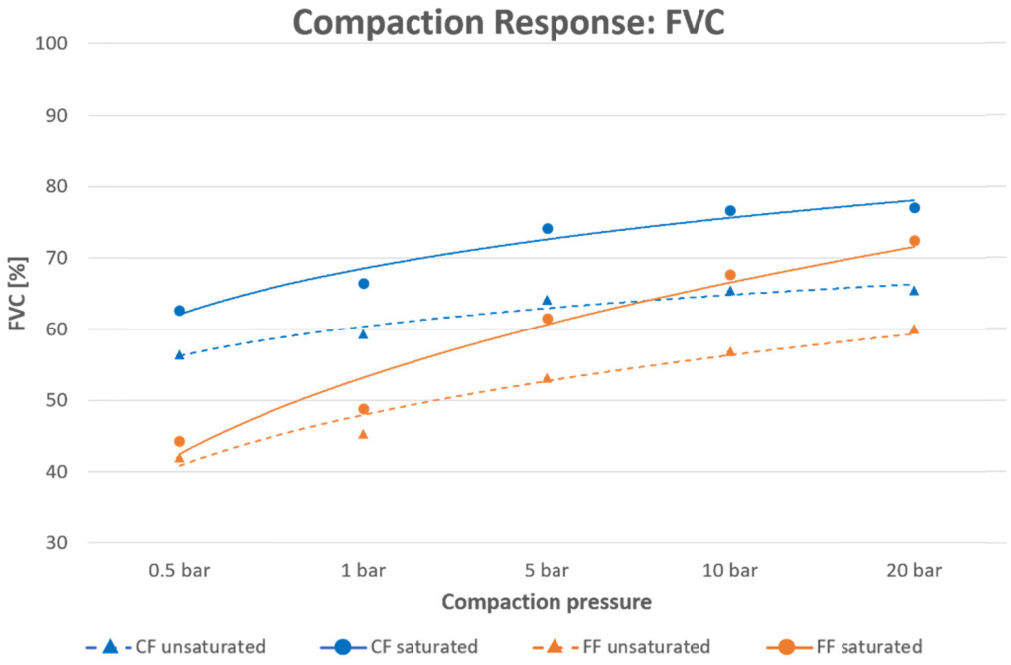

Fig. 2: FVC response of saturated and unsaturated CF and FF fibers .

3. LIGHTWEIGHT POTENTIAL

Method

The mechanical properties of pure CF, FF and CF/FF hybrid laminates are characterized by standardized three-point-bending tests. Each of the analyzed samples is produced by two different manufacturing processes, the hand lamination and the autoclave prepreg technique. Based on the mechanical properties, the so-called lightweight potential of different materials and material combinations can be calculated in a further step. This calculation is a methodological approach to find replacement laminates with same tensile-, compression-, bending- strength and stiffness in order to substitute a pure CF laminate. The calculation method computes the alternative material thickness in order to reach the structural constraints. This allows to evaluate which replacement configurations are lighter or heavier compared to the reference CF laminate at the same load case. From this analysis, it can be deduced for which load cases hybridization makes structurally sense and what are the benefits or drawbacks in terms of weight.

Results

Although there is a difference in the local fiber volume contents between carbon and flax, hybrid laminates with only 16% less flexural modulus and 17% less flexural strength compared to the pure CF reference laminate could be produced. Comparing the mechanical properties of the samples manufactured by hand lamination and autoclav process, it is noticeable that the hand laminated ones perform significant poorly.

As illustrated in Figure 3, from the calculation of the lightweight potential emerges that CF/FF hybrid structures can be built up to 8% lighter than a pure 0° CF structure, having the same compression- and bending strength as well as the same bending stiffness. This effect can be seen as well in a 0° UD arrangement with the flax (in the middle of the specimen) and the carbon in 0° direction as when they are arranged in a cross ply configuration where the 0° fibers are from carbon and the 90° fibers (in the middle of the specimen) are from flax. The biggest benefit appears at a hybridization ratio of 60/40 vol.% (CF/FF). From the preferred load cases, such as compression strength, bending strength (limited by buckling) and bending stiffness, it can be said that buckling critical structures hold a great lightweight potential for incorporating CF/FF hybrid laminates.

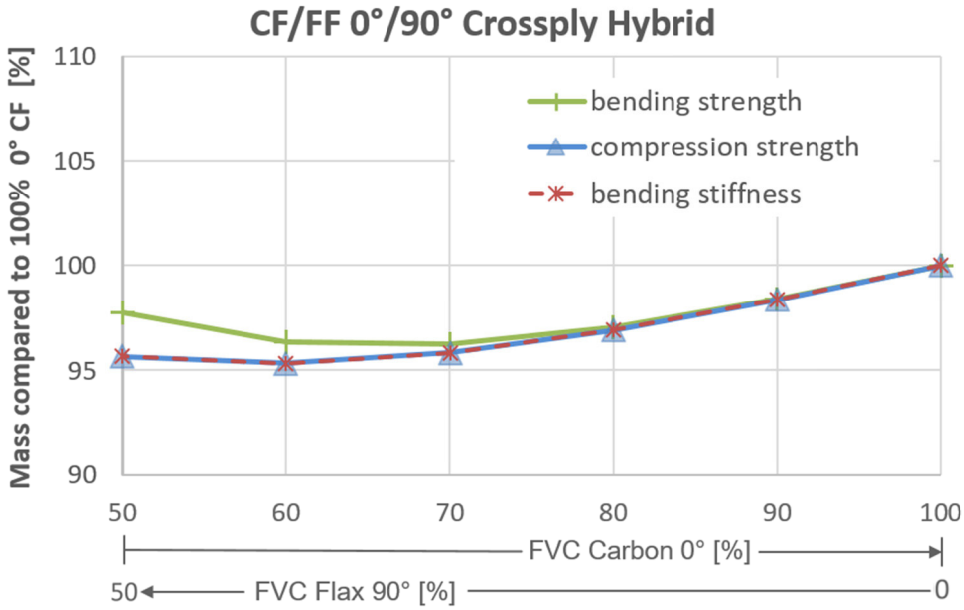

Fig. 3: Mass comparison of CF/FF cross ply hybrid, referenced to 0° CF for the preferred load cases.

4. CONCLUSION

It could be shown that flax fibers have lower fiber volume contents at the same compression pressures compared to carbon fibers. The deviation is strongly pressure depended and can be reduced by increased compaction pressures from a maximum of 30% to a minimum of 10%. Means higher processing pressures will result in lower local FVC deviation between the CF and FF layers within a hybrid laminate and therefore increased mechanical properties. Combined with the good resulting mechanical properties it can be concluded that carbon and flax can be very well processed together to hybrid laminates using the conventional composite manufacturing processes.

Resulting from the lightweight potential calculation, hybridization makes no sense in the case of tensile loading and compression stiffness since in this cases the carbon fibers are dominating with their high tensile stiffness and strength properties. By contrast, the properties of flax have a much greater impact on the load cases bending strength/stiffness and compression strength (limited by buckling), thus enabling to even reduce the weight under these loads. It can be said that hybridization in a pure structural sense only makes sense for these three load cases. The flax fibers unfold their full potential when combined as a kind of sandwich laminate with the carbon fibers. The maximum lightweight construction potential is achieved by sheathing the flax fibers (low density) as core material with carbon fibers (high stiffness & strength) as facings. A maximal weight reduction of up to 8% could be achieved by a CF/FF, 0° UD laminate and by a CF/FF, Cross ply laminate with 90° flax fibers arranged as core sheets. In both cases meaningful hybridization ratios are between 50-60/50-40 vol.\% (CF/FF). This insight quantifies that hybridization not only helps to improve the eco- and cost structure of laminates, but additionally offers a potential for lightweight design exceeding the one of pure carbon laminates within the preferred load cases.

REFERENCES

[1] Schmid, Jonas: Assessment of the lightweight and cost potential of carbon/flax hybrid laminates, Mater Thesis at CMAS Lab, ETH Zürich; 2018

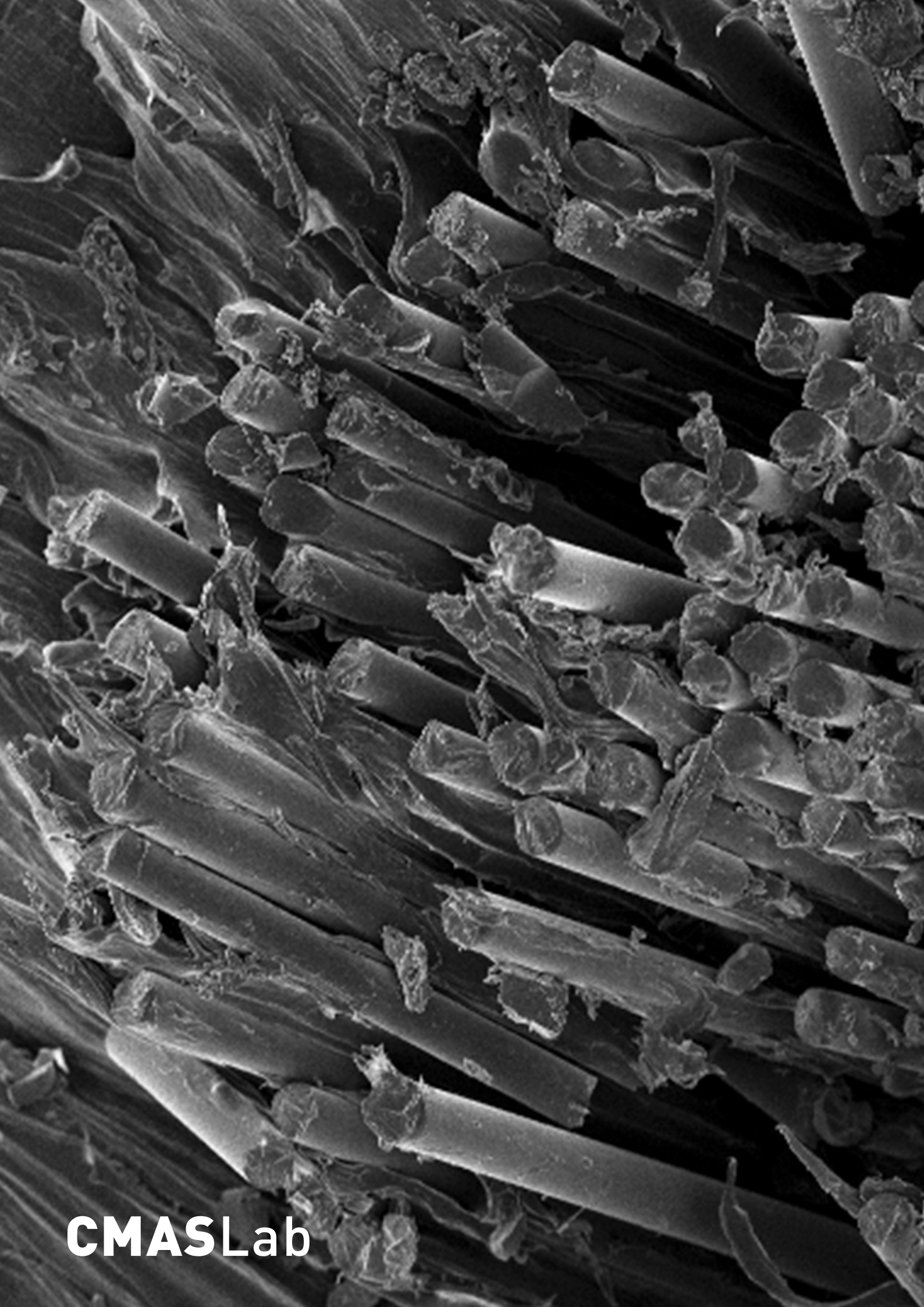
CMASLab